Republic of Iraq
Ministry of Higher Education and Scientific Research
University of Misan/College of Engineering
Civil Engineering Department

NUMERICAL ANALYSIS OF STEEL-CONCRETE COMPOSITE BEAM CURVED IN PLAN

A THESIS
SUBMITTED TO THE COLLEGE OF ENGINEERING OF
MISAN UNIVERSITY IN PARTIAL FULFILLMENT OF
THE REQUIREMENTS FOR THE DEGREE OF MASTER OF
SCIENCE IN CIVIL ENGINEERING
(STRUCTURES)

By
SABA LAITH KAREEM
B.Sc. in Civil Engineering, 2016

Supervised by
Prof. Dr. Abdulkhaliq Abdulyimah Jaafer

October 2020   **Rabi Al-Awwal 1442**

بسم الله الرحمن الرحيم

(قالوا سبحانك لا علم لنا إلا ما علمتنا إنك
أنت العليم الحكيم)

صدق الله العلي العظيم

سورة البقرة – الآية (٣٢)

DEDICATION

To my Parents

To those with whom I have acquired boundless power and love……

To those with whom I knew the meaning of life……….

To my Sister

To a spiritual twin and a companion for my path... to the one who has a kind heart and good intentions……

To who accompanied me since my childhood until now……

To my Brothers

To my companion for my path and support after my father……

At the end of my career, all thanks to them for their noble stances with me……

To my Close Friends

To whom stood beside me, for their support and encouragement……

I present my effort to them with all my respect and appreciation.

Acknowledgements

In the Name of Allah, the Most Gracious, the Most Merciful

Supervisor Certification

I certify that the preparation of this thesis entitled **"Numerical Analysis of Steel-Concrete Composite Beam Curved in Plan"** was presented by **"Saba Laith Kareem"**, and prepared under my supervision at The University of Misan, Department of Civil Engineering, College of Engineering, as a partial fulfillment of the requirements for the degree of Master of Science in Civil Engineering (Structures).

Signature:

Prof. Dr. Abdulkhaliq A. Jaafer

Date: 20. 7. 2020

In view of the available recommendations, I forward this thesis for discussion by the examining committee.

Signature:

Assit. Prof. Dr. Samir M. Chassib

(Head of Civil Eng. Department)

Date: 20 - 7 - 2020

IV

EXAMINING COMMITTTEE'S REPORT

We certify that we, the examining committee, have read the thesis titled (**Numerical Analysis of Steel-Concrete Composite Beam Curved in Plan**) which is being submitted by (**Saba Laith Kareem**), and examined the student in its content and in what is concerned with it, and that in our opinion, it meets the standard of a thesis for the degree of Master of Science in Civil Engineering (Structures).

Signature:

Name: **Prof. Dr. Abdulkhaliq A. Jaafer**

(Supervisor)

Date: 18/ 10/2020

Signature:

Name: **Assist. Prof. Dr. Ali N. Attiyah**

(Member)

Date: 18/ 10 /2020

Signature:

Name: **Dr. Nasser Hakeem Tu'ma**

(Member)

Date: 18/ 10 /2020

Signature:

Name: **Assist. Prof. Dr. Abbas O. Dawood**

(Chairman)

Date: 18/ 10 /2020

Approval of the College of Engineering:

Signature:

Name: **Assist. Prof. Dr. Abbas O. Dawood**

Dean, College of Engineering

Date: 18/ 10 /2020

Abstract

This study presents a numerical analysis on curved steel–concrete composite beam to investigate the effect of various parameters on the beam behavior. Composite steel-concrete beams with normal strength of concrete with or without steel beam openings designed as simply supported. Furthermore, a strengthening technique were conducted by adding intermediate steel stiffeners.

The work is done on forty-five specimens designed as simply supported with 6 m span length. The specimens were constructed of a concrete slab with a 500 mm width and 120 mm depth connected to a rolled steel beam Type 200UB29.8 using sex parameters. 3D finite element analysis is employed by using ABAQUS 2017 software to ascertain the accuracy and validity of FE procedure. Finite element analysis efficiency is proved through comparing with experimental tests through load-deflection curves, ultimate load, ultimate deflection, and cracks propagation. The validated models are used to asses some of the key parameters such the span/radius of curvature ratio, transverse web stiffeners, partial interaction, concrete compressive strength, steel beam yield stress, opening depth, shape of steel beam web stiffeners for retrofitting the beams strength. From the obtained results, it is evident that the span/radius of curvature ratio reduces the loading capacity, yield, deflection and ductility by 50%, 53%, 52% and 41% and increase the twisting of the beam due to the torsional effect. The presence of transverse stiffeners in the curved composite beam enhance the beam capacity and ductility index by about 57% and 63%. In addition, increasing the stiffeners number contribute to decrease the vertical separation and the beam twisting at the beam mid-span due to decrease the

beam torsion, transferring the failure to the concrete slab. Furthermore, increase the partial interaction show a significant reduction in the vertical and interface separation between the steel beam flange and concrete slab with an increasing the beam capacity by about 30%, while the deflection and ductility index reduced by 50% and 20%. The loading capacity and the curved composite beam ductility increased by 58% and 61% as the steel beam yield stress increased while the flexural cracks appear to be effective on the top and bottom faces of the reinforced concrete slab.

Increasing the opening depth lead to reduce the strength capacity of the beam and yielding of the beams becomes earlier. Maximum reduction was recorded for 75%h opening depth for yield load, ultimate load and vertical deflection by approximately 48%, 18% and 8% for curve by approximately 18%. An increasing in the flexural and diagonal torsional cracks has been observed when the opening depth increases. Moreover, presence of elongated circular opening in the mid-span reduce the beams capacity by 24% approximately, in which the beams exhibited less ductility by 14% where the response of the specimens softening and the beams yield in an early stage. Web stiffeners are considered a good way to enhance the beam capacity by 11%. They provided a semi complete restoring to the strength loss due to the opening presence with enhancement in the beam performance.

List of Contents

List of Tables

List of Figures

Nomenclatures

d_c	Damage parameter value of the compression of concrete……………	
d_t	Damage parameter value of the tension of concrete…………………	
E_{cm}	Secant modulus of elasticity of concrete……………………………….	MPa
E_s	Modulus of elasticity of steel material………………………………….	MPa
k	Coefficient; Factor……………………………………………………………..	
K_c	The ratio of the second stress invariant in the tensile meridian to compressive meridian………………………………………………………..	
f_{cm}	Mean value of measured cylinder compressive strength of concrete…..	MPa
f_{ck}	Characteristic value of the cylinder compressive strength of concrete at 28 days…………………………………………………………………	MPa
f_t	Concrete tensile strength………………………………………………	MPa
f_y	Steel yield strength……………………………………………………………	MPa
f_u	Steel ultimate tensile strength………………………………………...	MPa
U_i	Translational displacements………………………………………...	mm
α	Angle; ratio……………………………………………………………………	
ε	Tensile strain in the concrete…………………………………………	mm/mm
ε_{0c}^{el}	Elastic strain………………………………………………………………….	mm/mm
ε_c	Compressive strain in the concrete…………………………………..	mm/mm
$\tilde{\varepsilon}_c^{in}$	Inelastic strain……………………………………………………………..	mm/mm
ε_{c1}	Compressive strain in the concrete…………………………………..	mm/mm
ε_{cu1}	Ultimate compressive strain in the concrete…………………………	mm/mm
ε_t	Tensile strain in the concrete at the peak stress f_t………………….	mm/mm
ε_t^{ck}	Cracking strain…………………………………………………………	mm/mm
ε_t^{pl}	Plastic strain ………………………………………………………………..	mm/mm
σ	Tensile stress in the concrete…………………………………………..	MPa
σ_c	Compressive stress in the concrete……………………………………..	MPa
σ_{to}	Initial failure stresses……………………………………………………..	MPa
$\dfrac{\sigma_{b0}}{\sigma_{c0}}$	Strength ratio in the biaxial state to uniaxial strength state…………….	
v	Poisson's ratio………………………………………………………………..	

Abbreviations

AISC ……………………………………………American Institute of Steel Construction

C3D8R ………………………………. Eight-node brick element with reduced integration

CCBF.. ………..Curved in plan composite steel-concrete beam with full shear connection

CCBP………Curved in plan composite steel-concrete beam with partial shear connection

FE ………………..…………………………...…………………………….. Finite Element

FEA ……………...………………………………………… Finite Element Analysis

FEM …………………………………………………………...……. Finite Element Method

T3D2 …………………………………….………………. Two-node truss element

UB……………………………………………………………...…. Universal beam

CHAPTER ONE

CHAPTER **1**

Introduction

1.1 General Overview

Recently, conventional composite steel-concrete structures have been vastly used around the world sometimes one of the most economical construction in the civil engineering structures. They are commonly employed in contemporary buildings and highways for decades due to multiple benefits of mechanical properties of combining two materials, steel and concrete compared to the traditional construction of reinforced concrete structure.

Composite beams provide multiple properties and advantages than non-composite sections. The ideal combination properties of the most widespread building materials, i.e. steel and concrete, provided economic and safe structures was by combining stiffness of the concrete slab and ductility of steel beam. Since the structural steel beam and the concrete slab carrying the load, the required size of the steel beam would be smaller. This reduces the overall depth of steel structure and the total building height that led to reduce the structures cost and time of construction [1].

In recent years, the horizontally curved members have been dramatically employed in highway bridges, balconies and interchanges design essentially at the approaches in an urban area, whereas the complex geometry and the curvature are required as can be seen in Fig. (1-1) [2][3]. In addition to the aesthetic purpose, these structures have an economic purpose to fulfill the requirements of buildings and highway structures in a pre-determined manner to define the alignment of the roadway according to the design code requirements. [4].

Figure (1-1): Horizontally curved composite steel-concrete structure [2][3].

Curved members are different from the straight members in the analysis where the torsional effect is always present due to the curvature at which the torsional effect may be developed that vanished in straight members [5]. However, as a result of asymmetrical loading or complexity of member geometry, twisting moment combined with flexural moment to be developed in such members. Due to the complexity of stress state, a predict of strength

and structural behavior of curved in plane members under the action of combined bending and twisting moments may be tricky to fulfill. The available international codes such as AISC [6] and Eurocode 4 [7] do not cover these effects of combined actions [8].

1.2 Composite Action

The most important key parameters effect on the flexural stiffness, strength and associated with the connection between the steel beam and concrete slab in the composite member is the composite action. This phenomenon is illustrated in conjunction with the upper and lower limits of the composite beam behavior, i.e. full, partial interaction and no interaction.

Under loading condition, if a deliberate and appropriate connection maintained between the reinforced concrete slab and steel beam by an infinitely stiff and sufficient shear connector; the two components behave comparatively as one with fully yield strength provided for the tension flange or the beam chord [9]. This situation is described as completion or full interaction. Furthermore, the relative slip and strain differences between the two components is relatively close to zero everywhere with assuming that the plane section remain plane. Otherwise, if no connection provided between them, the two components have independent behavior with relative slip or separation occur at the interface. The effect of the composite action is described in Fig. (1-2) [10].

During the state of loading history, the considered mechanical properties may be varied. Thus, the sections in the composite member may properly be varied in the behavior, ranging from a section with no

interaction to that of typical or perfect interaction. Comparatively, assuming composite member with perfect connection during the analysis with deformable shear connectors overestimates their stiffness and the strength properties. Furthermore, the deficiency of physical connection in the interface between the synthesize of steel and concrete components is too conservative. Thus, the stiffness and strength of mechanical shear connector must be considered for the analysis accuracy.
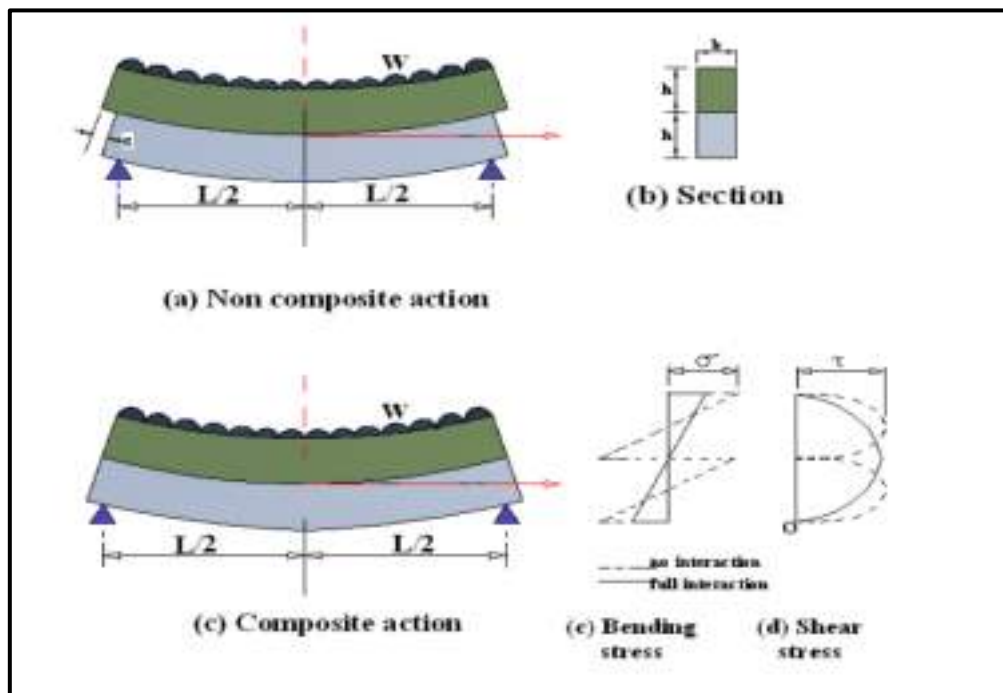
Figure (1-2): The composite action effect [10].

1.3 Shear Connector

Composite action has been providing between the pre-fabricated units such as prestressed or precast reinforced concrete or steel beam and cast in place concrete, in order to act as a single unit. Although there is a certain amount of natural bond between concrete slab and steel beam at least at the initial stages, this bond cannot be relied upon because it is likely to be

deteriorated due to over load and frequent use. Mechanical shear connectors provided to help the steel and concrete element to act in a composite manner ignore the contribution made by the inbuilt natural bond towards this effect. Typically shear connectors are proposed to resist the horizontal movement between the two components and to spread the horizontal shear between the concrete slab and steel beam. Shear Connectors are also used to prevent vertical separation of the slab from steel girder at contact surface.

1.3.1 Shear Connectors Types

Various types of shear connectors are specially shaped to provide adequate resistance to uplift as to separation. The connection is a region of severe and complex stress that defies accurate analysis. Methods of connection have been developed empirically and verified by tests. In a broad sense, connectors may be divided into two categories: [11]

I. Rigid connectors

Rigid type of shear connectors is very stiff and they undergo very less deformation under large shear force as compared to the other types of connectors. Their resistance is mainly generated from the bearing pressure on the concrete, and most of the times they fail due to the failure of concrete surrounding. Angles, Short bars and T-sections are common examples of rigid type of the connectors. Some other devices such as hooped bars are connected with rigid type of connectors to avoid vertical separation [12]. This type of connectors is shown in Fig. (1-3).
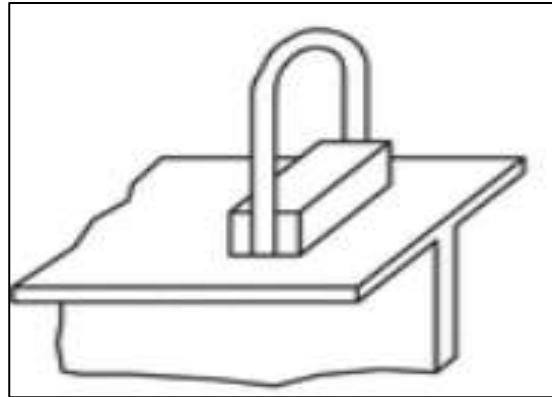
(a) Angle connector   (b) short bar connector

(c) T-connector

Figure (1-3): Typical rigid connector [13-15].

II. Flexible connectors

These are the most commonly used connectors. Headed studs and channels come in this category. Their stress resistance is mainly generated through bending and they undergo large deformation before failure. Typical flexible connectors are shown in Fig. (1-4). The stud connectors are the types used broadly. The shank and the weld collar nearby to steel beam resist the shear loads while the head resists the uplift [12].

(a) Stud shear connecror
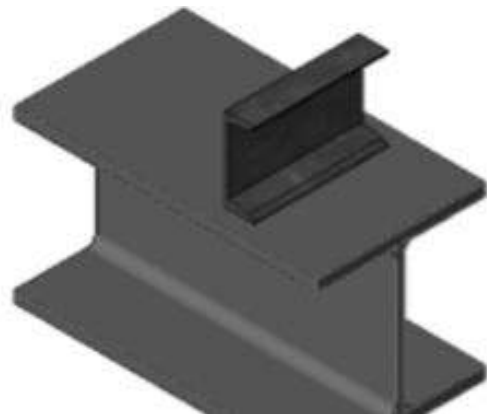
b) Channel connector

Figure (1-4): Typical flexible connector [16][17].

In practice, while using the rigid type of shear connector at the interface of steel-concrete composite beam it is assumed that there is no slip at the interface. But from the studies over the years it was found that even by using rigid type of connector in composite beam there is always some slip at the interface [12].

However, regardless of the shear connector type some relative movement does occur between steel section and concrete slab. Fig. (1-5)

show the mechanism example of this relative movement using flexible connector type.
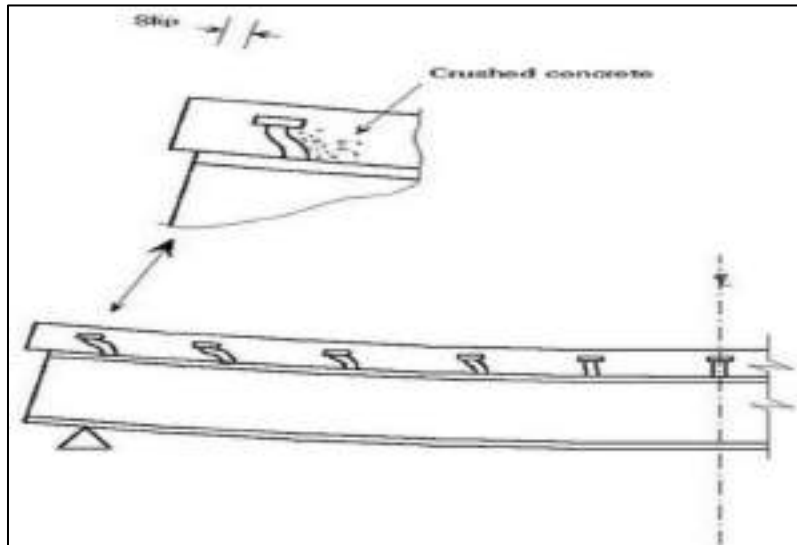
Figure (1-5): Slip at interface in the composite beam [11].

The concrete near the weld level may crush that allows some deformation for connector itself. However, near the head of connector the concrete is not very much stressed and the head of connector will not move from its earlier original position Fig. (1-6).
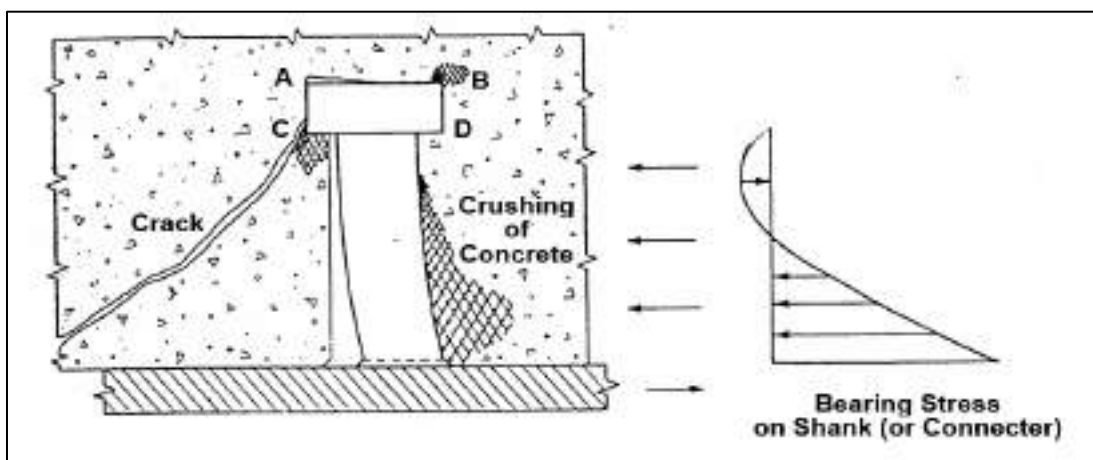
Figure (1-6): Shank stress distribution of the shear connector [11].

Results in the bending deformation of connector that can be seen in Figs. (1-5) and (1-6). Long and the flexible type of connectors are more likely to deform into this pattern and subsequently have a tendency to be ductile. On the other hand, the short stocky type of connector tends to be brittle and thus unwanted. Because of this reason most of the stud connectors are preferred to be at least three to four times longer than their diameter as per codes [12].

1.4 Needs for Curvature in Plan

The curved members are aesthetically considered an excellent solution that encourage increasing the designs of curved configurations members. Steel technology reached to a stage that all universal sections ranges and European sizes may be properly curved, taking into consideration the section size limitation and the length or material grades [18]. Horizontally curved beams found in various applications, including balconies, modern bridges and buildings, and interchanges as mentioned above. Many roads on the highway bridges are on curved alignment. Bridges with link roads and lower speed roads may have a 90 m radius of curvature, this properly needs to an angular change in the carriageway direction, which leads to a remarkable effect on the construction and design of the bridge. Furthermore, the higher speed roads definitely need to longer span due to increasing the radius of curvature [13] in which the longer-span bridges reduce the detailed of bearing and the expansion joints number.

In the past, a series of straight members had been used to form a sequence of curve chords, resulting in large and unequal overhang of the decking works that lead to undesirable appearance and uneven shadowing of

the members [19]. The fabrications of curved girders were costly and more difficulty with the complexity in the analysis process. However, the modern development and the invention of high-quality equipment's have overcome any difficulty in theses curved member. Whereas the analytical software plays an important role in the analysis of curved configurations members using curved members instead of series of straight girders being more popular, reducing the total cost and in the overhangs slab outside girders.

1.5 Behavior of Curved Beam

Horizantaly curved beam with vertical loading will be subjected to longitudinal bending stresses develop to the same extent as in a straigth beam in conjunction with a significant torsional stress due to geometric complexity and bending moment plane changing along the curve. The significant torsional moments tend to twist and distort the beam cross-section producing warping and torsional stresses incoporating with normal stresses due to the flexural bending [18]. The rotaion magnitude will be a fucntion of the beam torsional stiffenses [19]. A significant torsion (per unit length) will be associated with the bending moment and it can be determined from the following formula [18]:

$$T = \frac{M_y}{R} \qquad (1.1)$$

Where M_y (kN.m) and R (m) are the flexural moment about y-axis, and the radius of curvature of the curve beam, respectively. For I-section beam a tosion can be equivalent to the lateral (or radial) force per unit length as in equation below:

$$F = \frac{T}{h_f} = \frac{M_y}{Rh_f} \tag{1.2}$$

Where h_f (m) is the distance from the flange centroids. The St Venant torsion provides the major compenent of the torsional moment at the ends. The corresponding warping moment in each flange is greatest at mid-span.

The predscribed behavior is related to the elasticity status of the beam. Furthermore, for the placticity behaviour an additional complexity is considered in their analysis. In which the typical rotaion show almost a significant increaseing resulting in non-negligible bending in minor axis (beam axis seems to be non-vertical).

1.6 Curved Composite Beams Behavior

The behavior in the curved composite beams are comparable to the curved beam effect, i.e. flexural moments plus torsional moments generated due to the geometric curvature of the beam. However, the composite beam has a much greater warping stiffness than a single beam (such as I-section), because any twist would require vertical bending of the beam and the horizontal bending of the slab. Although the resistance to twist is due mainly to warping stiffness, it will be more readily seen as a transfer of vertical loading from one beam to another. However, as well as the overall twist, there are distortional effects because the radial forces in the bottom flange try to change the geometry of the cross section. The stiffness and strength of the web, bending out of its plane (even when there are transverse web stiffeners) is generally too weak to restrain the effects due to the typical plan curvature which necessarily need to provide steel section restraint [18].

An addtional complixity have been considered and associated in the beam analysis. The pure bending moments can accurately be coducted by using the AASHTO LRFD [20] procedure to compute the plastic moments for the curved compsoite member[19]. Whilst the ultimate torsion moments for the curved steel-concrete composite beam could be obtained using the proposed formula conducted by Tan and Uy [21] as shown in Eq. (1.3).

$$T_u = T_c + T_s + (\leq T_j)$$ (1.3)

T_u= Utimate theorotical torsional moments.

T_c= Concrete contribution to the ultimate torque.

T_s= Steel reinforcement contribution to the ultimate torque.

T_j= Steel beam contribution to the ultimte torque.

Also, a graphical representaion for the ultimate torsional moments contribution in the curved steel-concrete compsoite besm can be shown in Fig. (1-7).
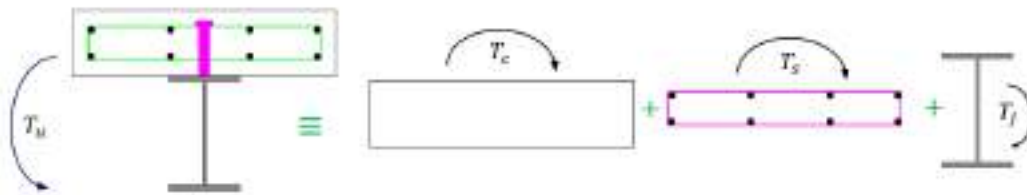
Figure (1-7) : Ultimate torsional moments in the curved composite beam.

In horizontally curved girder bridges there are two general types of cross sections: box girders and I-girders [22]. The box girders are able to resist significant torsion if their shapes are maintained with sufficient internal

bracing. The bridge type was initially popular for that reason [4]. On the other hand, I-girders are commonly used in curved bridges because of their constructability, but they have sometimes relativel low torsional stiffness due to their open web sections, and the thin plates used in their construction. This required the need to develop transverse web stiffeners, the strength and the stiffness of the web with the bending in its out of plane is properly too weak to resist this influnce because of typical plan curvature. Therfore, cross frames or diaphragms are frequently used to provide lateral supports for the girders Fig (1-8) [18].

Figure (1-8): Cross frames or diaphragms in horizontally curved girder bridges [18].

1.7 Study Objectives

The main goal of this study is to develop a three-dimensional FEA of composite steel-concrete curved in plane beam, to study the influences of some parameters on the beam behavior. The analysis of beams were done by using ABAQUS software; validity of the used procedure is examined by comparing their outputs with the literatures. The load versus vertical

deflection curves, flexural and torsional cracks, vertical and interface separation, the twisting and beam yielding are the most factors for current study.

The span to radius of curvature ratio, transverse web stiffeners, shear connectors ratio, concrete slab compressive strength, yield strength of steel beam, opening, fixation boundary condition are the main parameters used in this thesis to investigate their effects on the composite steel-concrete beams performance.

1.8 Thesis Layout

The present thesis offers five chapters as shown in Fig. (1-9) as follows:

Chapter 1 (Introduction): This chapter gives some background on composite steel-concrete structures, especially the curved members. Also, it gives a description of application, advantage and general behavior of the curved beam and curved composite beam, and objectives, in addition to the research outline.

Chapter 2 (Review of Literature): This chapter reviews a number of numerical studies and scientific experimental researches on horizontally steel curved beam and steel-concrete composite member curved in plane.

Chapter 3 (Finite Element Modeling and Formulation): This chapter develops the basic relationships and the material modeling in the finite element theory with concrete and reinforcing steel, steel beam and the shear connector representation, and the specimen modeling.

Chapter 4 (Numerical Application and Results): This chapter carries out the finite element results and their discussions.

Chapter 5 (Conclusions and Recommendations): This chapter summarizes the conclusions and recommendations for future studies.

CHAPTER TWO

CHAPTER 2

Review of Literature

2.1 Introduction

This chapter develops a brief review of significant conclusions and findings from previous studies that are related to this study. This chapter covers the previous experimental and analytical investigations of the horizontally curve steel beam and curved composite steel-concrete member behavior under the effect of static loading conditions.

2. 2 Horizontally Steel Beams Curved in Plan

Comparing to the counterpart's straight member, the behavior demonstrated by curved members is far more complex. In which, the beam curved in plane exposed to lateral loads, subjected not only to vertical deformation but to twist deformation also with respect to its longitudinal axis. This flexure-torsion interaction depends on the cross-sectional rigidity as well as curved girder geometry. However, the horizontally curved alignments of the modern highway bridges or an urban interchange, considerably increased in recent years was necessary to construct the curved in plane structures. The available curved members open new vision for inventive design of structural steel, whereas 70 years ago successive researches had begun for analysis and

design of horizontally curved sections. **Umanskii** in 1948 [23] conducted the first treatment of the curved girder who presented solutions for numerous conditions of loading by presuming initial parameters in the solution procedure. Following series of experimental and computer programs of curved flexural member had been adopted to investigate the linear and nonlinear large-deflection behavior of horizontally curve members by the University Research Consortium in the United States [24], to better understand and improve its behavior in the subsequent years.

In 1965 **Konishi and Komatsu** [25] presented a three-dimensional (3D) analysis of curved girders by deriving relations between strain and stress components for a very curved beam where the elastic flexural stress distribution along the beam depth could be nonlinear. In the mid-sixties, US Steel published an approximate procedure called (V-load analysis) for determining moments and shears in horizontally curved girder bridges [26]. Similar developments were also made in Japan by **Watanabe** [27]. **Conrad et al.** [28] in 1972, **Yoo et al.** [29] in 1974 and **Heins et al.** [30], [31] in 1976 and 1982 developed computer programs to design or analyze curved girder bridges for highway systems.

Fukumoto and Nishida in 1981 [32], used the transfer matrix method to obtain the inelastic ultimate strength of horizontally curved beams simply supported at both ends. The transfer matrix method includes the second order effects associated with geometric and material nonlinearities, and also the effects of residual stresses. The study has shown that the ultimate strength of horizontally curved 1-beams is dependent on a variety of parameters included:

type of loading, span-length, curvature, initial residual stresses and boundary conditions.

Rosen and Abromovich [33] in 1984 derive equilibrium equations describe the three-dimensional behavior of curved beams. These equations include first order geometric nonlinear influences. The equations are solved by the Galerkin method. The method is very general and allows general variation of the geometric and structural properties along the beam. Any combination of boundary conditions is possible and the most general distribution of loads along the beam can be treated. Numerical results for a few examples are presented and compared to other theoretical and experimental results. The agreement between the results is generally good. It is shown that Galerkin method is an efficient method which enables one to solve the problem using small number of unknowns compared to other methods which are in use.

The next traced theoretical treatment was carried out by **Yang and Kuo** [34] in 1987 derived the nonlinear differential equations based on virtual displacement principle with a continuum mechanics basis, to explore the curved I- beam buckling behavior under various loading action. The curvature effect [with an included subtended angle $(0 \leq \beta \leq 180)$ Fig. (2-1)] is considered through three factors: (1) The introduction of a Jacobian in the volume integral; (2) use of coupled generalized stress-strain relations; and (3) inclusion of radial stresses in the virtual work expression. Generally, it had been shown that the Jacobian and radial stress contributions to the buckling of a curved beam are significant. Such effects can only be neglected for very small subtended angles, say, for $(\beta < 20°)$.
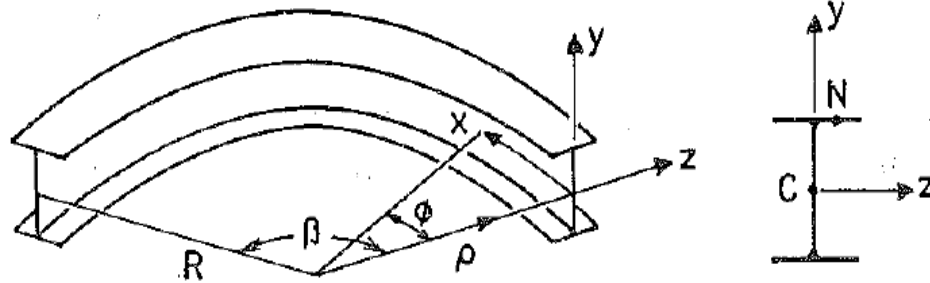
Figure (2-1): I-Section beam with Vertical Web [34].

Liew et al. in 1995 [35] presented the behaviour and design of horizontally curved I-beams by the analytical studies and the finite element using ABAQUS program, for further analysis and design the large –displacement inelastic behavior of I-beams curved in plane. The beam span length and radius of curvature represented the main study parameters. The ratio of (span/curvature) (L/R) was ranged (0.008 to 0.08). The results revealed that, the failure mode of a beam with shorter span length is due to the coupling effects of distributed plasticity and lateral-torsional instability whereas the failure of beams with longer span length is mainly by lateral-torsional instability. The study has also demonstrated that the effects of residual stress on the ultimate strength of the beams curved in plan is significant for beams with intermediate slenderness ratio larger than 0.3 and less than 1.5.

Yoo, et al. [36] in 1996 studied the buckling behavior of curved beams. Based on results from the lateral bifurcation buckling of horizontally curved beams, the authors put forward a regression equation representing the reduction in critical moment due to the simple addition of curvature. In 1997 **Davidson and Yoo** [37] did a parametric study and found that degree of curvature, span length and flange width were the parameters with most significant effect on the behavior of curved beams. Besides, the authors

developed an equation to provide a preliminary design limit for cross-frame spacing interval.

In 2000 **Pi and Bradford** [38] presented 3D finite element analysis using ABAQUS software for analysis curved steel I-beam under equal bending moment with $(0° \leq \theta \leq 90°)$. Early approximations are not made for the coupling between the displacements and the twist rotations, so that higher-order terms of twist rotations are included in the nonlinear strains. The numerical simulations emphasized that for curved beams with a small angle $(\theta \leq 1°)$, bending is the major action, the inelastic behavior of these curved beams is similar to those of straight I-beams, and the near inelastic flexural-torsional buckling may occur. The postbuckling displacement response is associated with the load decrease. For curved beams with an included angle $1° < \theta < 20°$, both bending and torsion are important, and as the included angle increases, the significance of bending decreases and the significance of torsion increases. For curved beams with a large included angle $(\theta \geq 20°)$, torsion is the major action, and the nonlinear inelastic behavior develops very early. When the near inelastic lateral buckling occurs, the vertical displacements and twist rotations are very large.

Pi and Bradford in 2001 [39] outlined a numerical analysis by ABAQUS software for the nonlinear elastic-plastic load-deflection behavior of the curve steel I-beam under the combined influence of bending and torsion. The strength interaction relationship between the dimensionless bending and torsion was related to many factors including beam slenderness, span length, minor bending axis and secondary torsion, lateral configuration bracing, and an angle $(0 \leq \theta \leq 90)$. The interaction equation was introduced as below for

unbraced, centrally braced and continuously braced as typically employed in the analysis.

$$\left(\frac{M_u}{M_{bx}}\right)^{\gamma_x} + \left(\frac{T_u}{T_P}\right)^{\gamma_s} \le 1 \tag{2.1}$$

where, for an unbraced member, $\gamma_x = \gamma_s = 1$, for a centrally braced member $\gamma_x = 1.5$, and $\gamma_s = 1$, and for a continuously braced beam $\gamma_x = 2$, and $\gamma_s = 1$.

Based on the outcome results, at a constant subtended angle with varied length, both the ultimate dimensionless bending moment and torque decrease with increasing the span length, and vice versa at increasing particularly the beam angle. Furthermore, at the stationary value of length and angle the incorporate effect of ultimate dimensionless torque and bending increase with an increase in the lateral bracing.

Jung and white [40] in 2006 employed FEM for studying the shear strength of curved steel I-girder. The study focusses on the influence of horizontal curvature on the maximum strength of transversely stiffened members with web slenderness approximately equal to the largest value permitted in AASHTO. The other parameters were also investigated in this study as imperfections, residual stresses and flange size. The results showed that decreasing the flange sizes contributes to reduce the beam shear capacity accompanied by decreasing the elastic bucking strength for the curved I-girder. The residual stresses and imperfection were less pronounced with less web slenderness than the largest one. Otherwise, by considering the post-buckling strength, the transversely stiffened curved I-girders could be

designed for maximum strength loading conditions based I-girder shear capacity equations of AASHTO [41].

Kim et al. [42] in 2007 the behavior of one- and two-sided transverse stiffeners in straight and horizontally curved steel I-girders is investigated by full nonlinear finite element analysis. Proposed design equations are developed based on providing adequate transverse stiffener bending stiffness and strength. From the outcome results, it was showed that this is a more important consideration in developing shear postbuckling resistance than the satisfaction of an area or axial force requirement. Otherwise, it was found, regardless of the type of the stiffeners, girders with a given slenderness (D/t_w) and web panel aspect ratio $(d_\circ/D)$ had essentially the similar strength in designing based on the suggested equations.

In 2009**, Madhavan and Davidson** [43] studied the curvature effect on the curved I-girder compression flanges flexural capacities due to local buckling. Theoretical model was used to define the non-compact section limit and the effect of stress gradient on elastic buckling of slender flanges. The results demonstrated that design criteria should not be based upon the buckling behavior of isolated half-flanges for load situations that result in a significant stress gradient across the flange. Furthermore, the one-third rule approach adopted in AASHTO 2007 is appropriate for curved compact sections, but becomes increasingly conservative with increases in compression flange slenderness since the effects of stress gradient on elastic buckling were negligible within typical bridge design parameters. Finally, flexural resistance equations for flange local buckling of curved I-girders were formulated and evaluated using finite element analyses.

In 2013 **Hayder and Kadhim** [44] presented 3D finite element analysis using NFHCBSL computer program to investigate the strengthening effect of the bottom flange on the ultimate strength behavior of the simply support horizontally curved steel I-girder under concentrated static load. The strengthening includes increasing the thickness of bottom flange at finite region which contributes to increasing the steel volume. The curvature (θ) influence employed at angles of 5°, 10°, 15°, 30° and 45°. For each value of θ eight values of angle of strengthening (φ) investigated ($\varphi = 0\%\ \theta$, 5% θ, 15% θ, 25% θ, 35% θ, 45% θ, 55% θ and 65% θ), thus forty cases were studied. The outcome results showed a sufficient improvement of the ultimate strength of such beam nearly 35% by strengthening the bottom flange of beam by ($\varphi = 55\%\theta$) with $\theta \leq 5°$, whilst the vertical and horizontal deformation shows a particular decreasing by 67% and 69%; respectively, at a strengthening angle ($\varphi = 65\%\ \theta$). Otherwise, when the angle of curvature (θ) increases, the ultimate loads of beam decrease for any value of angle of strengthening (φ), but this decrement increases rapidly if (φ) increases.

El-Khoury et al. [45] in 2014 developed numerical analysis by ABAQUS program to investigate the flexural behavior of horizontally curved steel I-girder as a function of the position of a single longitudinal stiffener at various locations along the depth of the web. Relative to the web depth (D), six various locations of longitudinal stiffener were studied. The most significant finding was observed that, the optimal location of stiffeners for horizontally curved plate girder were under pure bending where was D/5 from the compressive (top) flange, matching AASHTO recommendation for straight plate girders location. Otherwise, longitudinal stiffeners were more beneficial with respect

to enhancing curved girder flexural capacities for slender webs ($D/t_w = 300$) that were studied at higher girder radii.

Visuvasam et al. [46] 2017 devoted non-linear analysis using ANSYS program for the curved steel I-beam. Some governing parameters were carried out on the curved beam including the radius of curvature to the span ratio (R/L), flange and web slenderness (B/t_f), (D/t_w); respectively. The flexural behavior and the ultimate load carrying capacity for various curvature radii have been investigated for each parameter. The study showed that the beam flexural resistance significantly increasing with radii increasing because it gives a comparable behavior to the straight beam. Moreover, a higher (B/t_f) value, introduces higher resistance to flexural than beams with smaller (B/t_f). Although, the bending resistance was anticipated to increase at higher (D/t_w) ratio, the beam with smaller R/L ratio gives gentle increase and almost straight line, which shows the lesser radius of curvature beam with any web depth to thickness ratio, will not have an effect on its bending resistance.

2.3 Steel-Concrete Composite Member Curved in Plan

In the preliminary design phase, the composite beams preferred a newly-built high-speed railway due to the economic performance and their excellent mechanism. Curved composite steel-concrete beam construction could found in industrial buildings, bridges and in an urban interchange as mention in previous chapter due to their excellent achievement in large flexural stiffness terms and higher loading capacities. Depending on the beam geometry, a curved composite member tends to buckle in a simple mode by a combination

of flexural and torsion. For the curved composite steel-concrete members, the earlier analytical and experimental studies that conducted are listed below:

An experimental research had started by **Colville** [47] in 1973 that attitude an experimental series tests programs on the steel-concrete composite curved beams to explore the behavior of shear stud connector. Form test data, the quantified of vertical deflection for the three test specimens exceeded the predicted values by at least 50%, which indicate that with further torsional application to the composite steel-concrete beams there was a pronounced increase in the vertical deflection. Furthermore, a proposed formula was provided as seen in Eq. (2.2) for the composite steel-concrete beams undergoes the combined influence of flexural and torsion.

$$T_p = (\frac{K_c}{t_c})\sqrt{56.2f_c^{'} + \sqrt{f_c^{'}}(\frac{M}{S})} \qquad (2.2)$$

where;

T_p: Ultimate capacity of the torsional moment in the steel-concrete composite beam (N.m).

K_c: The concrete slab torsional rigidity (N.m^2).

t_c: The concrete slab thicknesses (m).

$f_c^{'}$: The characteristic concrete compressive strength (MPa).

M: The bending moment applied (N.m).

S : Plastic shear modulus (GPa).

Heins [48] in 1978 recommended erection and fabrication procedures depended on numerous erectors or fabricators organizations combined with premature work research on composite box-girder bridges curved in plane.

Otherwise, **Arizumi et al.** [49] in 1982, developed an analysis on composite curved girders using finite strip method with incomplete interaction, utilizing curved strip elements for the steel girder and concrete slab. Two-dimensional spring element along the nodal line for the shear connectors. A following of series papers discussed by (e.g. **Maeda et al.** [50] in 1973, **Yoda et al**. [51][52] 1980, 1981, **Nakai et al**. [53] (1981), **Arizumi et al.** [54][55][56] 1982, 1987, and 1988) were published on the design of curve composite or curved bridges. An experimental study developed on Cyrville Road bridge by **Ng. et al.** [57] in 1993, on a 1/24 linear scale model. A curved composite aluminum-concrete girder bridge with four-cell box was modeled. The model was tested elastically under various OHBD (The Ontario Highway Bridge Design) truck-loading conditions and continuous over the central support.

Thevendran et al. [58] in 1999, outlined a numerical analysis by ABAQUS software for predict the nonlinear behavior of the curved composite beam under combined loading effect. The approach represented by using four-noded isoperimetric thick shell element incorporating with membrane and bending stiffness for the concrete slab and the steel beam. Whilst the shear stud connector was simulated using rigid beam element. The results show that that the tangential stresses at the top surface of concrete slab in outer curvature side at midspan are greater than those at inner curvature side. At quarter span, the stress distribution along slab width is reversed and the tangential stresses at outer curvature side are less than those at inner curvature side.

Thevendran et al. [59] in 2000, performed an experimental investigation on horizontally curved composite steel-concrete beam. Five beams were tested with different span/radius of curvature ratios ranged from [0 to 0.5].

The typical geometry of the tested specimens shown in Fig. (2-2). The study explored the ultimate flexural moment capacity, stress distribution along the span, failure modes, and the beam loading capacity. The test results indicate that the load-carrying capacity decreases with the increase in the span/radius of curvature ratio. Moreover, the relative beam mode failure observed to change from flexural to combined effect of bending and torsion as well as the curvature increase. Fig. (2-3) show the beam twisting and crack patterns at failure.
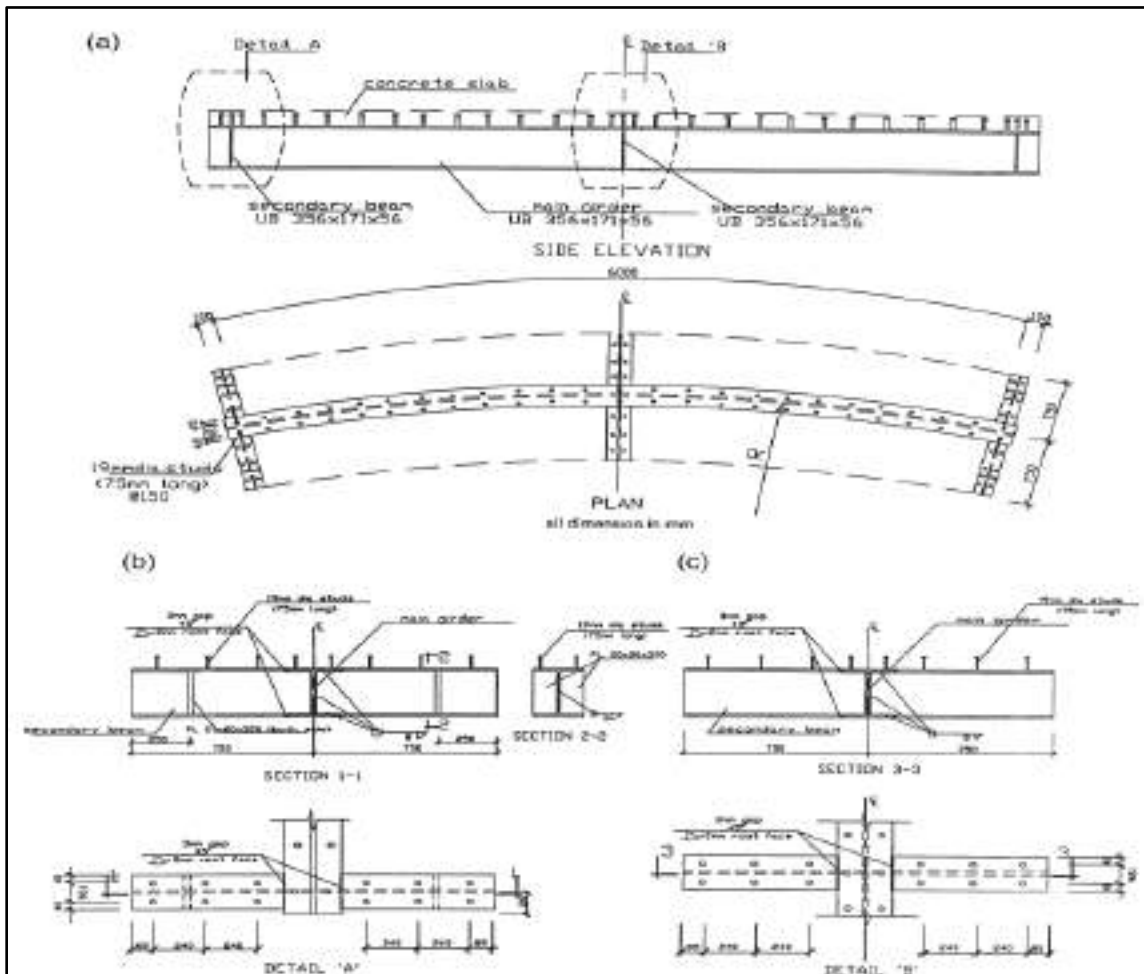
Figure (2-2): Typical specimen details, a) Steel structural components, b) Detail A, c) Detail B [59].
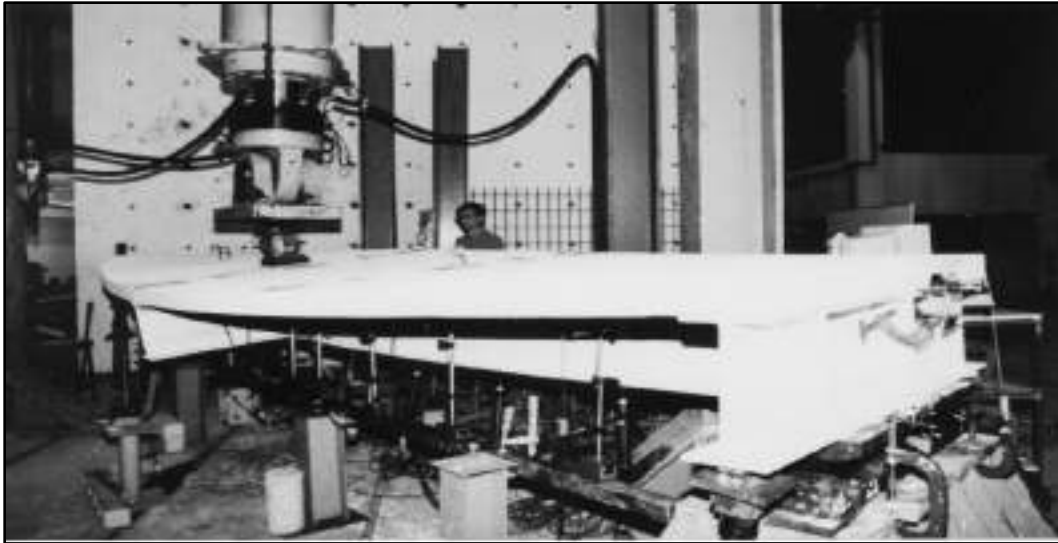
(a)

(b)

Figure (2-3): Mode of failure for the curve composite beam [59].

The simply supported straight and curved composite bridge was presented by **Sennah et. al** [60] in 2003 to investigate the structural response for different parameters. In this study an extensive parametric study, using an experimentally calibrated finite-element model, in which the straight and curved prototype bridges are analyzed to determine their shear distribution

characteristic under dead load and under AASHTO live loadings. Based on the generated data, an empirical simpler formula for maximum shears (reactions) are developed that are suitable for the design office. Furthermore, it was demonstrated the presence of solid end diaphragms at the abutment supports enhances the transverse shear distribution, and significant enhance in the transverse shear distribution was observed. The transverse shear distribution could be improved significantly by using stiffer cross bracings and decrease lifting upward at the abutments. Furthermore, bridge curvature as well as partial AASHTO live loading on the outer lanes produces high uplifting forces at the innermost support bearings.

In 2005, **Al- Hashimy** [61] discussed the effect of curvature, girder spacing, span length, number of girders and lanes, loading conditions and cross bracing on lateral load distribution factor of curve composite steel I-girder bridges using SAP2000 software. Research result used to develop empirical formulas for deflection and shear distribution factor. Analysis results showed that the curvature was the most significant factor that plays an important role in increasing the shear distribution factor with its increasing. Otherwise, increasing the girder number as well as the span length show significant effect on increasing the SDF (Shear Distribution Factor), while the cross bracing had less effect.

In 2007, **Samaan et al.** [62] conduct a 3D finite-element analysis of 180 continuous curved and straight composite multiple-box girder bridges. The effects of bridge configurations, loading positions, and vehicle speed on the impact factors were examined. Bridge configurations involve, span length, span/radius of curvature ratio and number of boxes and lanes. The static and

dynamic analyses were carried out in the parametric study along the parameters. The span-to-radius of curvature ratio has a measurable influence on the magnitude of the impact factors regardless of the span length of the bridge, while the number of lanes and boxes show no influence on it. Results showed that the impact factors for uplift reactions are generally underestimated by all current North American Codes.

Erkmen and Bradford [63] in 2009, extended numerical analog by sophisticated ABAQUS shell element models Fig. (2-4) with the elastic total Lagrangian formulation to derive the strain expression and explore the partial interaction effect in the radial and tangential direction as well as the geometric nonlinearity and initial curvature. Fig. (2-5) showed a simply support specimen with a combination of eccentric and vertical distributed loading resulting from the steel beam and concrete slab. The results showed that the partial interaction should be considered in the inelastic analysis of the curved composite beams. The proposed formulation had been extended and compared it with the experimental measurement to explore time-dependent creep and shrinkage of curved composite members by **Erkmen and Bradford** [64][65] 2011a, b and **Liu et al.** [66] in 2013.
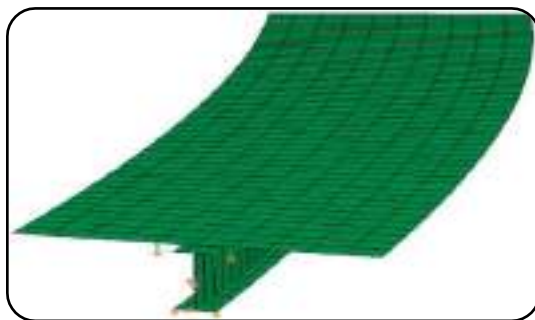
Figure (2-4): Beam modeling with shell element type [63].
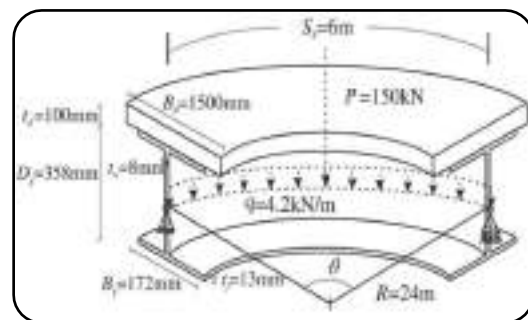
Figure (2-5): Geometric and boundary condition with Beam modeling [63].

The accomplished study considered the influence of materials and geometry nonlinearities carried out numerically by **Liu et al.** [67] in 2009. The calibration performed with experimental results, taken into account the partial interaction and initial curvature effect on the non-linear inelastic analysis of composite beams curved in plane.

Tan and Uy [21] in 2009, devoted an experimental work on the composite steel-concrete beam curved in plane under the combined bending and torsion to adopt the ultimate strength of such beam. The experimental program consisted of eight specimens designed and tested with full and partial interaction (four with full interaction, and the other with partial interaction) with different ratios of span/radius of curvature. Based on experimental results, the diagonal torsional cracks observed at both ends of the beam and start to open up and progress at the concrete slab as can be revealed in Fig. (2-6)a. Furthermore, the curvature played an important role in the beam torsional twisting that was noticed intensively at beam mid span. Furthermore, it casing uplift separation between steel beam and concrete slab at the ends of the member as seen in Fig. (2-6) b and c. The ultimate flexural moment capacity decreased with curvature increases. The failure mode was changed from flexural to combined effect of flexural and torsion with increasing the curvature. The results showed that in presence of flexural, the torsional strength ratio shows a higher increase in the case of the full interaction than the partial shear connector series. A suggestion was made that at decreasing level of the shear connectors, the contributed steel beam torque significantly remarked to decrease.

(a)

(b)   **(c)**
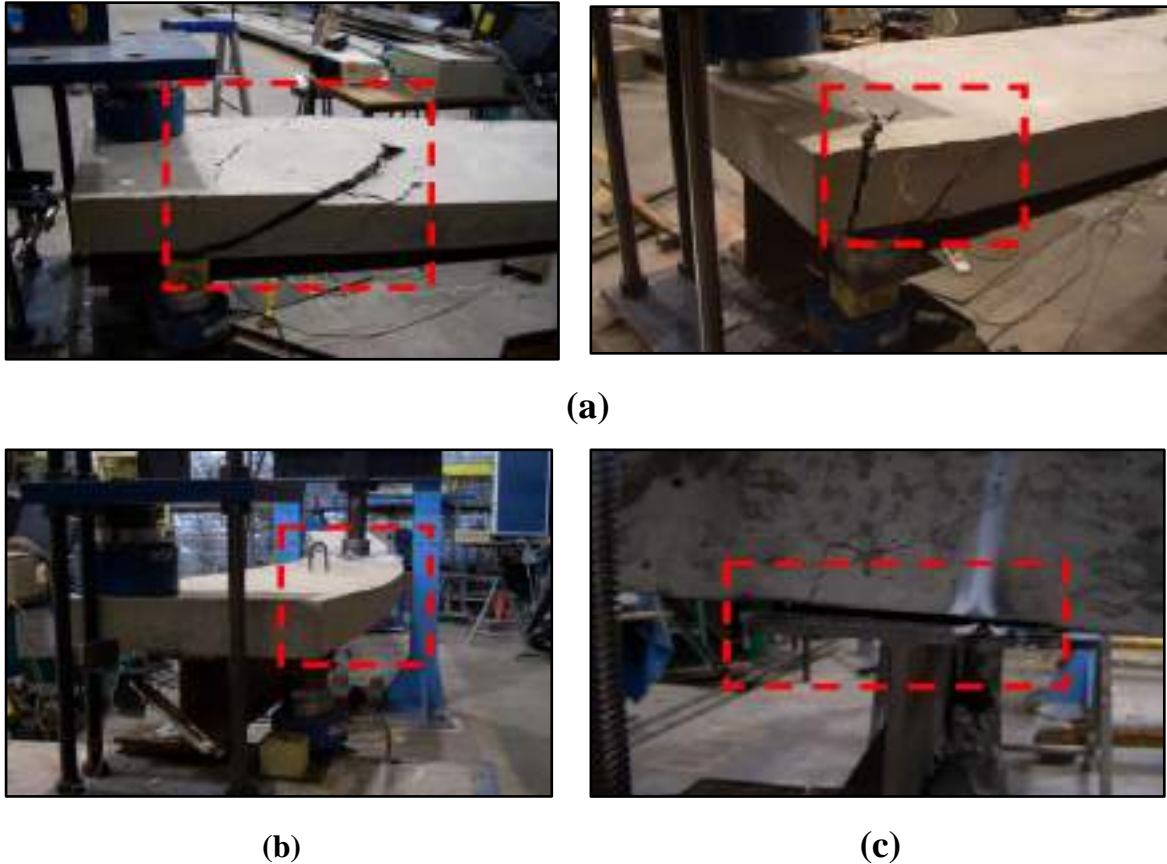
Figure (2-6): Curved composite beam mode failure: a) diagonal torsional crack, b) Mid span twisting, c) The concrete slab and steel beam separation [21].

Finite element analysis accomplished by **Tan and Uy** [68] in 2011, to idealize the partial interaction and beam span length effect on the straight and curve composite steel-concrete beams exposed to combined of flexural and torsional moments. All the simulated models deigned based on statically approached according to the AS/NZN (Australian Standard) and Eurocode 4 (British Standard Institution, 2005). Totally two hundred specimens were divided into two series (100 for straight and the other for curved composite member) and exposed to static concentrated load. Based on numerical results, a new phenomenon was noticed as significant issue called torsion induced vertical slip due the beam twisting was developed as revealed in Fig. (2-7). This phenomenon made the plane section remain plane invalid. In addition,

the flexural-torsion interaction relationship was not influenced by the partial shear connection, whilst the span length greatly effects on it. From the parametric study, it was concluded that the torsional strength ratio in the straight composite member depended mainly on the span length and neutral axis location. For the curved composite members, this rate significantly affected by the lateral torsional buckling of the steel web due to increasing the steel web depth when the span length increase.
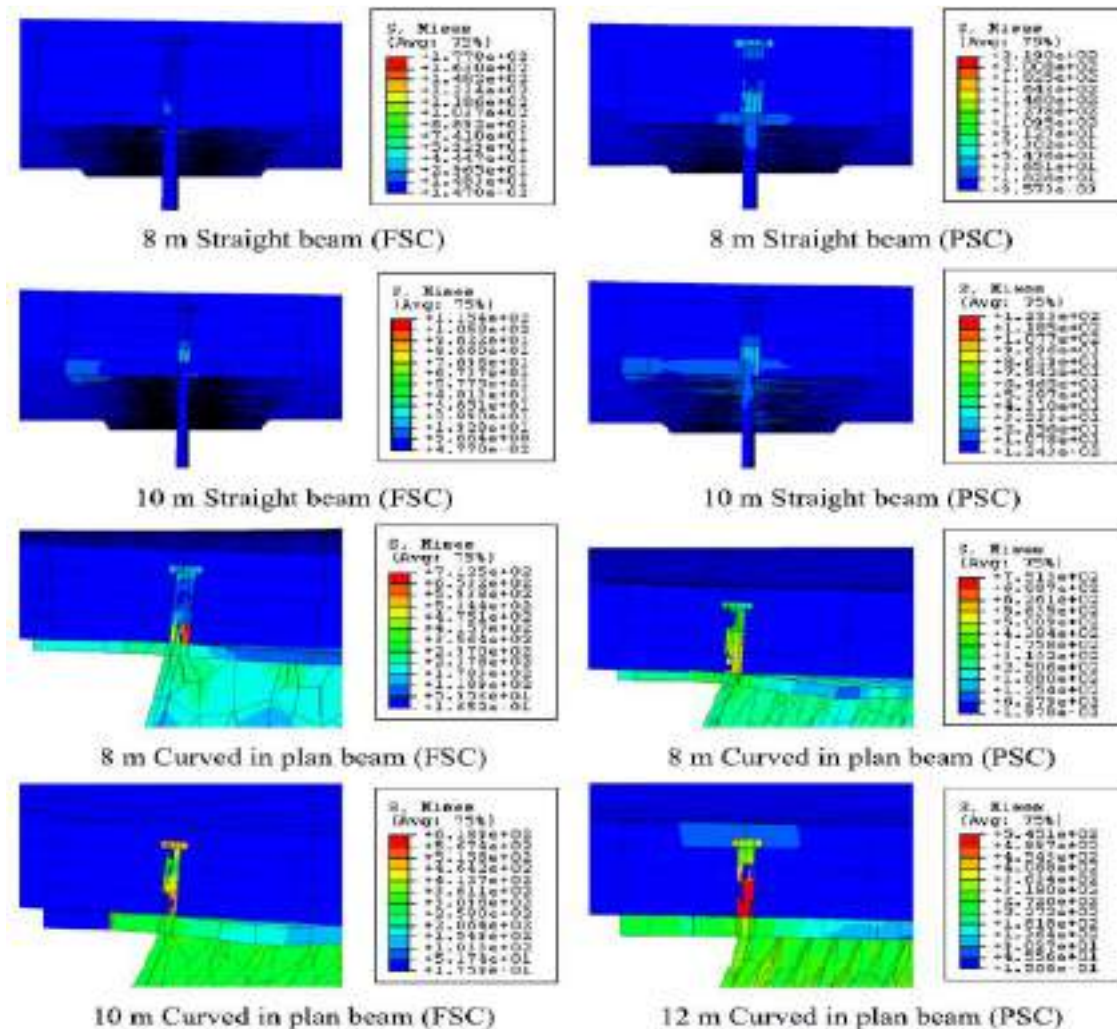
Figure (2-7) Views the concrete-steel interface at mid-span section under pure torsion for the composite beam [68].

Lin and Yoda [69] in 2014, established nonlinear 3-D finite element models by DIANA software to investigate the steel-concrete composite beams curved in plane subjected to hogging moments. Totally six simply supported curved composite I-girder simulated with various central angles (5°, 10°, 15°, 20° and 30°). The main conclusions of the study were:

1- The initial crack, yield and ultimate loads decreases linearly as the curvature significantly increased ($0 \leq \theta \leq 30$), Fig. (2-8).
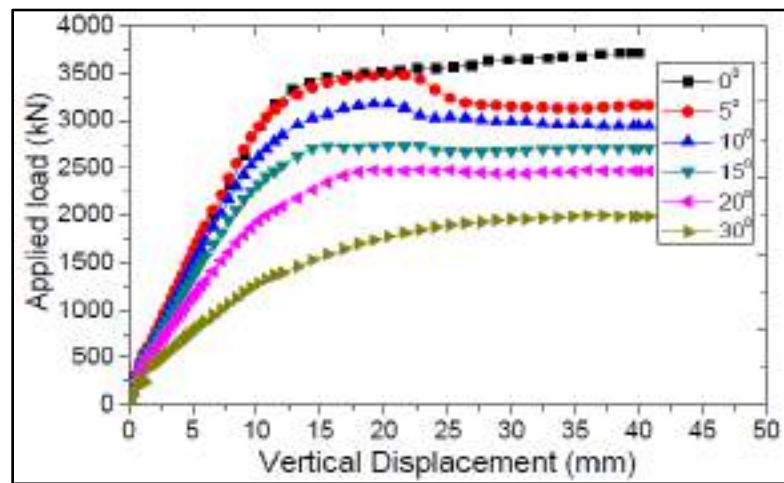
Figure (2-8): Load-deflection of the models [69].

2- Due to the concrete slab cracking as well as the presence of interface slip, the plane section assumption was no longer valid in the inelastic analysis.

3- The strain of reinforcement bar was found to be different according on its location and those differences increased with the increasing curvature whereas these particular differences increased with the increasing curvature due to further non-ignorable torsional moments.

4- The results confirmed that the mode of failure was changed from bending to torsional failure with the increasing of curvature. Also

proposed simplified bending-torsion interaction equation, for the curved composite beams under hogging moments was written as:

$$\frac{T}{T_u} = -3.71 \left(\frac{M}{M_u} - 0.5\right)^2 + 1.91 \quad (0 \leq \theta \leq 30) \qquad (2.3)$$

where;

T: Torsional moments at failure in test (N.m).

T_u: Theoretical values of ultimate torsional moments (N.m).

M: Flexural moments at failure in test (N.m).

M_u: Theoretical values of ultimate flexural moments.

θ: Central angle.

Zhang et al [70] in 2015 discussed the effects of diaphragm numbers, the span, the span-to-radius ratio, the girder height and the flange width on the stress (the ratio of the warping normal stress to the bending normal stress) of curved composite beam by using MIDAS program. The parametric analysis results indicate that the increase of the number of diaphragms, the stress ratio decreases exponentially; and with the increase of the span-to-radius ratio, the warping stress ratio increases linearly; additionally, longer span leads to reduced stress ratios, but the variation of the girder height and the flange width has little influence on the stress ratio. Calculation formulae for determining the required diaphragm spacing are obtained eventually by regression analyses take into account the radius of curvature, span and the expected stress ratio.

An analytical study presented by **Xi et al.** [71] in 2016 on the curved composite beam considering the partial interaction effect in the tangential direction. It was primarily developed to solve the static problem of the curve composite beam with interlayer flexible connection in the tangential direction. The principle of minimum potential energy adopted to achieve both the boundary conditions and the governing equations. The accuracy of the presented theory was verified by comparing with experimental and FEM of another researchers. The results showed that the reduction in the shear connector's stiffness had a significant effect on the torsional angle (in mid span section) and the vertical deflection at the mid span.

Qin et al. [72] in 2017 developed a modified rigid cross method to study lateral distribution of the multi-I composite curved bridge with slip effect. The finite element method by ABAQUS program is used to determine the stiffness interpolation coefficients of single composite curved beam and verify the lateral distribution calculation of multi-beam composite curved bridge. The numerical examples showed that the influence of interface slip to the lateral mid-span moment distribution factors can't be ignored for the composite curved bridge with shear connection, and the lateral distribution got by rigid cross beam method considering slip effect is in good agreement with that by finite element static analysis, which indicates that this method can accurately describe the load distribution characteristics of multi-beam composite curved bridge.

Androus et al. [73] in 2017 presented an experimental investigation on both elastic and ultimate behavior of composite box girder bridges in order to study the effect of internal cross bracing between box girders and curvature

effect at different loading stages. Three simply supported specimens of concrete deck-steel composite model of twin-box bridge, one straight and two curved, were tested up to collapse. The response of each model was monitored under free-vibration excitation, then an eccentric loading was applied and the corresponding deflections were recorded in the elastic range. The structural behavior of the three bridge models was compared at the three loading stages. It was noticed that the presence of an external cross bracing system between the steel boxes had an insignificant effect on the developed deflection and the fundamental natural frequency in the elastic range of loading. However, these external bracings assisted in decreasing the developed deflection approaching failure and in increasing the load carrying capacity by about 8.9%. In addition, the external bracing ensured a better distribution of the stresses under ultimate loading conditions.

Izzet and Mohammed [74] in 2018, carried out an experimental program to investigate the flexural behavior of horizontally curved composite I-girder bridge under the Iraqi standard live load effect. Five scaled simply support curve models fabricated with 3m central span length. Each specimen was built up with four girders, the first two models had 175 mm girder spacing and curvature (L/R) of 0.2 and o.3; respectively. The other three accomplished with 200 mm spacing and curvature ratio of 0.1, 0.2 and 0.3, respectively. To achieve the full-scale design bridge model, the applied loading comprises of superimposed dead and self-weight loads in addition to one of the Iraqi live bridge loading (Military; Lane loading: comprise of wheeled and traffic vehicle class 100). The outcome results confirm that the Iraqi wheeled load was the dominate case affecting on the bridge model; all the girder deflections were below the permissible AASHTO LRFD 2012 limit. The longitudinal

mid-span bottom flange girder strain was less than the girder yield strain and the maximum longitudinal mid-span concrete strain at the top surface was (469 micro-strains) which was lower than the ultimate concrete strain of (3000 micro-strains). The deflection and the longitudinal girder strains increased with the increasing curvature, whereas the girder spacing exerted only a very slight effect.

2.4 Summary

From the previous literature review in the field of the curved steel beams behavior and curve composite beams, it has been noticed that there are numerous analytical and experimental researches, which is being conducted in studying the curved girder or curved composite bridge behavior. However, there is no available data deals with curve composite steel-concrete beam strengthening with steel web stiffeners to prevent the web lateral torsional buckling. Therefore, this thesis extends a vulnerable information and better understanding of the demeanor of the curved composite beam under different parameters especially that web stiffeners are majorly utilized in steel beam, which are the primary components in enhancing the load-bearing capacity of such member.

Since the available studies that dealing with the behavior of curved in plan steel and steel-concrete composite beam are limited, many further studies are still needed to understand the influences of some parameters on the behavior and carrying capacity of composite beams. The main goal of this study is to develop a three-dimensional finite element analysis of curved steel-concrete composite beam using ABAQUS under the influence of combined flexural and torsion.

Moreover, a parametric study that is not well covered in literature is accomplished to investigate the effects on the composite steel-concrete beams performance of transverse web stiffeners, concrete slab compressive strength, yield stress of steel beam, shear connectors and radius of curvature.

CHAPTER THREE

CHAPTER 3

FE Modeling and Formulation

3.1 Introduction

There are many problems associated with composite steel-concrete members which are extremely difficult or impossible to solve exactly by the conventional analytical methods. Which may be due to the complicity of the composite nature of the materials, difficulties associated with the presentation of the load and boundary conditions or some constitutive stress-strain relations [75]. However, numerical methods such as the finite element and finite difference have been used to achieve approximate solutions for more complex problems in a much more realistic way.

On the other hand, during the last three decades, a rapidly developing in computers aided and finite element techniques provided an economical solution to perform 3D structural analysis. The goal of this chapter is to present nonlinear finite element analysis to investigate the overall behavior and the curved composite steel-concrete beam, general **F**inite **E**lement **P**rogram i.e. ABAQUS/CAE/2017 will be used.

3.2 Linear and Nonlinear Finite Element Analysis

3.2.1 Basic concept

Mathematical formulation of physical problems based on assumptions of neglecting certain quantities may reduce the problem into a linear one. In linear analysis, it is assumed that the displacements are infinitesimally small in which the material is linearly elastic incorporating with assuming unchanged boundary conditions during loading application of the finite element model. Linear solutions are easy and has less computational cost when compared to nonlinear solutions. On the other hand, in nonlinear analyses, the aforementioned assumptions are not valid. However, in some cases assumption of linearity may result in an unrealistic approximation of the response. The type of analysis, linear or nonlinear, depends on the goal of the analysis and errors in the system's response that may be tolerated. In some cases, nonlinear analyses are the only option left for the analyst as well as the designer [76].

3.2.2 Nonlinearities classification

There are two common sources of nonlinearity which are: nonlinear material analysis, nonlinear geometric analysis, and material and geometric nonlinear analysis. In nonlinear material analysis, the nonlinear effect lies in the nonlinear stress-strain relationship, with the displacements and strains infinitesimally small. Therefore, the usual engineering stress and strain measurements can be employed. In geometrically nonlinear analyses, the structure undergoes large rigid-body displacements and rotations. Finally,

combined material and geometrical nonlinear analyses have both nonlinear stress-strain relationship and large displacements and rotations experienced by the structure [77].

3.3 ABAQUS Description

ABAQUS is a suite of powerful engineering simulation programs based on the finite element method. The program is designed for ease of use on complex problems, with comprehensive data checking as well as a wide range of preprocessing and post processing output display options. ABAQUS can solve problems ranging from relatively simple linear analyses to the most challenging nonlinear simulations. Therefore, it will be used to execute the numerical analysis of steel-concrete composite beams behavior under torsional and flexural combined effect.

ABAQUS contains an extensive library of elements that can model virtually any geometry. It has an equally extensive list of material models that can simulate the behavior of most typical engineering materials including metals, rubber, polymers, composites, reinforced concrete, crushable and resilient foams and geotechnical materials such as soils and rock [78]. Problems with multiple components are modeled by associating the geometry defining each component with the appropriate material models and specifying component interactions. In a nonlinear analysis, ABAQUS automatically chooses appropriate load increments and convergence tolerances and continually adjusts them during the analysis to ensure that an accurate solution is obtained efficiently. ABAQUS/Standard will be employed in this thesis, as

it is an ideal solution technique for static event where highly accurate stress solutions are critically important.

3.4 ABAQUS Modeling Procedure

One of the most commonly used finite element analysis package is ABAQUS. Using ABAQUS/CAE, a wide range of input options is able to be input into the software for modelling such as geometry, element types, material properties, solution controls, loads, graphic user interfaces, automatic meshing, boundary conditions, contact and post processing controls. The simulating procedures are divided into four main stages in ABAQUS program as shown in Fig. (3-1), where;

1. Stage 1- Material and geometry modeling.
2. Stage 2- Constraint and boundary conditions.
3. Stage 3- Analysis output.
4. Stage 4- Results of Post-processing.

Stage 1: Includes modeling the section in the part field, defining the section properties, assembling the pieces and meshing each part in the field.

   a) Steel beam, concrete slab, reinforcement rebars and stud shear connector are modeled.

   b) Material field property includes linear and nonlinear stress-strain curves of the material as an input to the components in the part field.

   c) Mesh the components was adopted using various types of elements and assigned the member mesh number.
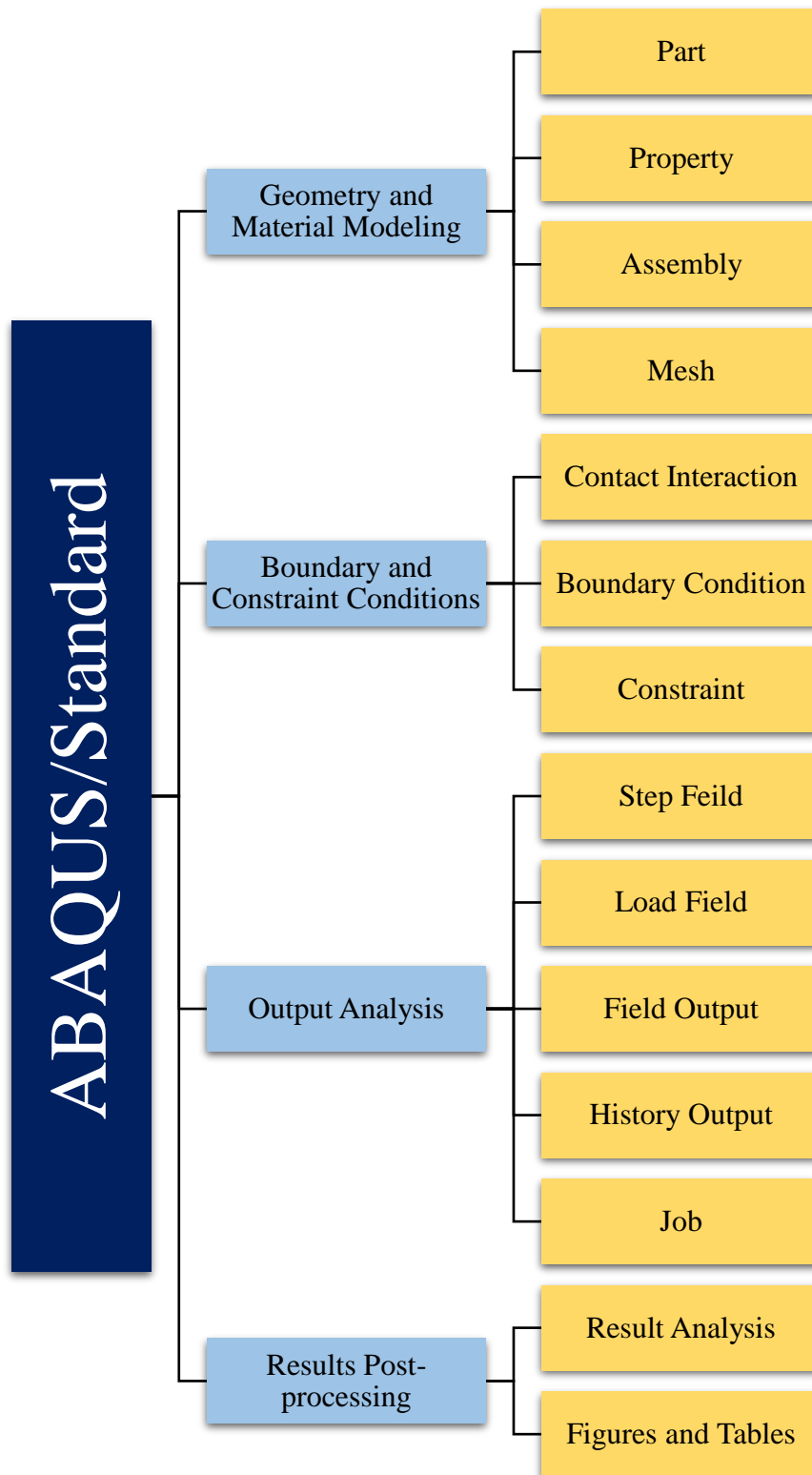
Figure (3-1): ABAQUS Modeling Procedure.

Stage 2: Including surface interaction, constraints and contact condition procedure in the program. In this stage boundary and loading conditions are also specified.

Stage 3: Discusses ABAQUS analysis procedure and outputs results of the composite steel-concrete beam such as the stress distribution, deflections and ultimate strength. Time increment, time period and load case are the input of the step field which is created in this stage during an analysis.

Stage 4: In this stage the results pose into tables and figures for the test comparison and validation.

3.5 Material Modeling

3.5.1 Concrete

Numerous researchers have come up with different methods and formulae in an attempt to make through algorithm to mimic the concrete behavior, both in compression and tension. Concrete itself is a composite structure. It is consisting of an aggregate material that is interlocked together and bound with cement. Therefore, an adequate concrete model needs to be utilized to ensure that the required reliability is obtained.

However, two major options are available in ABAQUS software for modeling the concrete plasticity, including concrete damaged plasticity and concrete smeared crack. Both models are utilized for plain concrete and reinforcement modeling. The prescribed models are applicable to model the concrete inelastic behavior according to the Sorensen and Karlsson [78]. The models are incremental, in which the total strain divided to elastic and plastic

parts. To model the nonlinear problem in ABAQUS, the load is divided into increments at each step. The structure response is solved by iteration to the load increments utilizing Newton-Raphson method [79]. The damage plasticity model (CDP) was used later in this thesis over concrete smeared cracking model because it was better to represent the inelastic behavior of concrete.

3.5.1.1 Concrete damage plasticity (CDP)

Concrete damaged plasticity model in ABAQUS provides a general capability for modeling concrete and other quasibrittle materials in all types of structures (beams, trusses, shells, and solids). The model uses concepts of isotropic damaged elasticity in combination with isotropic tensile and compressive plasticity to represent the inelastic behavior of concrete. In addition, the designed model is applicable for concrete under dynamic and/or monotonic loading under low confining pressure. The model combination of isotropic damage elasticity and non-associated multi-hardening plasticity to depict the irreversible damage that happen at fracturing process. Furthermore, the model allows user control of stiffness recovery effects during cyclic load reversals and can be defined to be sensitive to the rate of straining [78].

A. Strength hypothesis and its parameters

One of the strength hypotheses most often applied to concrete is the Drucker–Prager hypothesis Fig. (3-2). According to it, failure is determined by non-dilatational strain energy and the boundary surface itself in the stress space assumes the shape of an energy and the boundary surface itself in the stress space assumes the shape of a cone. The advantage of the use of this criterion is surface smoothness and thereby no complications in numerical

applications [80]. The CDP model used in the ABAQUS software is a modification of the Drucker–Prager strength hypothesis.
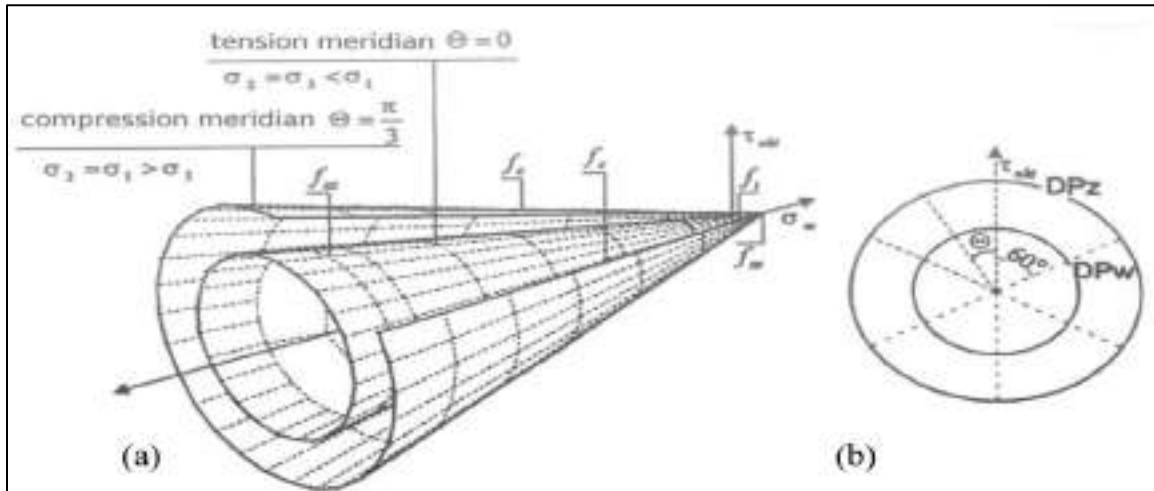
Figure (3-2): Drucker–Prager boundary surface, a) View b) Deviatoric cross section [80].

Following five basic parameters are available in damage plasticity model:

I. **Eccentricity (ϵ):** Plastic potential eccentricity, it is a small positive value which expresses the rate of approach of the plastic potential hyperbola to its asymptote. Along the hydrostatic axis, it is measured length between the hyperbola vertex and hyperbola asymptotes intersection (the hyperbola center). Eccentricity can be determined as a strength ratio of tensile to compressive strength [76]. $\epsilon = 0.1$ is the recommends value in CDP model, whilst the surface in meridional plane be a straight line at a $\epsilon = 0$ as seen in Fig. (3-3) (the strength hypothesis of Drucker-Prager) [78]. In this thesis $\epsilon = 0.1$ value was used.
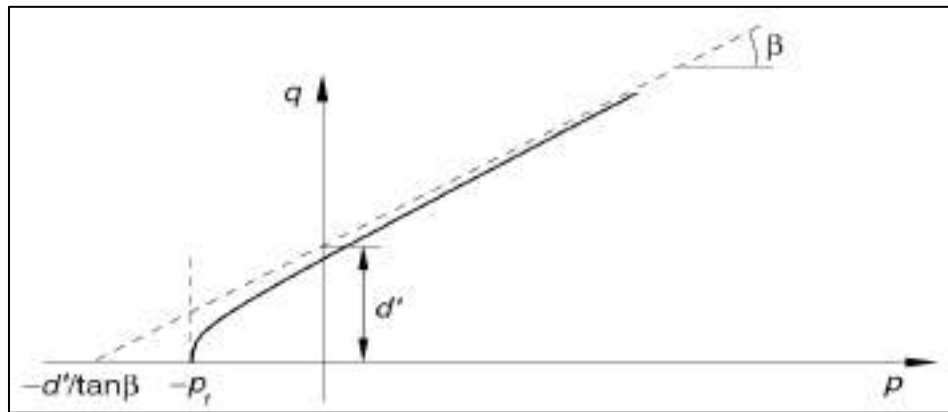
Figure (3-3): Hyperbolic surface of plastic potential in meridional (*p-q*) plane [78]. p_t: initial hydrostatic tension strength, β: friction angle, d: hardening parameter.

II. **Dilation angle (ψ):** Angle of inclination of the failure surface towards the hydrostatic axis, measured in meridian plan. When the value of the parameter is small the material develops a brittle behavior, in opposition, when the value takes high values the behavior is close to a ductile one. According to the experimental results of researchers on four-point loaded beam, it was observed that this parameter took values between 20° and 45°. Meanwhile, other researcher suggested values between 30 and 55 [81]. Defaults values in ABAQUS under compound stress is 36. Dilation angle ψ physically is clarified as an internal friction angle of concrete. Usually, in modeling ψ = 25° to 40° or more depending on concrete compressive strength. In this thesis, the inclination angle ranged between (34 -50) degree.

III. $\frac{\sigma_{b0}}{\sigma_{c0}}$ **:** Another parameter describing the material state is the point in which the concrete failure under biaxial compression. $\frac{\sigma_{b0}}{\sigma_{c0}}$ (f_{b0}/f_{c0}) is the strength ratio in the biaxial to the uniaxial state Fig. (3-4) [78]. The experimental results are the most reliable in this consideration that

reported by Kupler (1969). Under elliptic equation with this approximation, biaxial compression strength f_{cc} is equal to 1.1625 f_c [78]. The defaults values specify by ABAQUS user's manuals $\frac{\sigma_{b0}}{\sigma_{c0}} = 1.16$.
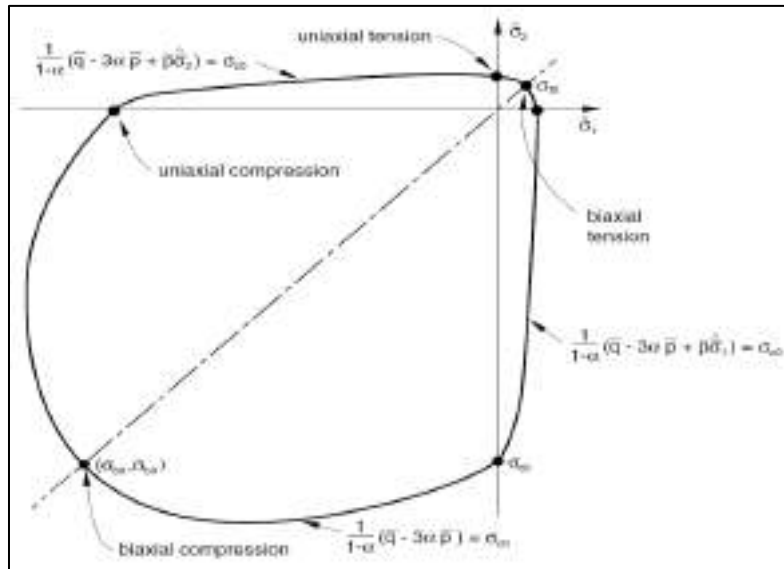
Figure (3-4): Concrete strength under biaxial stress in CDP model [78].

IV. K_c: Its parameter that governing the deviatoric failure surface of the cross section instead of a circle Fig (3-5). Physically, parameter K_c is interpreted as a ratio of the distances between the hydrostatic axis and respectively the compression meridian and the tension meridian in the deviatoric cross section. The default value is always above 0.5, while the failure surface of the cross section becomes a circle at 1.0 value (as hypothesis strength of Drucker–Prager). K_c= 2/3 is the recommended value in CDP model. This shape is similar to the strength criterion (a combination of three mutually tangent ellipses) formulated by William

and Warnke (1975). It is a theoretical-experimental criterion based on triaxial stress test results. [78]. K_c= 2/3 is the value used in this thesis.
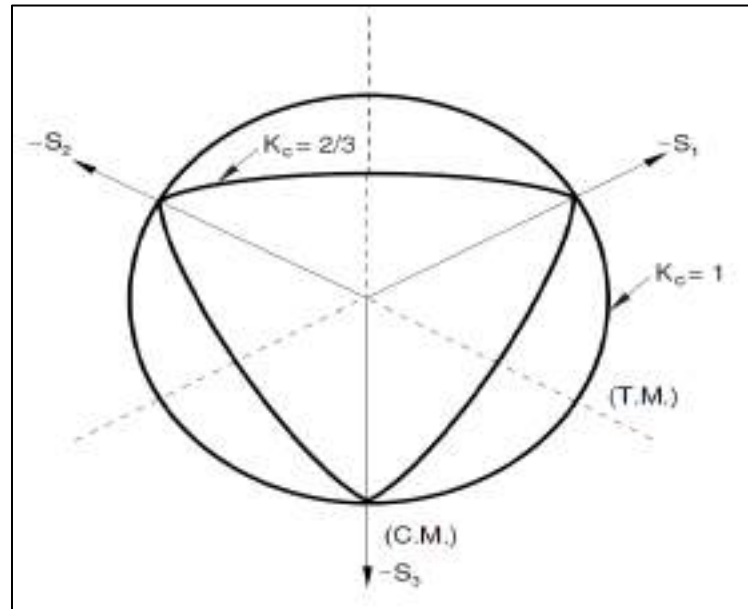
Figure (3-5): Deviatoric cross section of failure surface in CDP model [78].

V. **Viscosity parameter** (ŋ): is also known as the relaxation time. Advanced material models which develop stiffness degradation and strain softening, which lead to convergence issue. One of the most popular technique to overcome this kind of problems is the constitutive equations regularization, in which for small increments of time the tangent stiffness of the material become positive. In general, the value of visco-plastic regularization parameter is the hundred part of the maximum load values. Using small values generally helps the convergence development rate in the softening regime of the model, without results compromising. The viscosity parameter default value is zero in ABAQUS/Standard; thus, no viscoelastic regularization is employed [78]. Therefore ŋ=0.0001 was used in this thesis.

The unquestionable advantages of the CDP model are the fact that it is based on parameters having an explicit physical interpretation. The exact role of the above parameters and the mathematical methods used to describe the development of the boundary surface in the three-dimensional space of stresses are explained in the ABAQUS user's manual. The other parameters describing the performance of concrete are determined for uniaxial stress. In ABAQUS program the default parameters of the model's characterizing its performance under compound stress are shown in Table (3-1).

Table (3-1): Default parameter of CDP model under compound stress.

Parameter	Default Value	Used in Present Study
Eccentricity	0.1	0.1
Dilatation angle	36	34-50
f_{b0}/f_{c0}	1.16	1.16
K_c	0.667	0.667
Viscosity parameter	0	0.0001

B. Stress-strain curve for uniaxial compression

Tensile cracking and compressive crushing are the two available failure mechanisms assumed in CDP model. The control mechanism of yield surface was achieved by two hardening variables associated with the tensile and compression failure mechanisms, respectively. The concrete stress-strain relation can be precisely described according to the uniaxial compression tests carried out on it. Once the graph obtained from laboratory, the variables must transform Fig. (3-6). In CDP the inelastic strains $\tilde{\varepsilon}_c^{in}$ are utilized. To define

them the elastic part must be deduct (according to the undamaged material) from uniaxial compression test for total registered strains:

$$\tilde{\varepsilon}_c^{in} = \varepsilon_c - \varepsilon_{0c}^{el} \tag{3.1}$$

$$\varepsilon_{0c}^{el} = \frac{\sigma_c}{E_0} \tag{3.2}$$
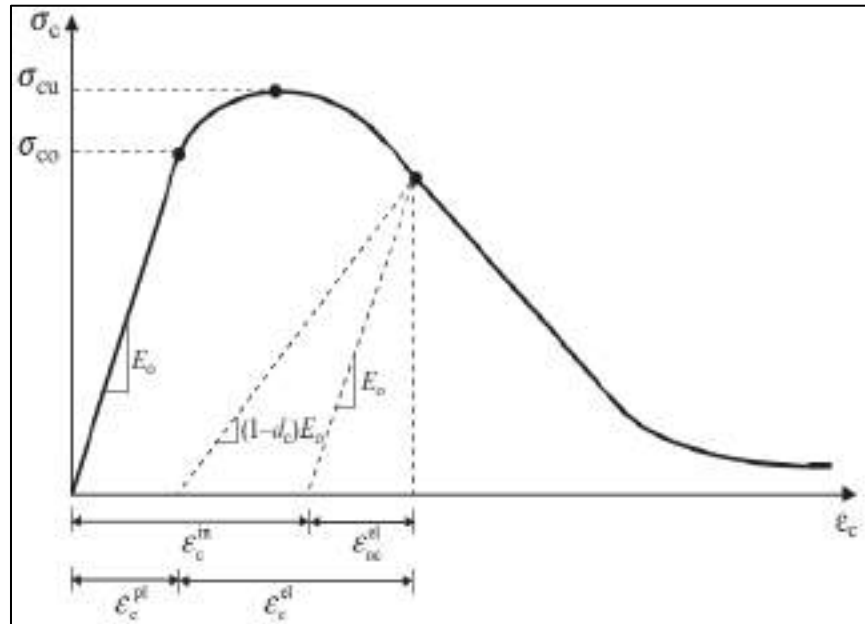
Figure (3-6): Inelastic compressive definition of strain $\tilde{\varepsilon}_c^{in}$ [78].

For elastic properties of the material, which specified that the modulus of elasticity to be secant in the range of $(0 - 0.4\ f_{cm})$ as in Eq. (3.3) and the possion's ratio (v) is of 0.2 according to Eurocode 2 [82], the concrte modulus of elasticity (E_{cm}) was adopted utilizing prescribed relation in Eurocode 2 [82].

$$E_{cm} = 22000 \left[\frac{f_{cm}}{10}\right]^{0.3} \tag{3.3}$$

$$f_{cm} = f_{ck} + 8 \tag{3.4}$$

Where f_{cm} is the mean cylinder concrete compressive strength (MPa) value and f_{ck} is the characteristic cylinder concrete compressive strength at (MPa) 28 days. Compression and tension behavior in the form of plasticity and damage coefficient are required to create the FE model. In uniaxial compression of concrete, the hardening region was determined by using Eurocode 2 [82] as described in following Eq. (3.5).

$$\sigma_c = f_{cm} \left[\frac{k\eta - \eta^2}{1 + (k-2)\eta} \right] \tag{3.5}$$

$$\eta = \frac{\varepsilon_c}{\varepsilon_{c1}} \tag{3.6}$$

The coefficient; Factor

$$k = \frac{1.05 \, E_{cm} |\varepsilon_{c1}|}{f_{cm}} \tag{3.7}$$

Where σ_c is compressive strength of concrete (MPa) that validated for $0 < |\varepsilon_c| < \varepsilon_{cu1}$, ε_c is the compressive strain of concrete, ε_{c1} is the concrete compressive strain at peak stress f_{cm}, and ε_{cu1} is the ultimate compressive strain in the concrete. The characteristic compressive strength of concrete taken as 0.0035 at an ultimatr strain 12-50 MPa as specified in Eurocode 2 [82]. For ε_{c1}, Majewski proposed approximating formula (high accuracy) to calculate ε_{c1} depending on the experimental result from the following expression:

$$\varepsilon_{c1} = 0.0014 \, (2 - e^{-0.024 f_{cm}} - e^{-0.14 f_{cm}}) \tag{3.8}$$

The schematic representation of nonlinear structural analysis for the concrete stress-strain relationship in compression in Eurocode 2 is seen in Fig. (3-7).
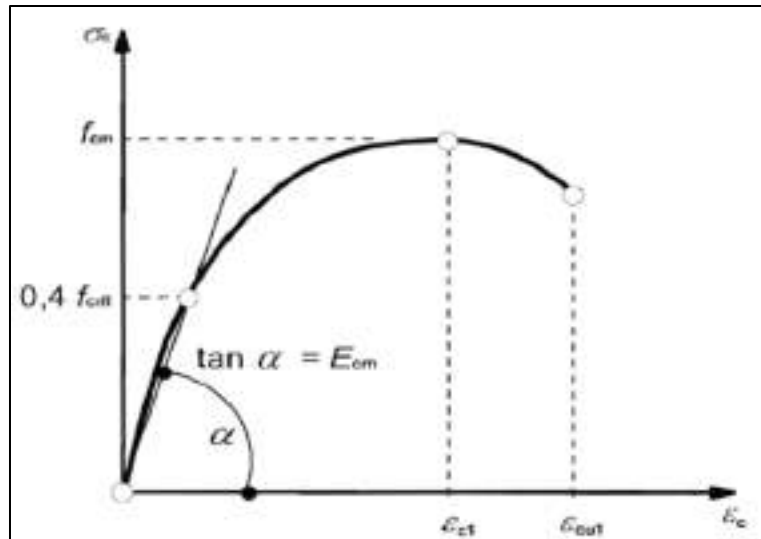
Figure (3-7): Schematic the stress-strain representation of concrete material [82].

C. Tensile strength of concrete

Fig. (3-8) presents the concrete stress-strain curve in uniaxial tension. The shape of the curve shows many similarities to its uniaxial curve in compression. The direction of crack propagation is normal for uniaxial tension to the direction of stress. However, the maximum tensile stress is much less than the maximum compressive stress.

The assumed tensile stresses varying linearly with concrete tensile strain increasing until concrete cracking. This hypothesis is applied to the continuation of the analysis process. However, the tensile stress is calculated in Eurocode 2 [82] as seen in Eq. (3.9):

$$\sigma = f_t \left(\frac{\varepsilon_t}{\varepsilon}\right)^{0.4} \tag{3.9}$$

Here, f_t is the concrete tensile strength, which is expressed by the following relationship as in Eurocode 2 [82]:

$$f_t = 0.3 \, (f_{ck})^{\frac{2}{3}} \tag{3.10}$$
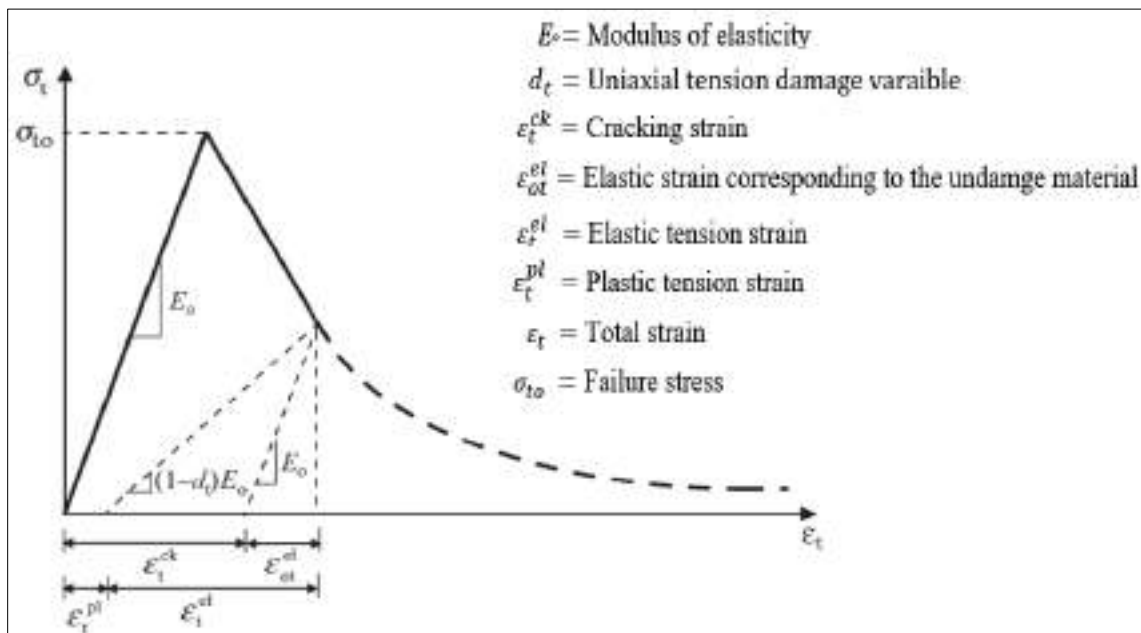
Figure (3-8): Schematic the stress-strain representation of concrete material [78].

D. Cracking of the model

Unlike concrete models based on the smeared crack approach, the concrete damaged plasticity model does not have the notion of cracks developing at the material integration point. However, it is possible to introduce the concept of an effective crack direction with the purpose of obtaining a graphic visualization of the cracking patterns in the concrete structure. Different criteria can be adopted within the framework of scalar-

damage plasticity for the definition of the direction of cracking. ABAQUS assumes that cracking initiates at points where the tensile equivalent plastic strain is greater than zero, and the maximum principal plastic strain is positive. The direction of the vector normal to the crack plane is assumed to be parallel to the direction of the maximum principal plastic strain [78].

E. Post-failure stress-strain relation

The post-failure behavior for direct straining is modeled with tension stiffening, which allows modelers to define the strain-softening behavior for cracked concrete. This behavior also allows for the effects of the reinforcement interaction with concrete to be simulated in a simple manner. Tension stiffening is required in the concrete damaged plasticity model. Modelers can specify it by means of a post-failure stress-strain relation or by applying a fracture energy cracking criterion.

In RC, the specification of post-failure behavior generally means giving the post-failure stress as a function of cracking strain ε_t^{ck}. The cracking strain is defined as the total strain minus the elastic strain corresponding to the undamaged material as illustrated in Fig. (3-8). To avoid potential numerical problems, ABAQUS enforces a lower limit on the post-failure stress equal to 100 of the initial failure stresses ($\sigma_{to}/100$) [78]. Tension-stiffening data are given in terms of the cracking strain, ε_t^{ck}. When unloading data are available, the data are provided to ABAQUS in terms of tensile damage curves, and the software automatically converts the cracking strain values to plastic-strain values [78].

F. Damage compression and tension variable (d_c) and (d_t)

Stiffness degradation for the concrete damaged plasticity for compression (d_c) and tension (d_t) material models are another important parameter in ABAQUS for damage plasticity model to describe concrete stresses evolution when the concrete material reaches to the peak stress. They are assumed to be functions of the plastic strains. If damage is not specified, the model behaves as a plasticity model; consequently, ($\varepsilon_t^{pl} = \varepsilon_t^{ck}, \varepsilon_c^{pl} = \varepsilon_c^{in}$) [79].

The evolution law [$d_c - \varepsilon_c^{in}$] was identified to consider the compression damage of concrete after its reaches to concrete peak stress, where d_c and ε_c^{in} are the compressive damage parameter and compressive inelastic strain, respectively. Similarly, the evolution law [$d_t - \varepsilon_t^{in}$] was specified to capture the tensile damage of concrete after reaches to the concrete tensile strength, in which d_t and ε_t^{in} are the tensile damage parameter and cracking strain of concrete, respectively. ε_t^{in} is determined as the total strain minus the elastic strain according to the undamaged material.

Numerous methods were available to achieve the damage parameter. Nguyen and Kim [83] present the following relations for defining prescribed parameters, $d_c = 1 - \dfrac{\sigma_c}{f_{cm}}$ and $d_t = 1 - \dfrac{\sigma_t}{f_{ctm}}$ for compression and tension, respectively.

3.5.2 Structural Steel Section

In uniaxial tension Fig. (3-9), the experimental test shows that structural steel behavior appears strain hardening rather than elastic-perfect plastic response [84]. Using strain hardening in the stress-strain curve in the nonlinear analyses have been shown well demeanor [85,86]. In the FEM, the behavior of reinforcement bar, the steel beam, transverse stiffeners and stud shear connector are similar using a bilinear stress-strain curve, representing elastic-plastic material with strain hardening.
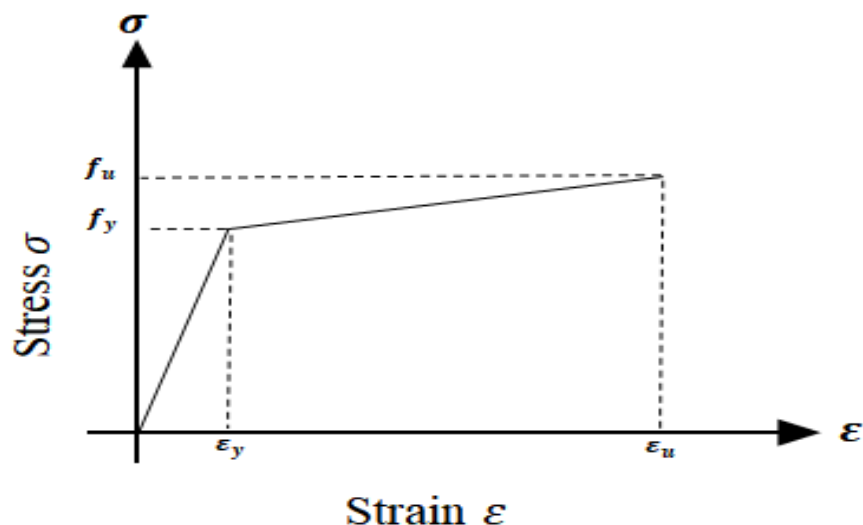
Figure (3-9): Uniaxial stress-strain relationship of the steel material.

Concerning this demand, ABAQUS requires input data of Young modulus (E_s), Poisson's ratio (v) to represent the elastic behaviour, yield stress (f_y), the ultimate stress of steel (f_u) and the inelastic strains for the purpose of define the plasticity behavior. Assuming that the tension behavior is identical and typical for the corresponding compression behavior.

3.6 Solution Technique

The solution is unique in linear analysis as for non-linear problems, may not be the best solution. Therefore, the accomplished solution may not necessarily be the solution sought [87]. For nonlinear analyses problems, various techniques are presented. Briefly, three methods will be described, namely:

- Incremental or stepwise procedure (Euler-Cauchy method).

- Iterative procedure (Newton-Raphson method).

- Combined methods.

The combined solution procedure is adopted in this thesis instead of these methods. The prescribed solution procedure combined of full or Newton-Raphson iterations method coupled with incremental load [87].

3.6.1 The Riks Method

The problems of nonlinear geometry sometimes involve buckling collapse demeanor or unstable post-buckling response where a negative stiffness matrix has been developed in the load-deflection behavior, in which some strain energy must be release to stay in equilibrium [85]. For the static analysis procedures, an automated version adaptive in ABAQUS/Standard software. Modified Riks method was adopted during the unstable response of the structure Fig. (3-10) in static equilibrium situation. Otherwise the method is employed to solve the status where the loading is proportional [87].
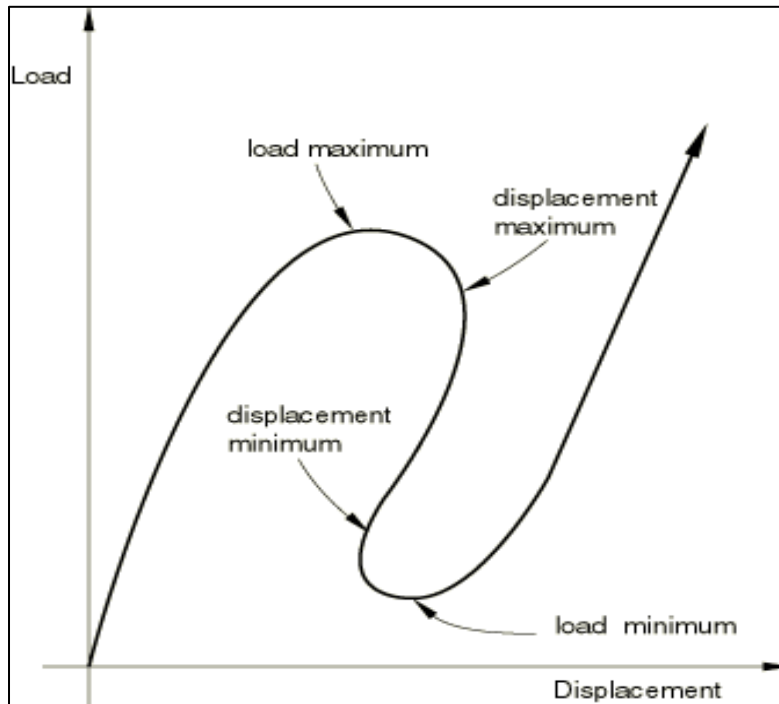
Figure (3-10): Typical unstable static response [87].

ABAQUS employed the standard Newton-Raphson method and the modified Riks method to solve the load versus vertical deflection nonlinear trace and nonlinear problems. For nonlinear equation, the standard Newton-Raphson method used iteratively and incrementally possesses the tangent stiffness matrix. This method solved simultaneously for displacement approached using the load as an unknown extension in the unloading response for structural buckling behavior. In the load-displacement approached, the arc length method (l) is adopted to accomplished this approached in static equilibrium method Fig. (3-11). Moreover, if the convergence issue fails in the finite element analysis, the initial increments must be modified, Finally, the load computed automatically after every increments. The final outcome will be either maximum displacement value or maximum load value [87].
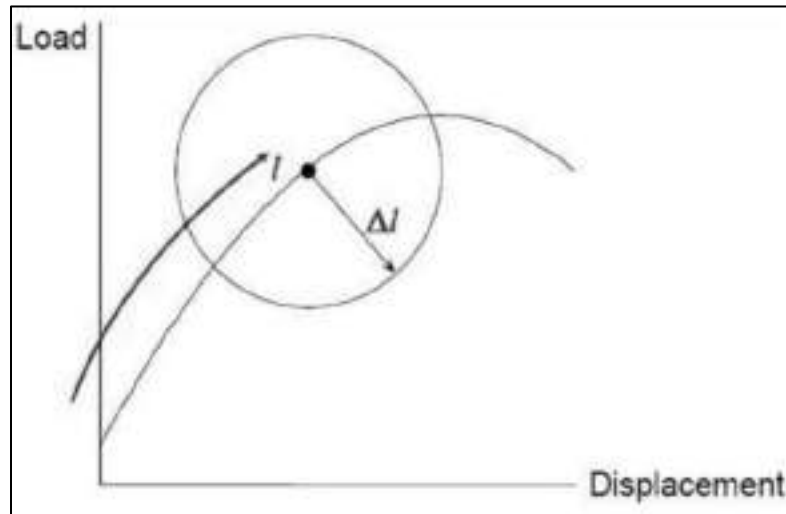
Figure (3-11): Arc length and arc length increment [87].

3.7 ABAQUS Finite Element Model

3.7.1 Element Mesh and Type

A. Solid element description

3-D solid elements are volume elements which are composed of a single homogeneous material or can included several layers of different material, for large deformations, plasticity and contact behavior during linear and nonlinear analyses.

For the concrete slab, structural steel beam, shear connector and steel stiffeners, a 3-D eight node element (C3D8R) as shown in Fig. (3-12) with linear approximation of displacement, reduced integration with hourglass control, eight nodes and three translational degrees of freedom was used. Stress at various points though out the thickness of the element can be provided at each integration nodes. The first-order interpolation elements such

as hexahedral exhibit potential stiff behavior with a slow convergence rate but prevents potentially mesh locking when a reduced integration analysis procedure is used, whereas second-order elements provide higher accuracy [88]. However, first-order elements were used to accurate the model for contact surfaces and prevent compact contact condition.
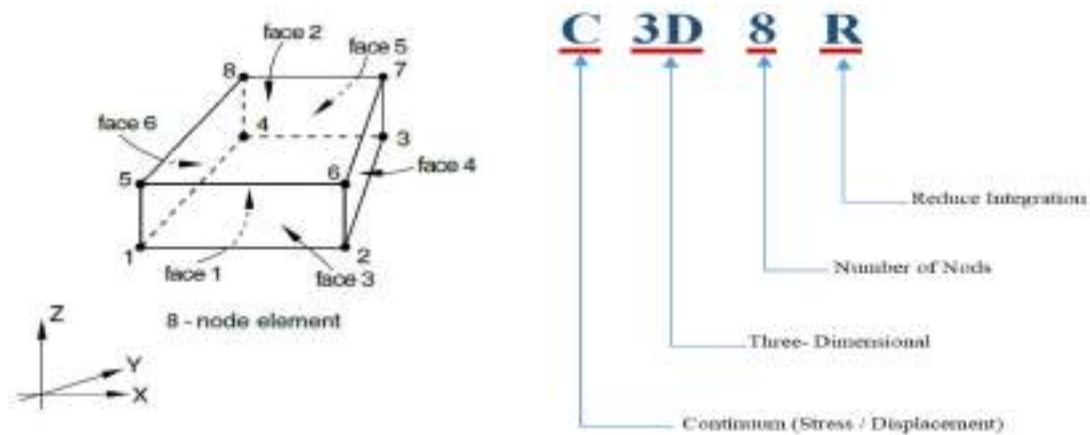
Figure (3-12): C3D8R element description [88].

B. Truss element description

Truss elements are used in 2-D and 3-D to model slender, line-like structures that support loading only along the axis or the centerline of the element. No moment or forces perpendicular to the centerline are supported. A 2-node straight truss element which uses linear interpolation for position and displacement and has a constant stress is available in ABAQUS/Standard. In addition, a 3-diamention curved truss element which uses quadratic interpolation for position and displacement so that the strain varies linearly along the element is available in ABAQUS/Standard [88] too. For the reinforcing steel, 3-D two-node truss element (TSD2) with linear

approximation of displacement, two nodes and three translational degrees of freedom per node was used as shown in Fig. (3-13).

Figs. (3-14) and (3-15) shows mesh sizes, the mesh and the type of elements used presented in the finite element model for curved composite steel-concrete beams.
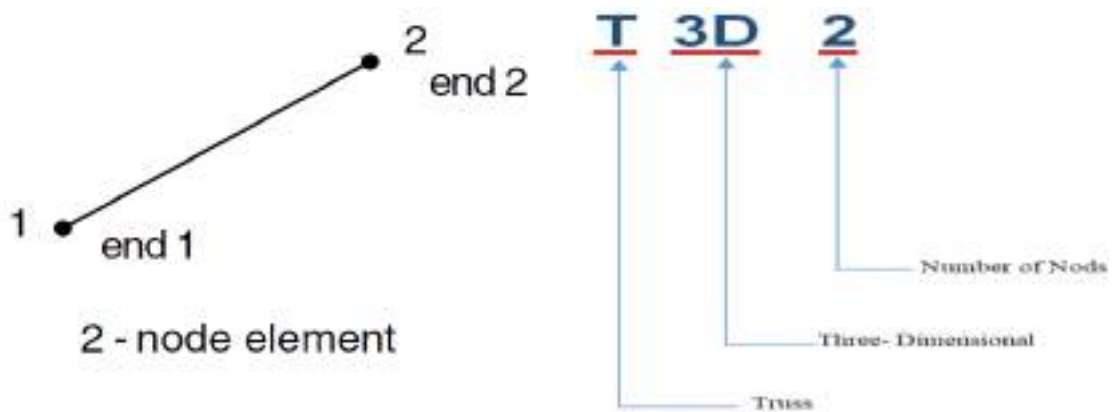
Figure (3-13): T3D2 element description [88].
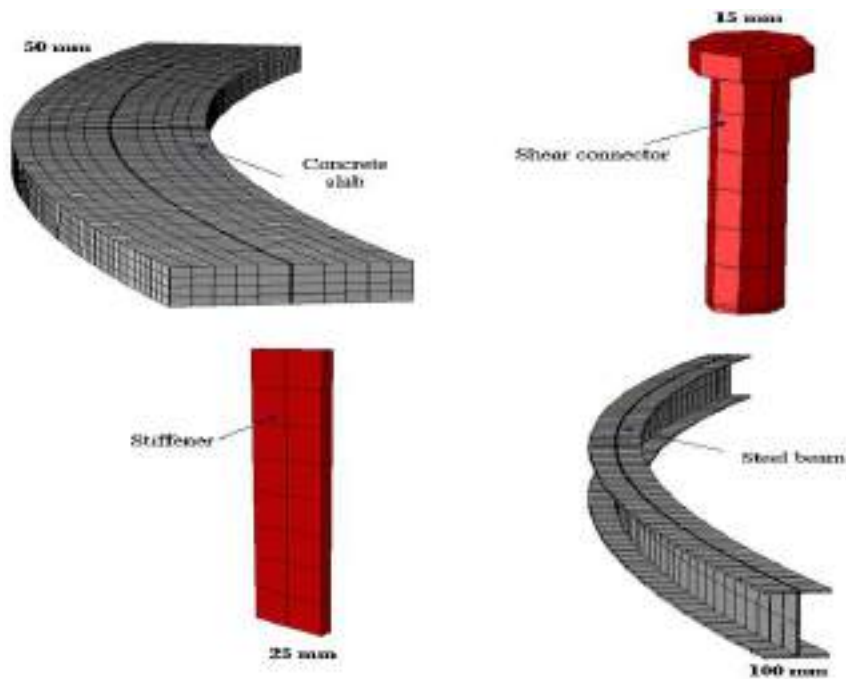
Figure (3-14): Mesh sizes for each part of the curved composite beam.
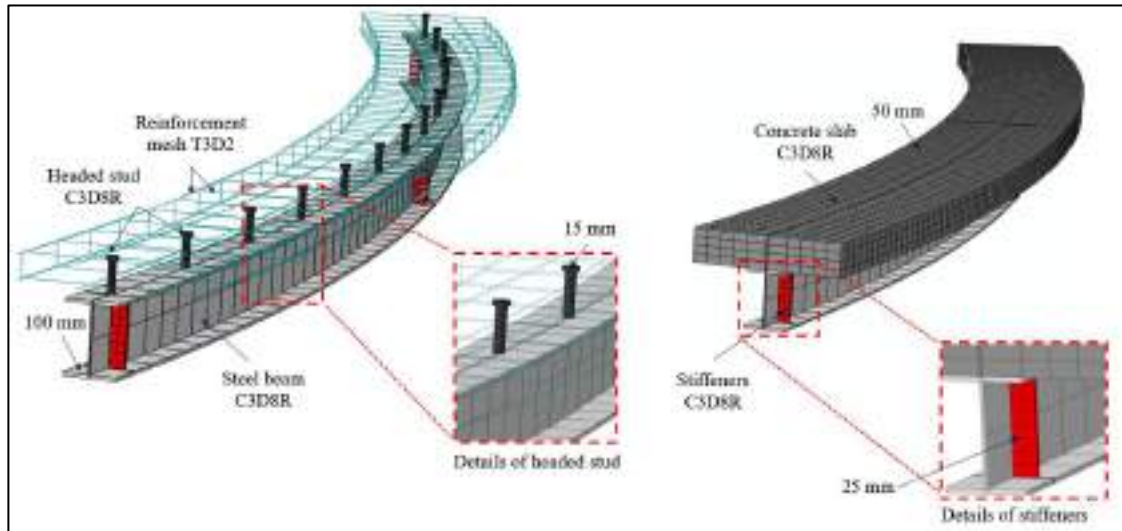
Figure (3-15): The mesh of the beam model in ABAQUS program.

3.7.2 Contact Interaction and Boundary Conditions

Once all parts are assembled at appropriate locations, a proper constraint used to describe the interaction between components as presented in Fig. (3-16). In FEM, the Contact interactions is an important aspect. The fact is that the physical processes are important aspects and must be taken into account in boundary conditions and surface interactions in numerical simulation. An inappropriate definition may have an undesirable effect on the simulation overhead, especially in the current thesis, due to the presence of several components in the simulation such as the steel beam, concrete slab, shear connector and rebars. ABAQUS/Standard provides more than one approach for contact definition compressing general contact, contact pairs, and contact elements [89].

2D and 3D structures may be either under finite or small sliding for the example the interface contact surfaces between the steel beam and concrete slab. Contact interactions can also be some types of kinematic constraints such surface-based tie and surface-based coupling constraints. Even boundary conditions are also a type of kinematic constraint in stress analysis because they define the support of the structure or given fixed displacements at nodal points.
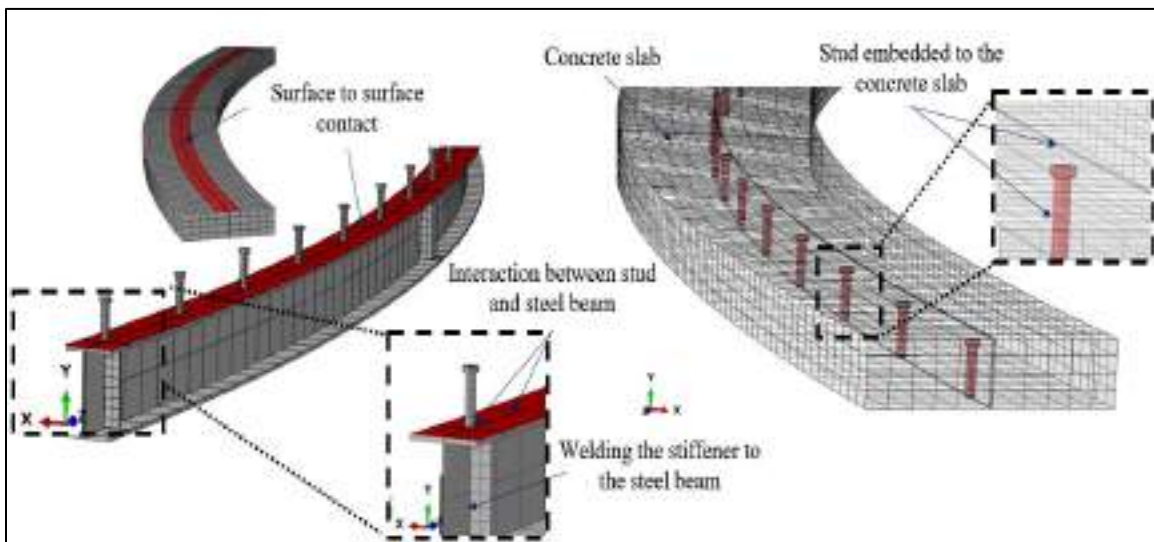
Figure (3-16): Interaction and the constraint condition in the model.

3.7.2.1 Defining contact pairs and properties of contact

For contact pair definition, the interacted surfaces pairs must be indicated or which surfaces must interact with themselves. All regions in the contact surfaces must be included far enough through an analysis. The nodes on the two contact surfaces by contact pair are not allowed to involve, but the master and slaves' surfaces must be choosing [89].

In a contact simulation, the contact interaction between bodies is defined by assigning property of contact to a contact interaction. Hard contact model utilized by ABAQUS is the default pressure-overclosure contact relationship, which has been adopted in this work.

3.7.2.2 Contact Type for the FE Modeling

A. Steel beam and concrete slab interface

Surface-based contact available in ABAQUS, utilized for interface contact between the concrete slab and the steel beam surfaces. The upper surface of the steel beam flange connected to the concrete slab bottom surface at the specific position. The concrete surface has been chosen to be the master surface whilst the upper steel beam flange to be a slave surface. Small-sliding formulation was used, in which the load was transfers to the master nodes according to the slave node of current position for geometric nonlinear analyses, the prescribed formulation presumes an arbitrarily large rotations but the slave node and the master surface will interact with the same local area throughout the analysis. This type can be used instead of Tie constraint to improve the model robustness. In the normal direction a hard contact relationship was used to reduce the slave node penetration and preventing the tensile stress transferring through the interface.

B. Reinforcing steel and stud shear connector contact interface to the concrete slab

Contrast to others constraint technique, the interface contact condition between the reinforcing steel bars and the concrete slab was represented less

important. No slippage was assumed between the steel reinforcement and the concrete slab during an analysis. Thus, the embedded element was utilized to constrain the reinforcement bar elements into the concrete slab elements. Whereby, the degrees of freedom at each node of the reinforcing bars element was eliminated into the concrete slab host element, thereby the node was considered as an embedded node [89].

Furthermore, similar technique is employed to represent the shear stud connector within the concrete slab by considering the top surfaces of each shear connector to be embedded within the concrete.

C. Shear stud and web stiffeners contact interface with steel beam

Surface-based tie contact interface was used to simulate the interaction between the shear studs to the top flange of the steel beam; transverse stiffeners to the web of the steel beam. This type of interaction is employed to eliminate the vertical separation between the two contact surfaces. It constrained each of the nodes on the shear stud bottom surface and the transverse stiffeners to have the same translational and rotational motions as well as all other active degrees of freedom as the point on the steel beam surface to which it was closest.

In surface-based tie constrain, two approaches have been used. There are node to surface approach or surface to surface approach. Surface to surface approached criteria have been utilized in this thesis. Over a finite area, this approach enforces to constraints in an average concept, rather than in the conventional node to surface approach which was at discrete points [81].

3.7.2.3 Boundary and loading conditions

Since the experimental models were designed as simply supported at both ends and the concrete slab had been restrained against twisting, thus the boundary conditions are to be assigned to each support as prescribed.

To simulate the analytical model as the test specimen conducted by Tan and Uy [21], one end of the bottom steel flange of the FE model was prevented from translationally displacement in the x, y and z direction and the other end support was restrained in the x and y directions Fig. (3-17).
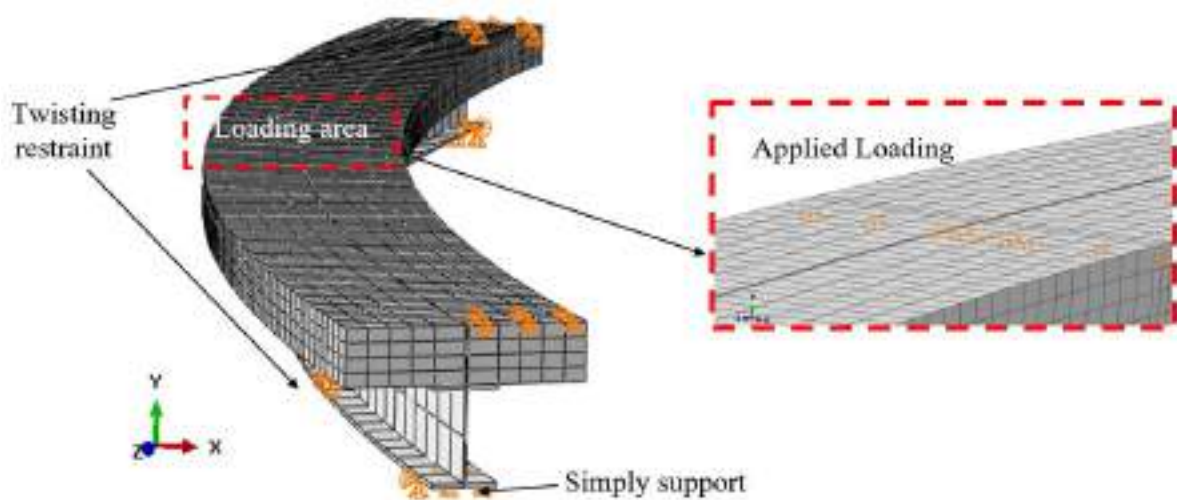
Figure (3-17): Boundary and applied loading conditions for the finite element modeling.

To simulate the twisting boundary conditions as experimental work, translational D.O.F in x and y directions are restrained at both ends of the concrete slab. Loading was applied as a displacement control, where the displacement applied as a downward pressure forces to avoid the high stress concentration on the concrete slab. Prescribed boundary conditions are summarized in Fig. (3-17).

CHAPTER FOUR

CHAPTER 4

Numerical Application and Results

4.1 Introduction

In this chapter, a comparison between the numerical with these of experimental for the curved steel-concrete composite beam is provided by the previous studies carried out in terms of load-deflection curves and crack patterns using ABAQUS/Standard 2017. Furthermore, this chapter will discuss the analysis of some important variables that affecting on behavior of such beams; the study is conducts to determine yield and ultimate loads, and the deflection at ultimate load.

4.2 Details of Study

The study developed in this thesis is adopted to conduct the curved composite beam structural behavior depending on the available experimental results tested by Tan and Uy [21].

Three of them were full shear connectors and identified as CCBF. The remaining other beams were partial shear connector with 50% which identified CCBP. The load was applied at mid span. The other detailed of the specimens are presented in Fig. (4-1).
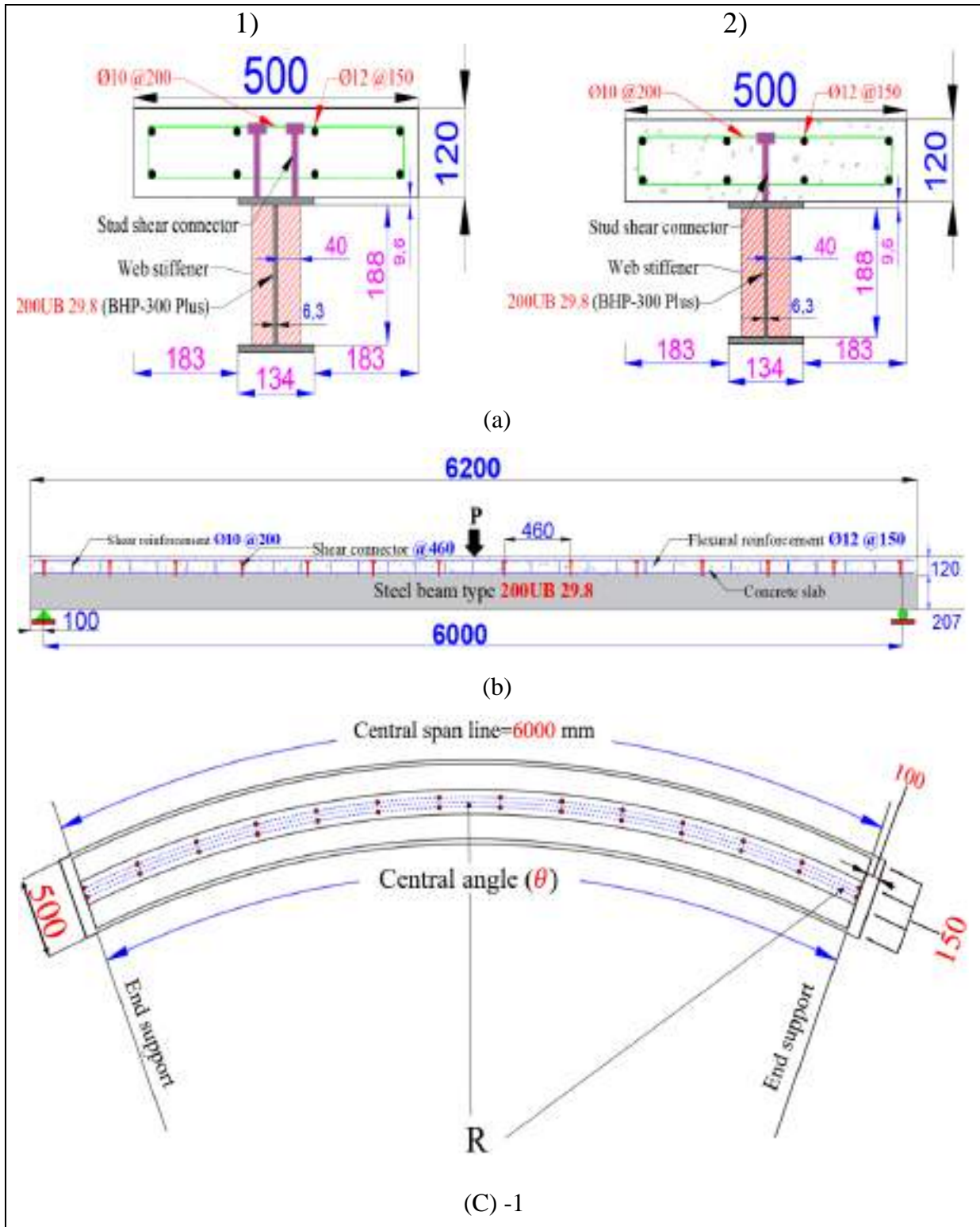
Figure (4-1): Geometry and dimensions of the curved composite steel-concrete beam (unit: mm): (a) Cross section for: 1-CCBF; 2-CCBP, b) Side view, (c) Plan for 1- CCBF; 2- CCBP.
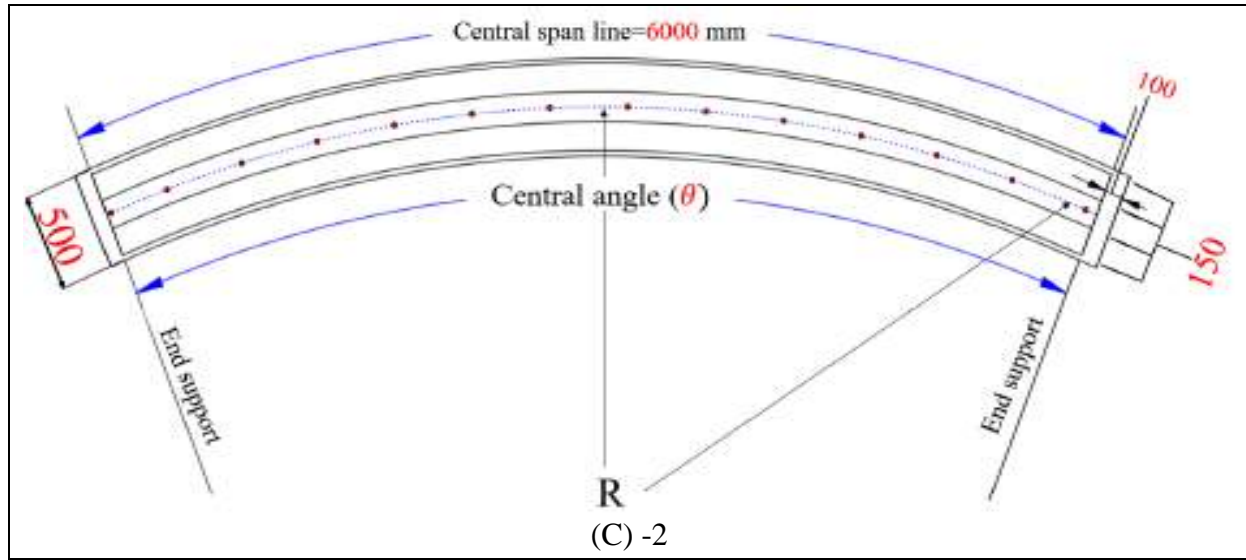
Figure (4-1): Continued.

The overall length of beam was 6200 mm and simply supported at 6000 mm. The specimens were constructed of a concrete slab with a 500 mm width (b_c) and 120 mm depth (t) connected to a rolled steel beam Type 200UB29.8 (Universal beam). The section was of 207 mm (beam depth h_s) × 6.3 mm (web thickness t_w) × 134 mm (flange width b_f) × 9.6 mm (flange thickness t_f). Reinforcements of diameters 10 mm and 12 mm were placed on the concrete slab for torsional and longitudinal reinforcement; respectively. Tables (4-1) to (4-3) demonstrates properties of concrete and reinforced steel for validated model.

Table (4-1): Model's details for the curved composite beams with full interaction.

Material	Beam identification	CCBF-1	CCBF-2	CCBF-3
	Span length (mm)		6000	
	Span/Radius	0.291	0.303	0.424
	Radius of curvature (mm)	20.62	19.8	14.15

Table (4-1): Continued, Model's details for the curved composite beams with full interaction.

Material	Beam identification	CCBF-1	CCBF-2	CCBF-3
Concrete slab	Thickness (mm)	120	120	120
	Width (mm)	500	500	500
	Compressive strength (MPa)	42.3	41.5	38.3
Steel beam	Type		200UB29.8	
	Total depth (mm)		207	
Steel flange	Thickness (mm)		9.6	
	Yield stress (MPa)		347	
	Ultimate stress (MPa)		495	
Steel web	Thickness (mm)		6.3	
	Yield stress (MPa)		374	
	Ultimate stress (MPa)		512	

Table (4-2): Model's details for the curve composite beams with partial interaction.

Material	Beam identification	CCBP-1	CCBP-2	CCBP-3
	Span length (mm)		6000	
	Span/Radius	0.275	0.294	0.455
Concrete slab	Thickness (mm)	120	120	120
	Width (mm)	500	500	500
	Compressive strength (MPa)	37.7	39.1	40.4
Steel beam	Type		200UB29.8	
	Total depth (mm)		207	
Steel flange	Thickness (mm)		9.6	
	Yield stress (MPa)		347	
	Ultimate stress (MPa)		495	
Steel web	Thickness (mm)		6.3	
	Web depth (mm)		188	
	Yield stress (MPa)		374	
	Ultimate stress (MPa)		512	

Table (4-3): Model's details for the curve composite beams.

Material	Beam identification	CCBF-1, CCBF-2, CCBF-3	CCBP-1, CCBP-2, CCBP-3
	Span length (mm)	6000	
Longitudinal steel reinforcement	Type (Top)	Ø12	
	Type (Bottom)	Ø12	
	Spacing (mm)	150	
	Yield stress (MPa)	586	
	Ultimate Stress (MPa)	683	
Stirrups steel	Type	Ø10	
Stirrups steel	Spacing (mm)	200	
	Yield steel (MPa)	399	
Stirrups steel	Ultimate stress (MPa)	498	
Shear connection	Type (mm)	Headed stud	Headed stud
	Diameter (mm) x length (mm)	$19 \, x \, 100$	$19 \, x \, 100$
	Number of rows	2	1
	Spacing (mm)	460	460
	Degree of shear connector (%)	100	50
	Yield stress (MPa)	395	395
	Ultimate stress (MPa)	499	499

4.3 Discretization of Finite Element

Three-dimensional finite element models using ABAQUS software are developed to simulate the curved composite steel-concrete beam.

An important step in the finite element modeling is mesh density selection. The convergence results are obtained by dividing the structure into

a sufficient number of elements. This is properly adopted when the mesh density has negligible influence on the results.

The same properties of the curved composite beam material were simulated with element size increasing. The load capacity for the same vertical displacement is the response parameters used for this comparison. 2980, 4860 and 6932 elements are used to carried out the accuracy of the convergence results. Table (4-4) shows the conclusions of comparison results and the two parameters response.

Table (4-4) Convergence of results

No.	Number of elements	solution time (minute)	Mid-span deflection (mm)	Ultimate load
1	2980	13	91	90
2	4860	26	119.1	115.12
3	6932	39	122.02	115.51

From this table, it can be observed that the model began to converge with 6932 elements. Therefore, this number of elements was adopted for the mesh density, which developed a good modification between the numerical solution stability and element size.

4.4 Finite Element Model Validation

The experimental and numerical comparison values produced by finite element analysis in this study for specimens (CCBF-1, CCBF-2, CCBF-3, CCBP-1, CCBP-2 and CCBP-3) in terms of load-deflection curve, ultimate load, flexural and torsional cracks are listed in Tables (4-5) and (4-6), and Figures (4-2) to (4-7).

Table (4-5): The ultimate load of the verification results.

Beams Symbol	Load Carrying Capacity P_u (kN)		$\dfrac{P_{uEXP} - P_{uABAQUS}}{P_{uEXP}} * 100\%$	$\dfrac{P_{uEXP}}{P_{uABAQUS}}$
	$(P_u)_{EXP}$	$(P_u)_{ABAQUS}$		
CCPF-1	104	107.46	-3.3%	0.97
CCBF-2	108	107.54	0.43%	1.00
CCBF-3	72	80.98	-12.5%	0.89
CCBP-1	122	122.02	-0.02%	0.99
CCBP-2	114	126.64	-11%	0.90
CCBP-3	78	83.71	-7.3%	0.93
Mean				0.947
Standard Deviation				0.0468

Table (4-6): The deflection at ultimate load of the verification results.

Beams Symbol	Deflection at ultimate load Δ_u (mm)		$\dfrac{\Delta_{uEXP} - \Delta_{uABAQUS}}{\Delta_{uEXP}} * 100\%$	$\dfrac{\Delta_{uEXP}}{\Delta_{uABAQUS}}$
	$(\Delta_u)_{EXP}$	$(\Delta_u)_{ABAQUS}$		
CCPF-1	86	102.37	-19 %	0.84
CCBF-2	95	68.46	27.9%	1.39
CCBF-3	45	46.35	-3 %	0.97
CCBP-1	115	115.51	-0.4 %	0.99
CCBP-2	68	80.69	-18.7 %	0.84
CCBP-3	47	51.13	-8.8 %	0.92
Mean				0.992
Standard Deviation				0.2051

The finite element in terms of load versus vertical deflection gives close relationships to experimental results, as can be shown in Fig. (4-2). Also, the

stiffness, strength and ductility are almost identified in both experimental and FE during each loading stages.

Tables (4-5) and (4-6) illustrate the comparison between the experimental results and the numerical ones for ultimate load and deflection, respectively.
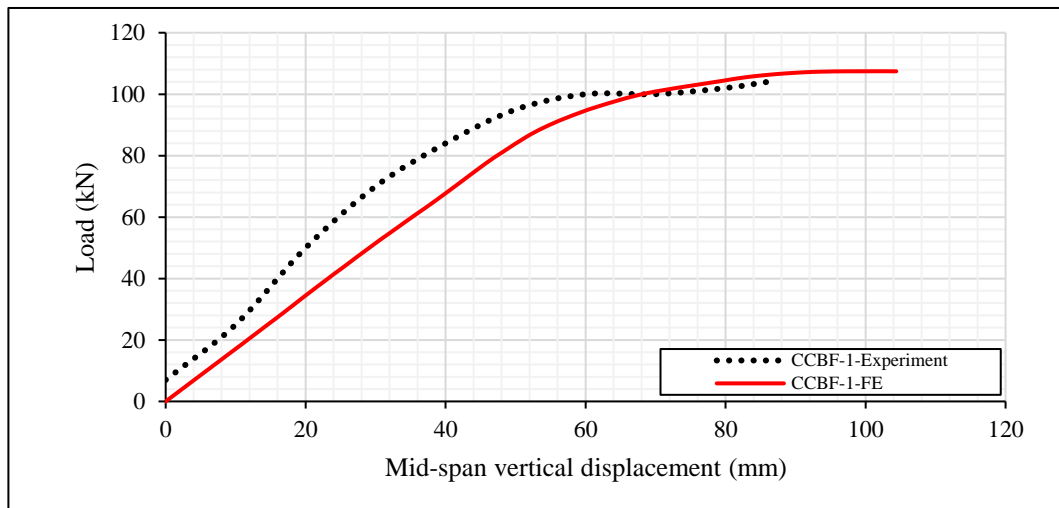
a) Specimen CCBF-1
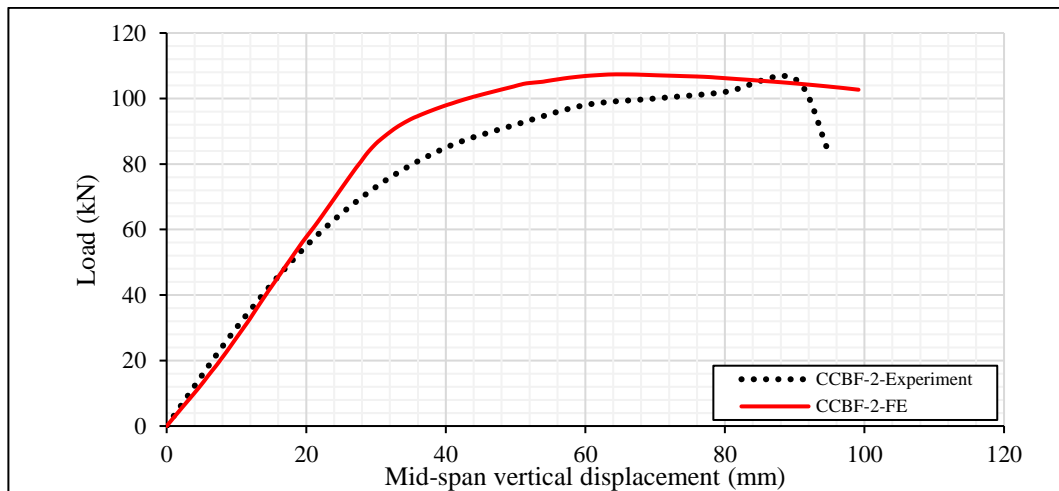
b) Specimen CCBF-2

Figure (4-2): Load-displacement curve between theoretical and experimental curved composite beams.
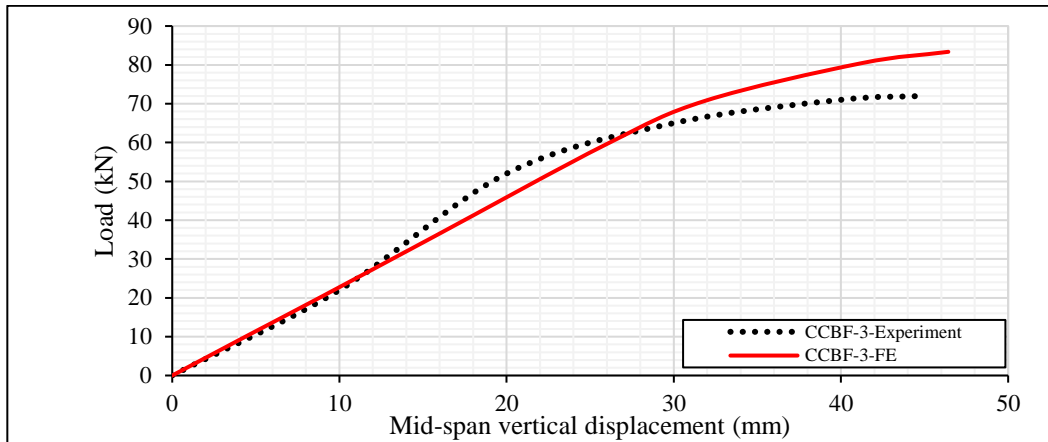
c) Specimen CCBF-3
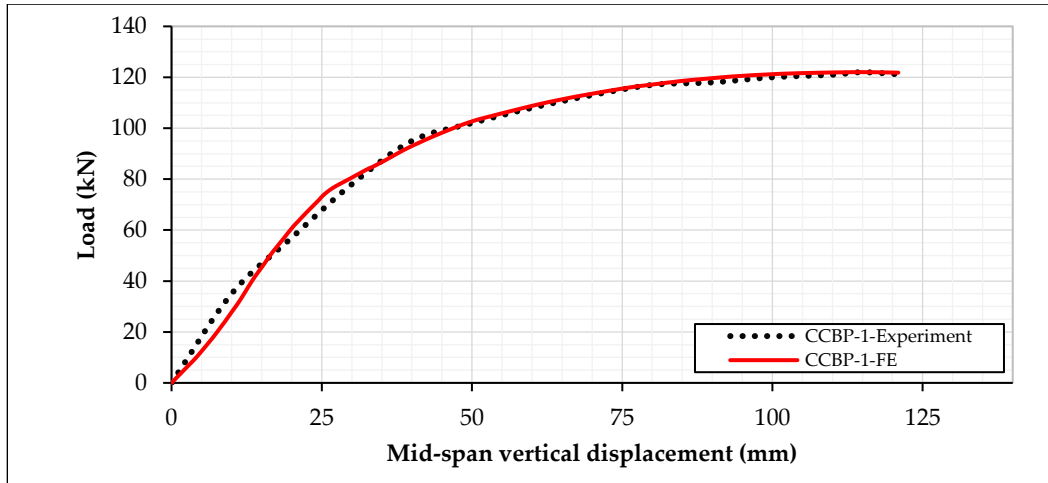
d) Specimen CCBP-1
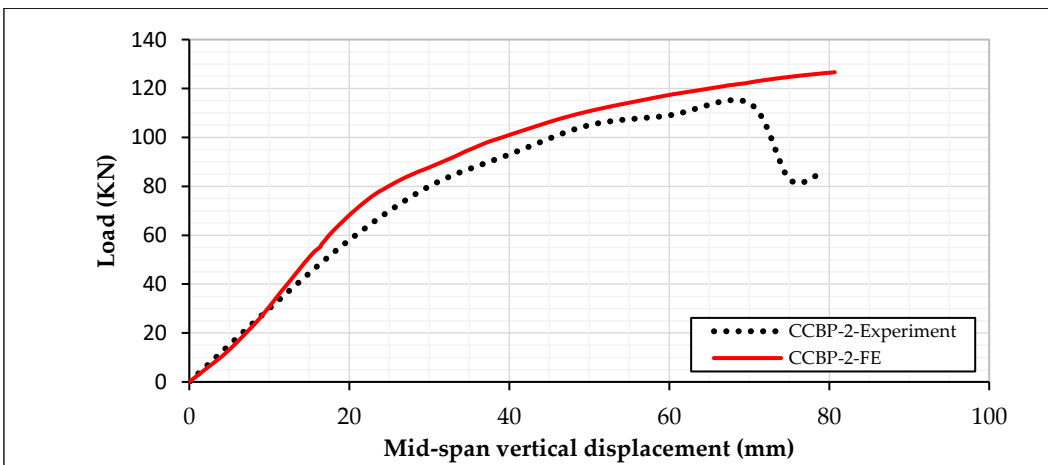
e) Specimen CCBP-2

Figure (4-2): Continued.
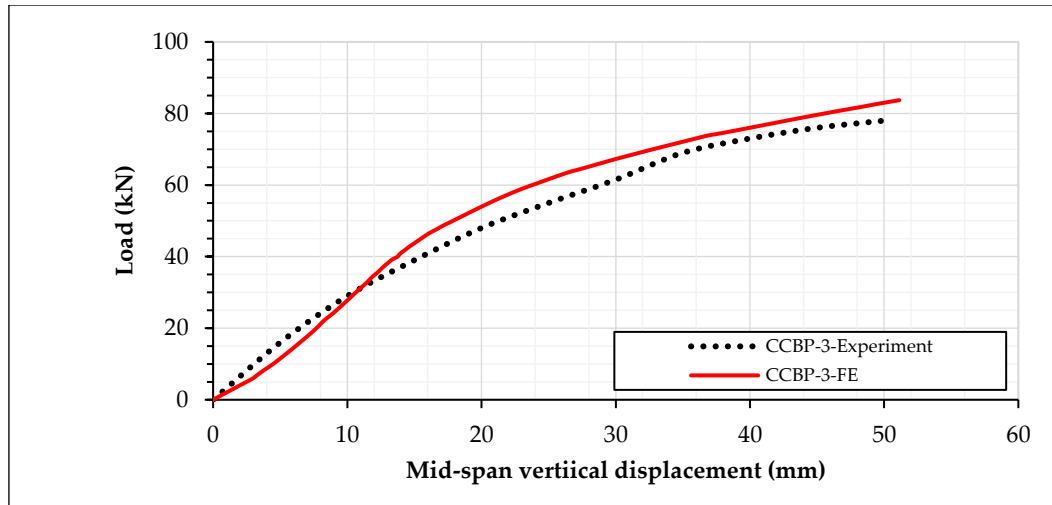
f) Specimen CCBP-3

Figure (4-2): Continued.

In the ratio of experimental to predicted values of ultimate load are 0.89 to 1.00 with an average value and standard deviation of 0.947 and 0.0468 respectively. Therefore, the suggested numerical models are consistent and can be utilized with confidence.

For the validated model CCBF-1, a few flexural cracks were developed firstly near to the mid-span of the modeled beam. At applied load increased to 23.4 kN, the diagonal torsional concrete cracks were developed as seen in Fig. (4-3) that was closed to experimental results tested by Tan and Uy [21] which was 20 kN. Moreover, the validated model CCBP-2 with partial interaction, shows the same behavior to the experimental specimens which was closer to the behavior of CCBF-1 but with more torsional and flexural cracks as shown in Fig. (4-4). The numerical and experimental results comparison appear that the cracks extended more than the areas in the experimental results.
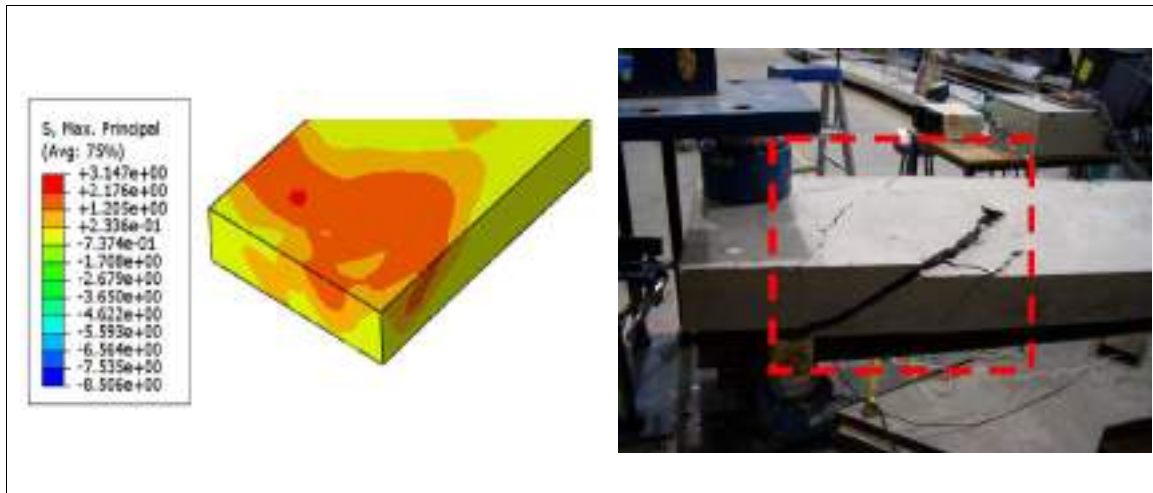
Figure (4-3): Diagonal torsional cracks for experimental and numerical of CCBF-1.
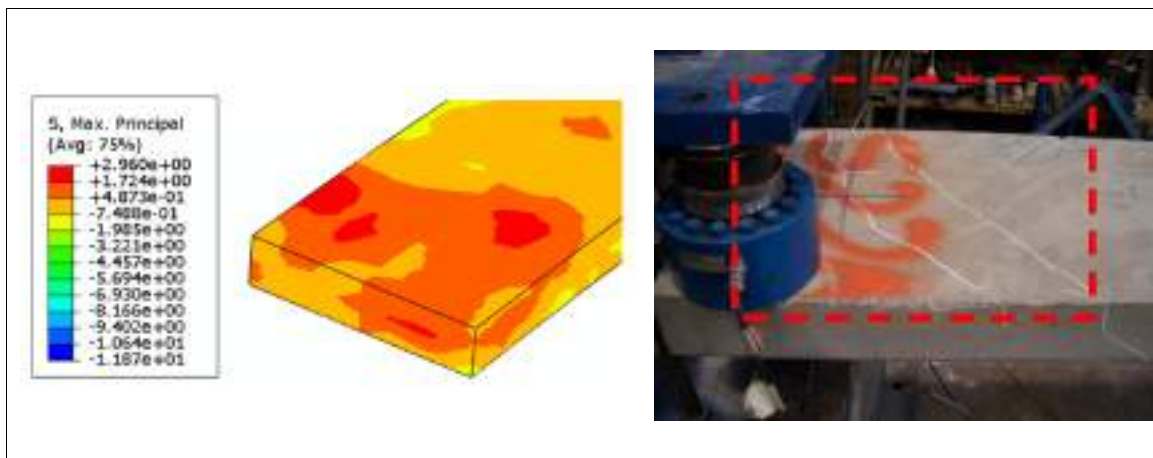
Figure (4-4): Experimental and numerical comparison of diagonal torsional cracks for CCBP-2.

For model CCBF-2, the diagonal torsional concrete cracks appear at both supports at loading increase incorporating with flexural cracks at the beam mid span as achieved for experimental results for specimen CCBF-2 tested by Tan and Uy [21]. Mid-span twisting comparison between experimental and numerical results for CCBF-2 show a good agreement as seen in Fig. (4-5).
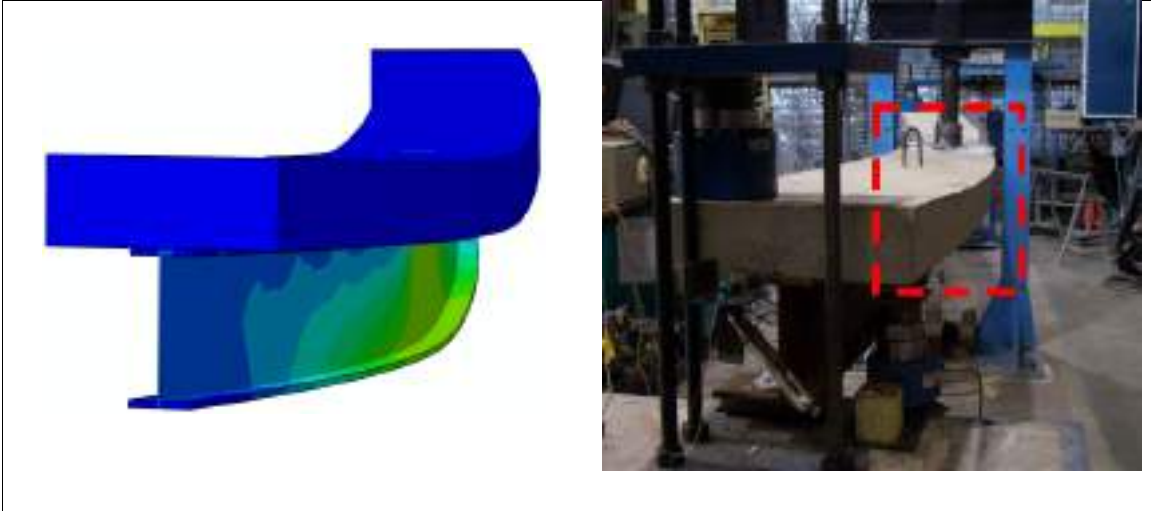
Figure (4-5): Beam twisting comparison between experimental and numerical results for CCBF-2.

For CCBF-3, a few flexural cracks were observed in this model, while the diagonal torsional cracks were observed as well as the applied loading increase as observed in tested beam. The twisting of the beam started immediately with applied load increase. Fig. (4-6) shows the experimental and numerical comparison of flexural cracks for CCBF-3. The comparisons between the numerical and experimental results appear that the cracks extended more than the areas in the experimental results.

The CCBP-3 model was with highest span to curvature ratio among the other models. The diagonal torsional cracks were formed at the end support and it was observed immediately as well as the load increase incorporating with flexural concrete cracks as depicted by the experimental results by Tan and Uy [21]. The model shows more torsional cracks than the regular existed in the experimental results as seen in Fig. (4-7).
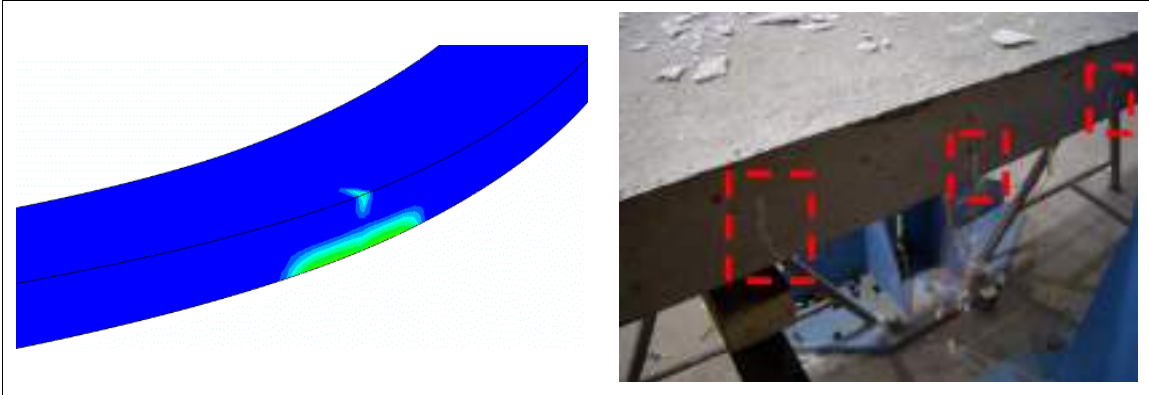
Figure (4-6): Flexural cracks comparison between experimental and numerical for CCBF-3.
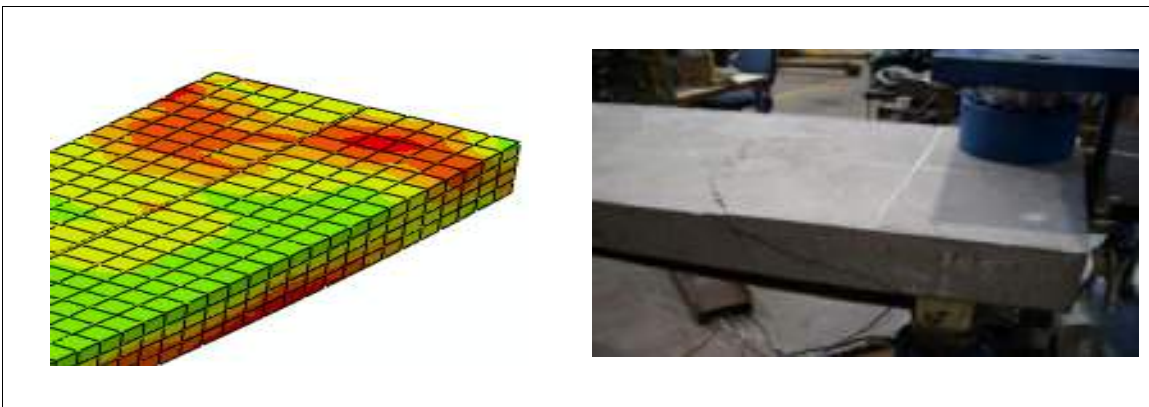
Figure (4-7): Experimental and numerical comparison of diagonal torsional cracks for CCBP-3.

Due to the difference between the experimental and theoretical condition for the flexural and torsional cracks, the extended area in the FE models was found to be distributed more than that exists in the experimental results. The concrete material modeling nature was the main reason. Furthermore, the distributed of the material degradation over all the element volume due to the cracking of the model may the main for the greater intensity of the numerical model.

After the results of FE become within acceptable limits relation to the experimental test, the parametric study may be implemented for some important parameters to know the effect of these variables on curved composite beams behavior. The test specimen's contact condition, material behavior, element type, and the solution technique are explained in previous chapter.

4.5 Ductility

Ductility is a measure of a material's ability to undergo significant plastic deformation before rupture or breaking, which may be expressed as percent elongation or percent area reduction from a tensile test.

Ductility index ratio was selected as an index to assess the ductility of curved composite beam models. The ductility index (μ_Δ) is defined as the ratio of the maximum mid-span displacement over the first yield displacement of beams. The first yield displacement Δ_y corresponds to the load- deflection curve and maximum displacement Δ_u, Fig. (4-8) [90].
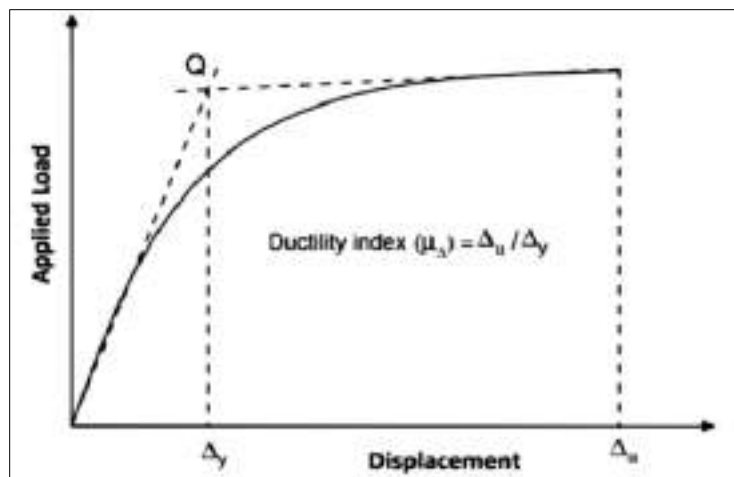
Figure (4-8): Show the ductility index calculation [91].

Therefore, the use of ductility ratio presents a better criterion in addition to the strength criterion for predicting the behavior of curved composite steel-concrete beams [90].

$$\mu_\Delta = \frac{\Delta_u}{\Delta_y} \tag{4.1}$$

4.6 Parametric Study

In the present study the essential objective is to investigate the effect of several important parameters that are not well covered in past the previous studies on the inelastic behavior, crack patterns, ductility, stiffness and strength of curved steel and concrete composite beams. The span to radius of curvature ratio, transverse web stiffeners, partial interaction, the concrete compressive strength and steel beam yield stress, steel beam opening and fixation boundary condition are the considered parameters in this study. The FEM was carried out and developed using the general commercial ABAQUS software.

The parametric study results of the parameters obtained from the FE modeling including the yield load (P_y), ultimate failure load (P_u) and the ultimate vertical mid-span deflection (Δ_u). The curve beam strength and the load versus mid-span deflection relation are included in each parameter involved to focus on the effect of these variables on all the numerical models.

To find out the phase of the curved composite beam yielding stage, a section is selected on the beam mid-span, this measured section was created

from the longitudinal reinforcement and steel girder portions [4]. Nine points are selected for measurement locations, where the typical four points located at reinforcement bar layers (two at the top and the other remaining two at the bottom), four at the top and bottom flanges (two for each flange) and one at the steel beam web as seen in Fig. (4-9). In those locations, the mean element stress is used and generated to determine the sectional yield stresses depending on the reinforcement bars and steel beam yield stress.
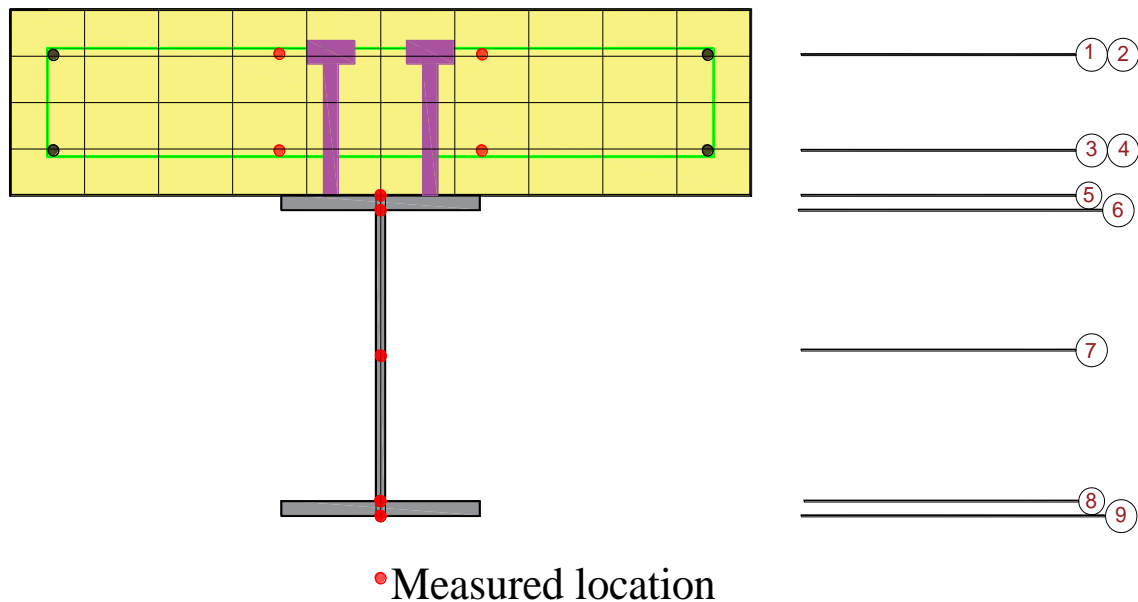
Figure (4-9): Measured location of section yield stress.

For all the studied modeled, the reinforcements of diameters 10 mm and 12 mm were placed on the concrete slab for torsional and longitudinal reinforcement, respectively. The yield stress of 12 mm and 10 mm of steel rebar, the steel beam web and flange were, 586, 399, 374 and 347 MPa; respectively. The concrete slab compressive strength was 37.7 MPa. Concrete modulus of elasticity, compressive and tensile stress of concrete was calculated by using prescribed relation in Eurocode 2 [82]. Modulus of

elasticity, compressive and tesile strength are according to the Eq. (3.3), (3.5) and (3.9). Table (4-7) show the specimens' detail.

Table (4-7): Model's details for the curve composite beams.

Specimen	Central angle (°)	Degree of connection (%)	Stiffeners number	Compressive strength (MPa)	Steel beam yield stress (MPa)
CCBF-1	16.7	100%	-	42.3	360.5
CCBF-2	17.4	100%	-	41.5	360.5
CCBF-3	24.3	100%	-	38.3	360.5
CCBP-1	15.8	50%	-	37.7	360.5
CCBP-2	16.8	50%	-	39.1	360.5
CCBP-3	26.1	50%	-	40.4	360.5
A-0	0	50%	-	37.7	360.5
A-10	10	50%	-	37.7	360.5
A-20	20	50%	-	37.7	360.5
A-30	30	50%	-	37.7	360.5
A-40	40	50%	-	37.7	360.5
WS1	26.1	50%	2	40.4	360.5
WS2	26.1	50%	3	40.4	360.5
WS3	26.1	50%	5	40.4	360.5
WS4	26.1	50%	6	40.4	360.5
WS5	26.1	50%	14	40.4	360.5
WS6	26.1	50%	16	40.4	360.5
ST30	16.8	100%	-	39.1	360.5
ST26	16.8	90%	-	39.1	360.5
ST24	16.8	80%	-	39.1	360.5
ST22	16.8	70%	-	39.1	360.5
ST20	16.8	65%	-	39.1	360.5
ST16	16.8	50%	-	39.1	360.5
ST12	16.8	40%	-	39.1	360.5
ST10	16.8	30%	-	39.1	360.5
ST8	16.8	25%	-	39.1	360.5
C30	30	50%	-	30	360.5
C40	30	50%	-	40	360.5
C50	30	50%	-	50	360.5
S200	16.8	50%	-	39.1	200
S250	16.8	50%	-	39.1	250
S300	16.8	50%	-	39.1	300
S350	16.8	50%	-	39.1	350
S400	16.8	50%	-	39.1	400
S450	16.8	50%	-	39.1	450

4.6.1 Span to radius of curvature ratio effect

The validated model CCBP-1 was contrived to investigate effect of the span to radius of curvature ratio ($\frac{L}{R}$) effect on the inelastic behavior of the curve composite beam. This parameter is studied with different ratios to produce different levels of combined effect of flexure and torsion.

Five curved composite beams were designed as simply supported, identified as A-0, A-10, A-20, A-30 and A-40 that represent the beams with central angles ($\theta = 0°, \ 10°, 20°, 30°$ and $40°$); respectively, as seen in Fig. (4-10) and Table (4-7), and were designed with partial shear connection. The headed shear studs were welded in a single row to the steel flange top surface with a diameter, length, and spacing with 19 mm, 100 mm, and 450 mm; respectively. The concrete slab compressive strength was 37.7 MPa.
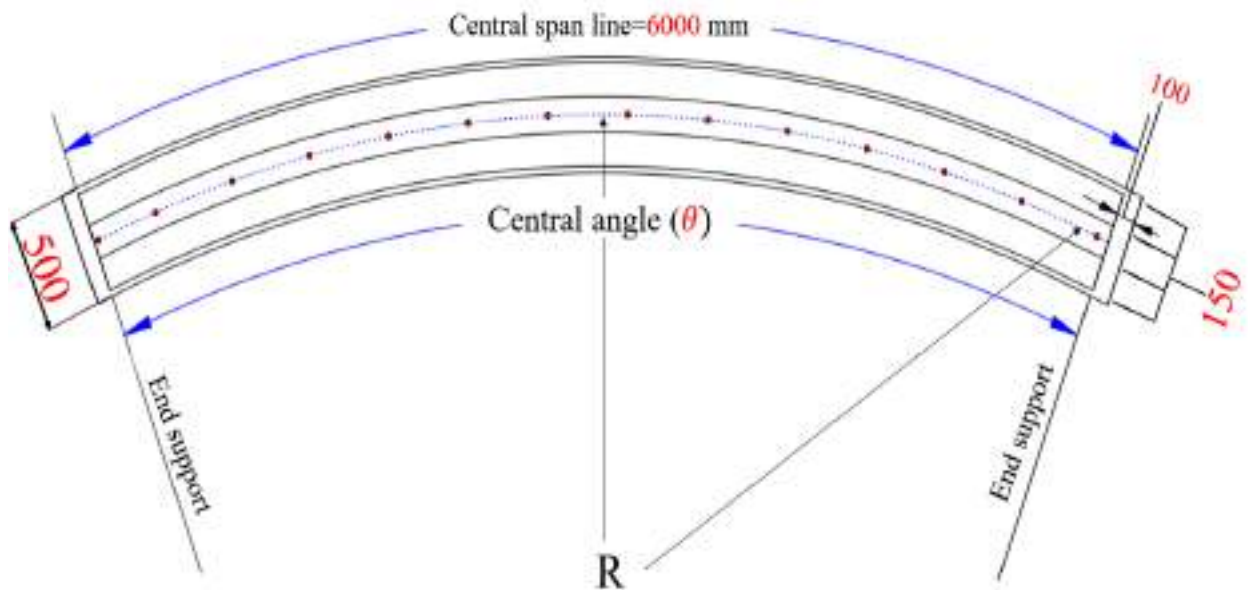
Figure (4-10): Plan view for the curved composite steel-concrete beam (unit: mm).

Table (4-8). Curve composite beam details for curvature effect.

Beam type	Specimen (A-i)	Degree of connection (%)	Central angle (°)	Beam modeling	Radius (m)	Span/Radius
CCBP-1	A-0	50	0		0	0
	A-10	50	10		34.3	0.175
	A-20	50	20		17.19	0.349
	A-30	50	30		11.45	0.524
	A-40	502	40		8.6	0.698

The headed shear studs were welded in a single row to the steel flange top surface with a diameter, length, and spacing with 19 mm, 100 mm, and 450 mm; respectively. The concrete slab compressive strength was 37.7 MPa.

From the model's analysis, in the beam mid span, the flexural cracks be the main cracks and expand toward the beam immediately with applied loading increase as seen in Fig. (4-11) with some cracks at end support. The vertical slip at the beam mid-span observed to be eliminate compared to the

other model with applied load increase as seen in Fig. (4-12). The ultimate load capacity is recorded at 167.3 kN with a vertical deflection of 163.3 mm. The flexural failure of the beam is the main failure of the beam.
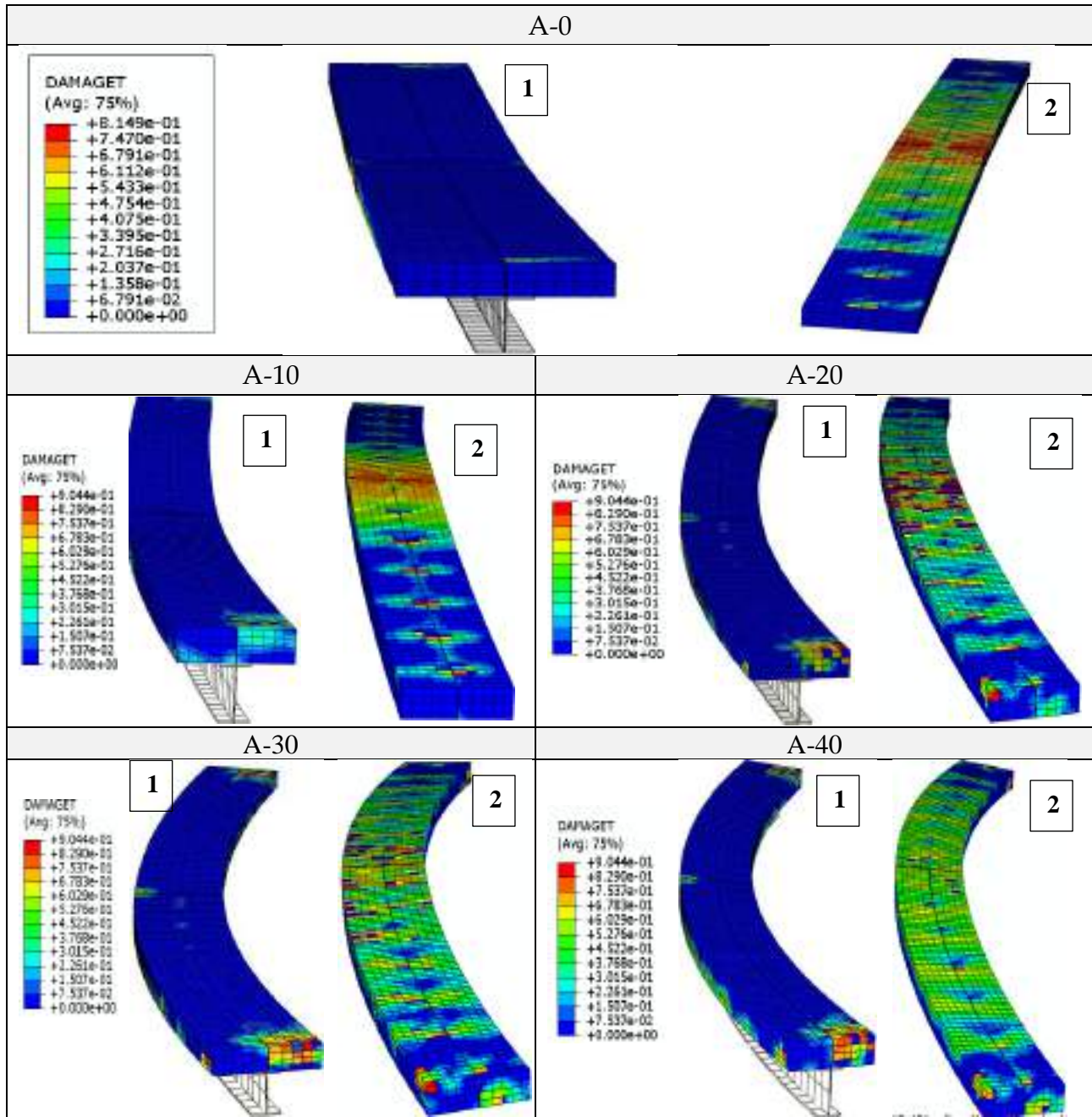
Figure (4-11): Effect of curvature on crack progression on the concrete slab, 1- Top surface of the slab, 2- Bottom surface of the slab.
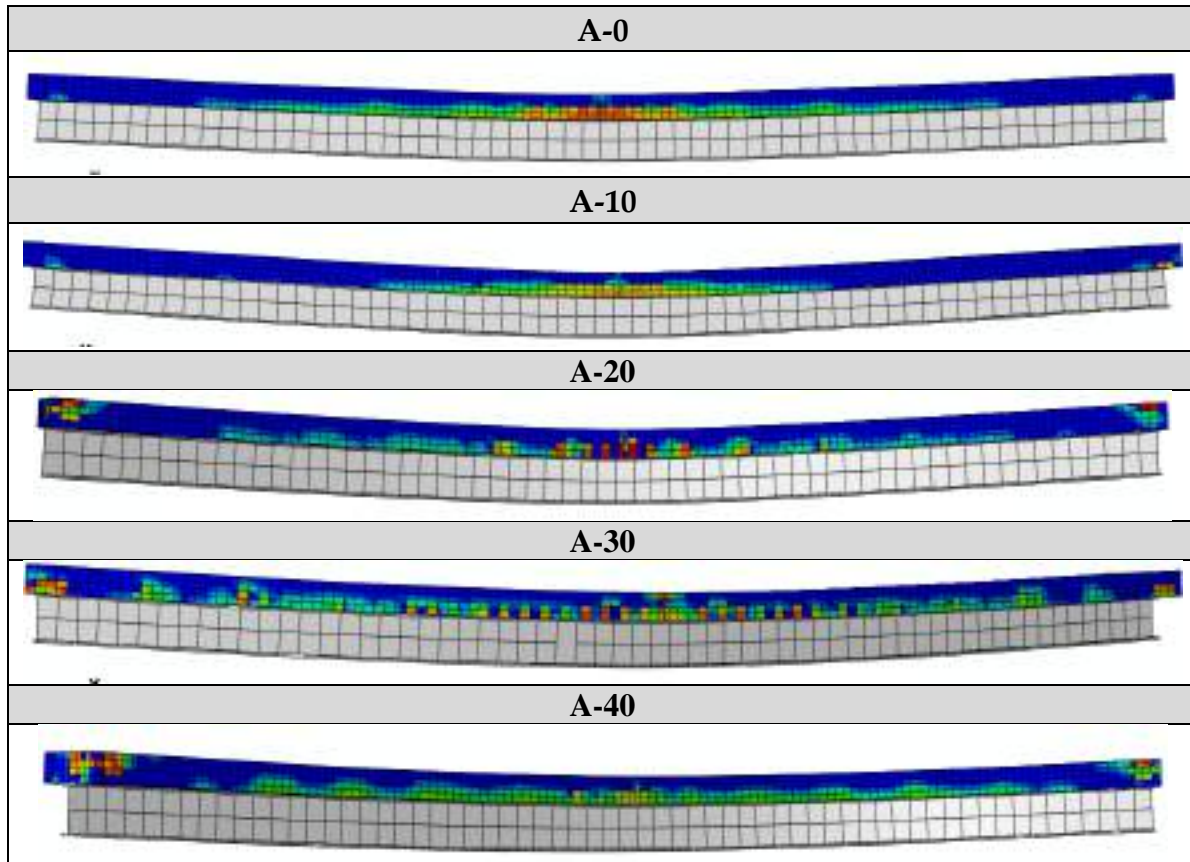
Figure (4-12): Effect of the curvature on the beam flexural cracks.

For A-10, in the vicinity of the mid span, few flexural cracks were observed. At both the support, the diagonal torsional cracks of concrete slab were beginning to be observed at applied loading increase to 32 kN as shown in Fig. (4-11). The maximum recorded load and vertical deflection was 138.8 kN and 146.3 mm, respectively. The beam fails due to increase the flexural failure.

Compared to A-10, A-20 has more torsional cracks as well as flexural concrete cracks as shown in Figures (4-11) and (4-12). For A-20, lesser ductility has been noticed where a vertical deflection of 122.4 mm at ultimate load of 120.7 kN. The vertical slip at the beam mid-span observed to increase

significantly with applied load increase incorporating with increasing the twist rotation of the beam as seen in Fig. (4-13). The model fails due to severe steel-concrete composite twisting beams.
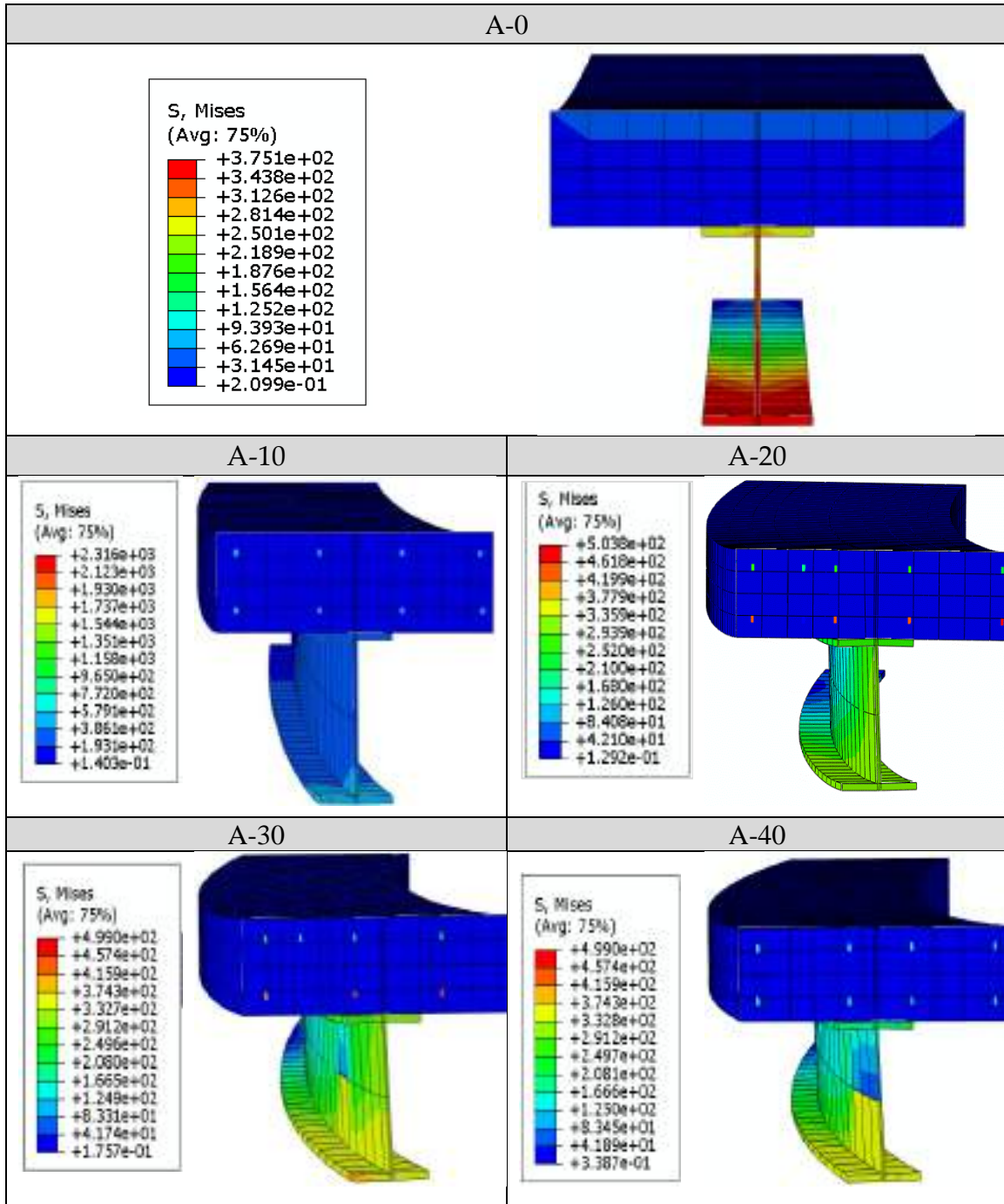
Figure (4-13): Effect of the curvature on vertical slip at mid-span.

Due to higher central angle, the steel-concrete composite beam subjected to higher torque for A-30. The flexural cracks of concrete are noticed immediately after the load was applied incorporating with diagonal torsional cracks with excessive steel-concrete composite beam twisting. Furthermore, twist rotation began to develop and increase with a slight loading increase as seen in Fig. (4-13). The ultimate load capacity is recorded at 104.6 kN with a vertical deflection of 111.1 mm. Excessive twisting of the beam is the main failure of the beam.

Among the other models, A-40 has the highest central angle. Diagonal torsional cracks of concrete slab began to develop and expand at the end support immediately with applied loading increase as seen in Fig. (4-11). Additional cracks are noticed compared to the models A-10, A-20, and A-30. Extra twisting of A-40 is the main reason for the model failing, in which the applied loading duration was short compared to the other models. The ultimate load recorded for this model is 79.44 kN with vertical deflection of 80.94 mm. In the top and bottom surface of the concrete slab, concrete cracks are expanded and widening with applied increase.

Figures (4-14) and (4-15) of the load versus vertical deflection and the load versus central angles relations of the specimens, it can be noted that the beam began to yield at an early stage the ratio increase, and inelastic nonlinear behavior developed early, as seen in Table (4-9). Compared to the specimen A-0, the other three specimens recorded a reduction in yield load by 17%, 28%, 34% and 50% for A-0, A-20, A-30 and A-40, respectively.

$P_{tc(i)} = torsinal\ crack\ load\ of\ model$
$P_{tc(A-0)} = 71\ kN$
$P_{tc(A-10)} = 32\ kN$
$P_{tc(A-20)} = 25.13\ kN$
$P_{tc(A-30)} = 18.86\ kN$
$P_{tc(A-40)} = 11.20\ kN$
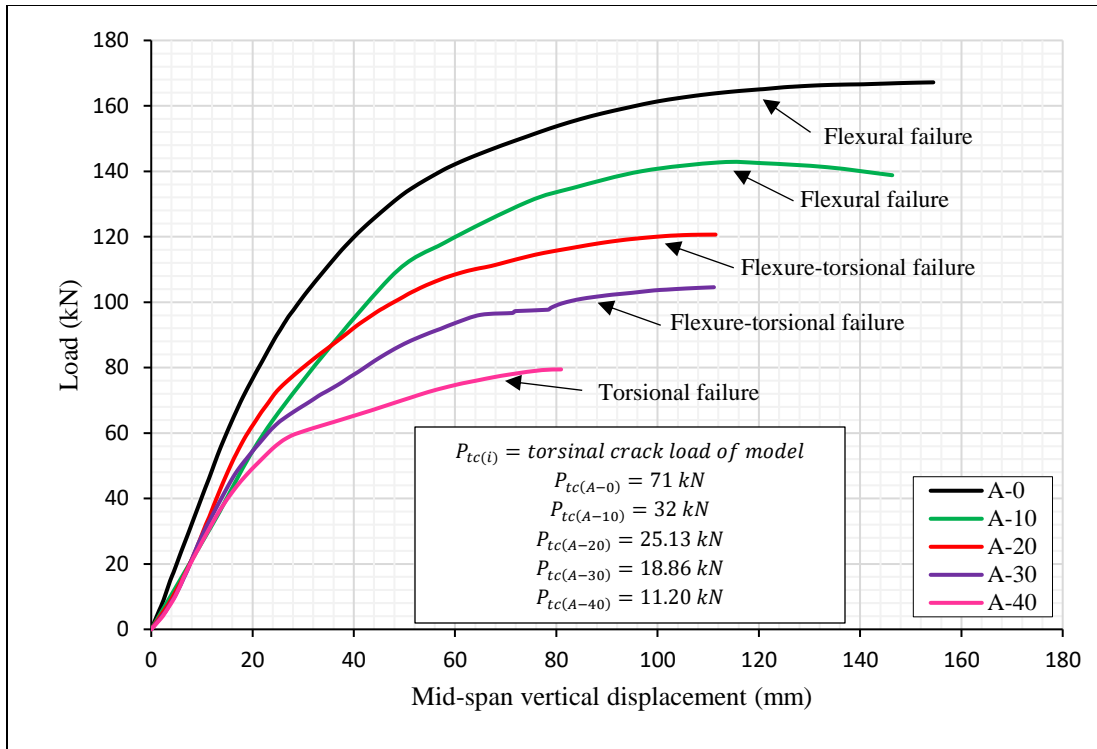
Figure (4-14): Curvature effect on the load-deflection curve of the curve composite beam.
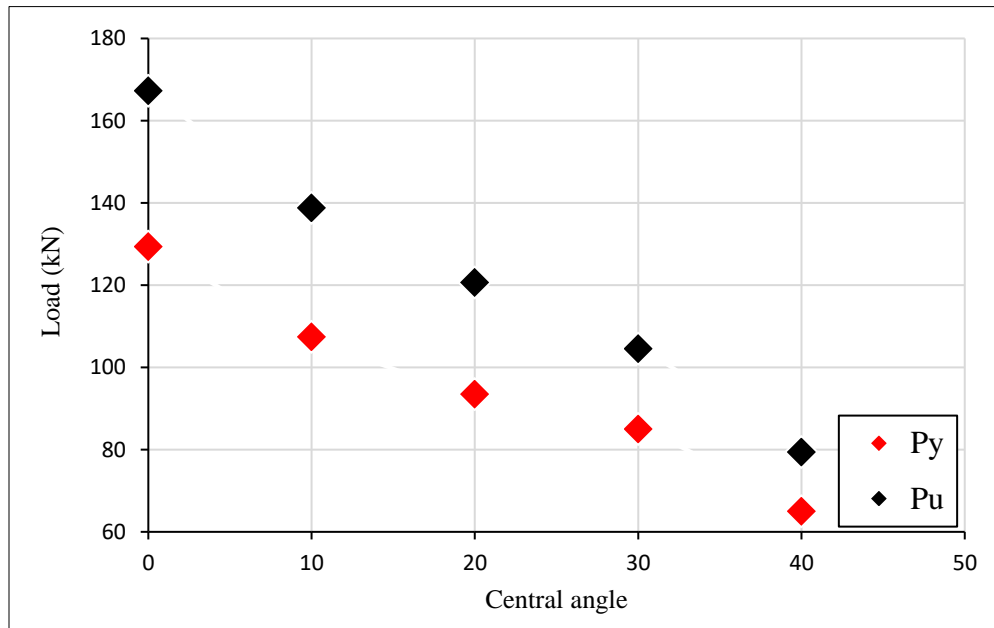
Figure (4-15): Yield and ultimate load vs central angle.

Table (4-9): Curve composite beam results under curvature effect.

Specimen (A-i)	F_{yA-i} (kN)	F_{uA-i} (kN)	Δ_u (mm)	$\dfrac{F_{yA-i}}{F_{yA-0}}$	$\dfrac{F_{uA-i}}{F_{uA-0}}$	$\dfrac{\Delta_{uA-i}}{\Delta_{uA-0}}$	Ductility index (Δ_u/Δ_y)
A-0	129.4	167.3	163.3	1.00	1.00	1.00	3.5
A-10	107.5	138.8	146.3	0.83	0.83	0.90	3.1
A-20	93.5	120.7	122.4	0.72	0.72	0.75	2.97
A-30	85.04	104.6	111.1	0.66	0.63	0.68	2.35
A-40	65.05	79.44	80.94	0.50	0.47	0.50	2.05

In term of load-carrying capacity, composite beams load seemed reduced in a range of 17%, 28%, 38% and 53 for A-10, A-20, A-30 and A-40, respectively, compared to A-0. The numerical ultimate vertical deflection decreases by 17%, 28%, 38% and 52% for a specimen A-10, A-20, A-30 and A-40, respectively compared to A-0. Furthermore, it can be observed from the load versus vertical deflection curves in Fig. (4-14) that all the numerical curves appear to reduce the ductility index of composite beams by 41% significantly with the increasing the span to radius of curvature ratio as seen in Table (4-9).

From above results it leads to the conclusion that the response of the specimens softens, and the beam yielding earlier. From Fig. (4-13), it is evident that increasing the ratio increase the vertical slip and the twisting at the mid-section and be more evident. This observation of the twisting and the vertical slip attribute to the effect of torsion as the curvature increases, where the failure of the beam change from flexural to a combined effect of flexural and torsion. Moreover, the torsion was found to be dominate and influential

on the inelastic failure mechanism and behavior of the specimen, especially in specimens with large span/radius of curvatures ratio, A-30 and A-40.

The crack patterns of the curved beams shown in Fig. (4-11) that the tensile zone was found to be initiated in the centroid zone then enlarged and propagated toward the whole slab when the curvature increased. The observed increase in the cracks Fig. (4-16) was due to the increase in shear stresses in the specimens when the curvature increased due to an increase the torsional effect. The cracks in the compression face were observed to be little in comparison to these in with the tension face. Furthermore, the strain distribution in the mid span, Fig. (4-17) show that the beams record a reduce in the beam strain with curvature increases.
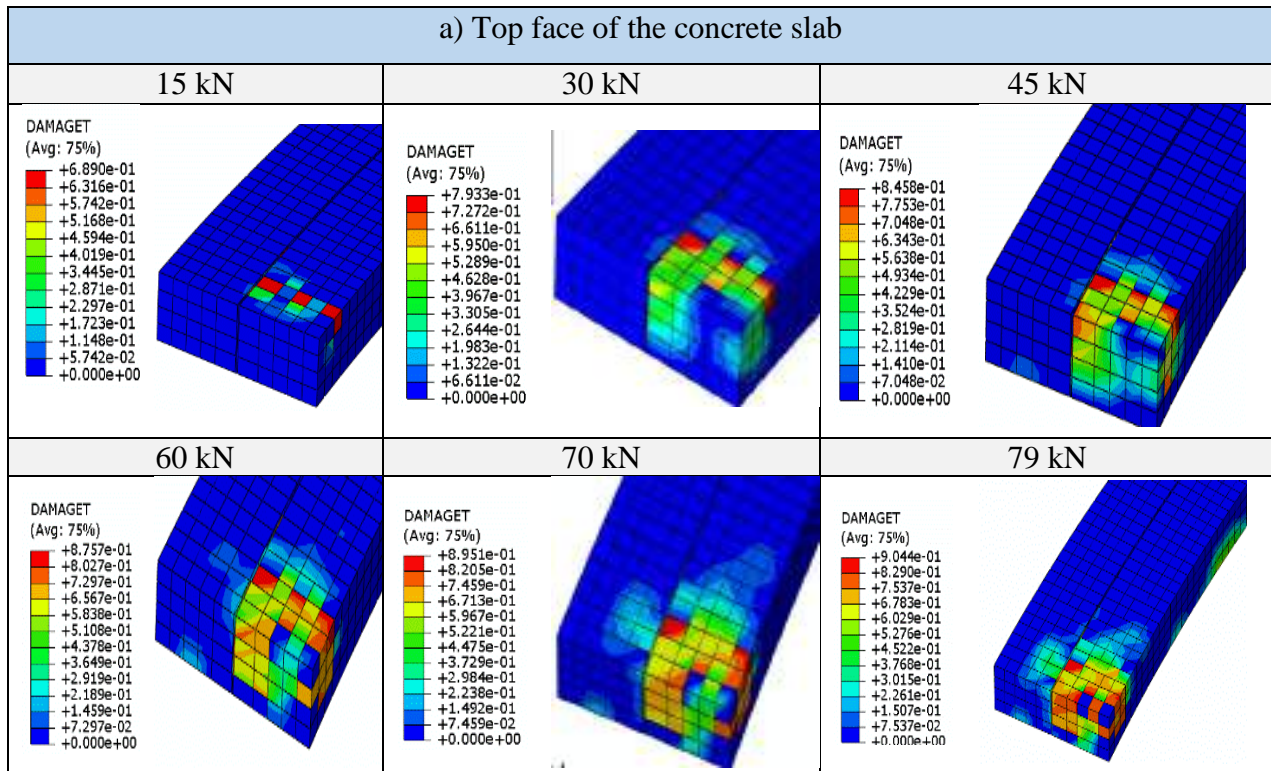
Figure (4-16): The crack progression in the concrete slab for model A-40 at different loading stage.

b) Bottom face of the concrete slab		
15 kN	30 kN	45 kN
60 kN	70 kN	79 kN
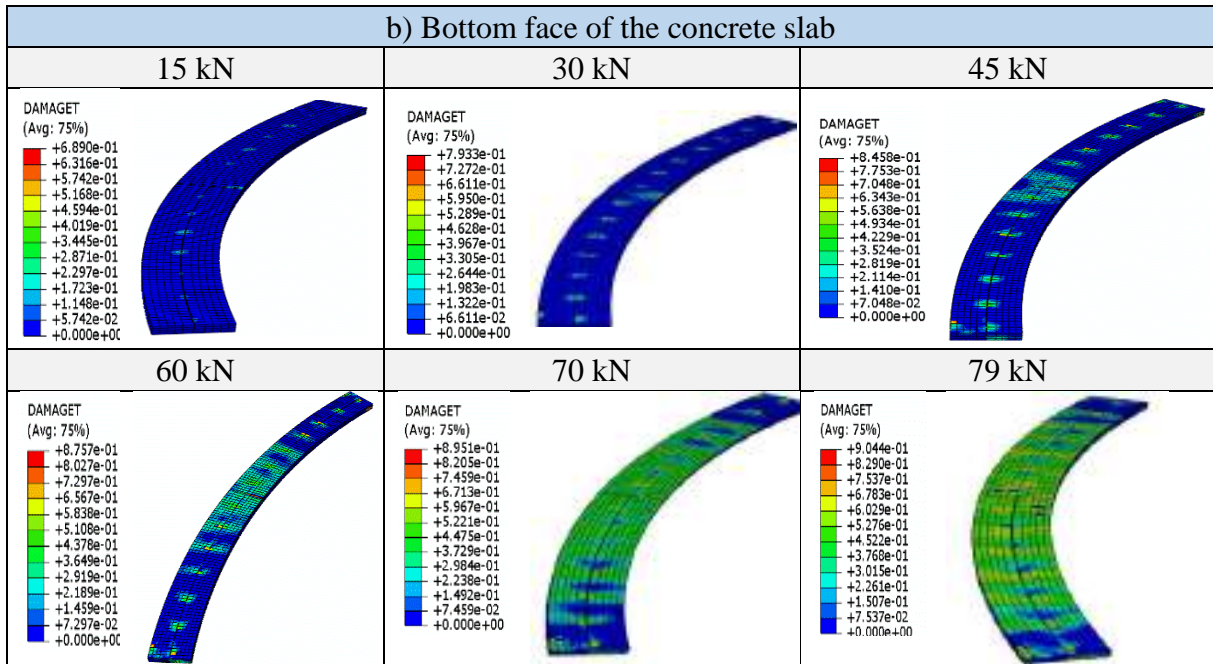
Figure (4-16): Continued.

A-0	
A-10	A-20
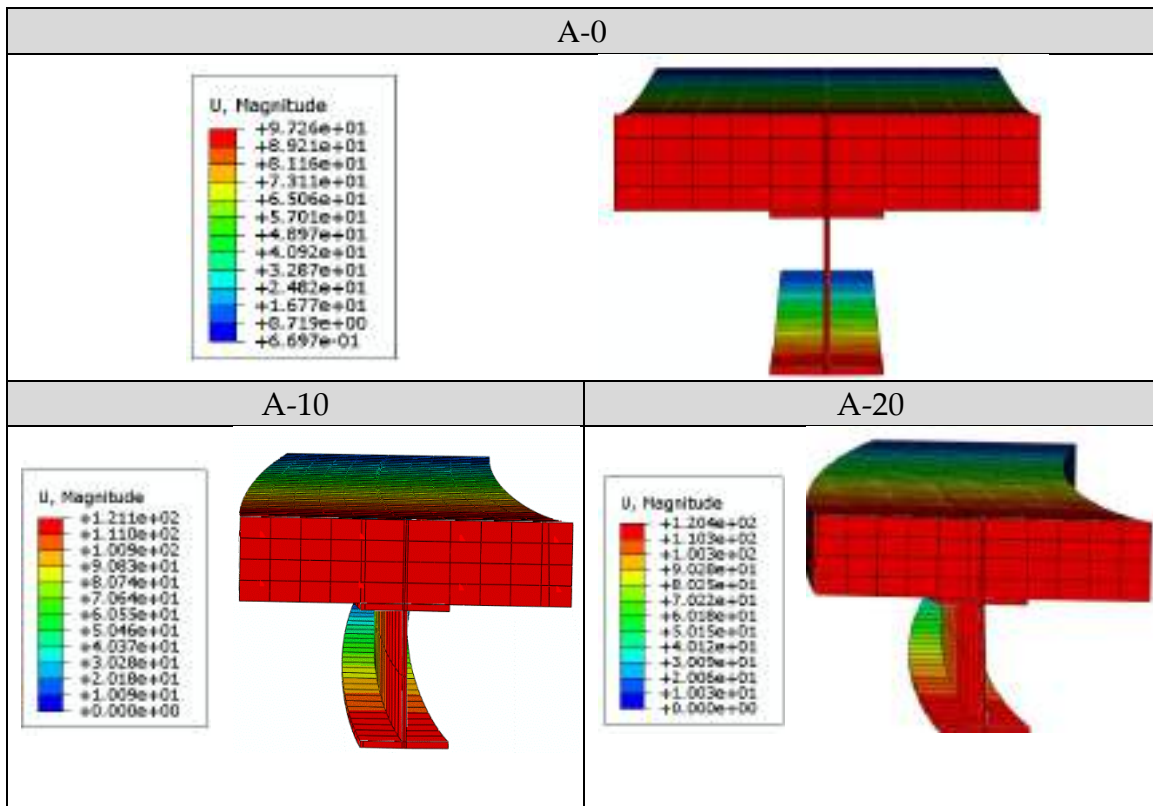
Figure (4-17): Effect of the curvature on strain distribution at mid-span.

A-30	A-40
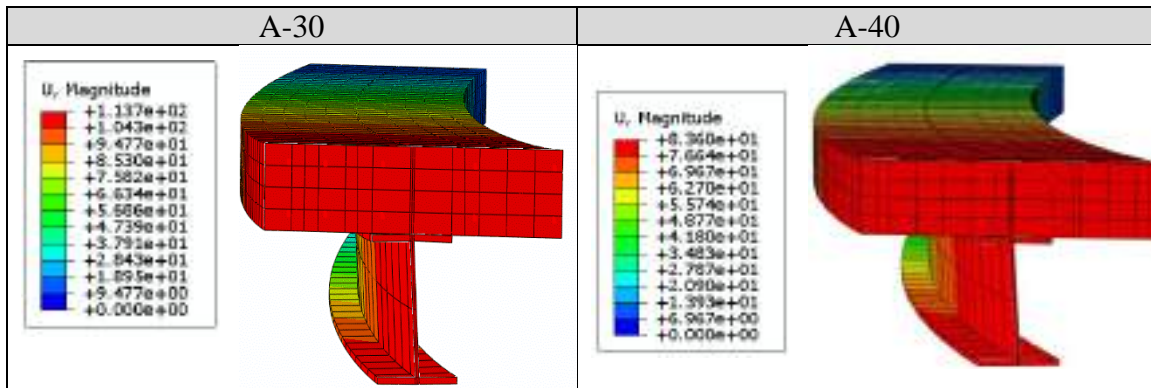
Figure (4-17): Continued.

4.6.2 Transverse web stiffeners effect

In order to illustrate the vertical web stiffeners effect on the inelastic behavior and the performance of the steel and concrete composte curved beams, group of beams with different numbers and locations of web stiffeners were analzed by using the FE method.

Six partial shear connection composite beams are prepared to study the effect of web stiffeners and the performance of the composite beams. The web stiffeners with nominal thickness of 6.5 mm are arranged in the validated model CCBP-3, as shown in Fig. (4-18). The central angle, span/radius, and degree of shear connector are 26.1°, 0.469 and 50% respectively. The web stiffeners number of these six beams are 2, 3, 5, 6, 14 and 16 for specimens identified WS1, WS2, WS3, WS4, WS5 and WS6, respectively. Distribution of web stiffeners along the beam and details are illustrated in Fig. (4-18). The headed studs were welded in a single row to the steel flange top surface with a diameter, length, and spacing of 19 mm, 100 mm, and 450 mm; respectively. Moreover, the concrete slab compressive strength was 40.4 MPa.

(a)

(b)
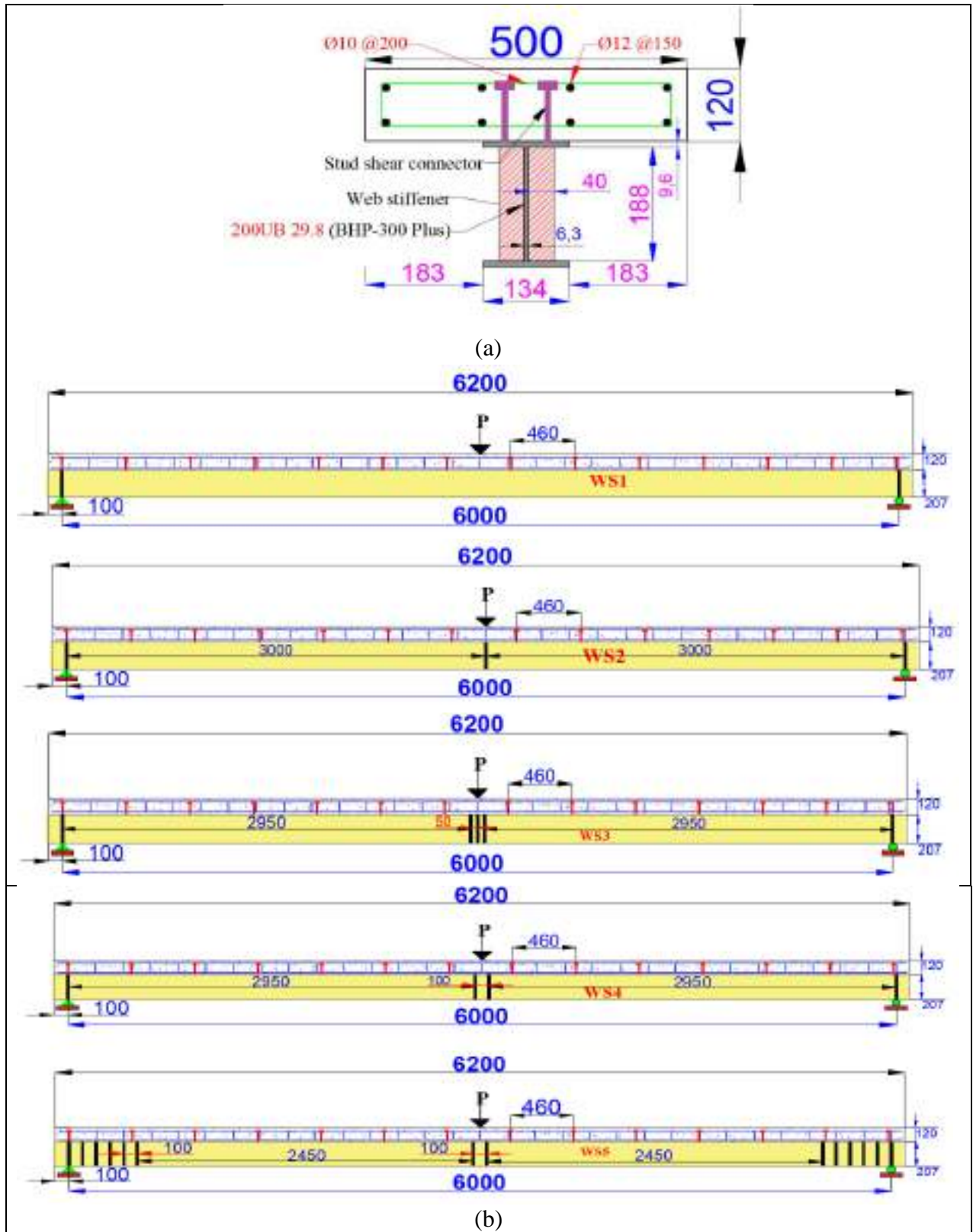
Figure (4-18): Geometry and dimensions of the curved composite steel–concrete beam with web stiffeners (unit: mm): a) Cross section, b) Side elevation.
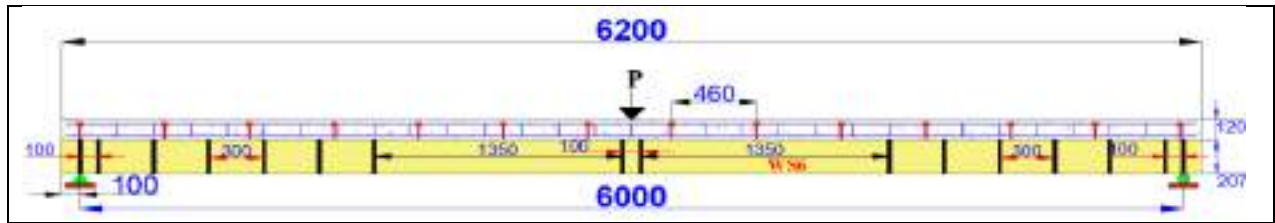
Figure (4-18): Continued.

For WS1 with two stiffeners (one stiffener at each support), the flexural concrete cracks observed immediately as the load is applied incorporating with diagonal torsional cracks with excessive remarkable beam twisting in the vicinity of the beam mid-span. Twist rotation was significant and effective with increasing the applied load as seen in Figures (4-19) and (4-20). 131.17 kN was the maximum recorded loaded with 115.32 mm vertical deflection. excessive twisting and the concrete slab failure are the main reason for the model failure.

For WS2 three stiffeners are used, one stiffener is placed at each end of beam and one at the center. The specimen WS3, five stiffeners distributed one at each support and three placed at the center, Fig (4-18). Six stiffeners are distributed in specimens WS4, two stiffeners at each support and the remaining two at mid-span. The diagonal torsional cracks and the flexural concrete cracks noticed at the beginning of loading stage, the twisting in the beam mid-span is reduced as well as the number of the stiffeners increase in this mid-span region as seen in Figures (4-19) and (4-20). The maximum recorded load for the specimens are 137.12 kN, 141.79 kN and 161.08 kN with 109.57 mm vertical deflection, 109.80 mm and 125.32 mm, respectively.

Fourteen stiffeners are used in WS5. The two stiffeners are placed near the supports and at the center, while the remaining stiffeners are located at

100 mm from each support, Fig. (4-18). The stiffeners in specimen WS6 are distributed as the same of WS5 except the distance between the stiffeners is 300 mm and only one stiffener are located at each support.
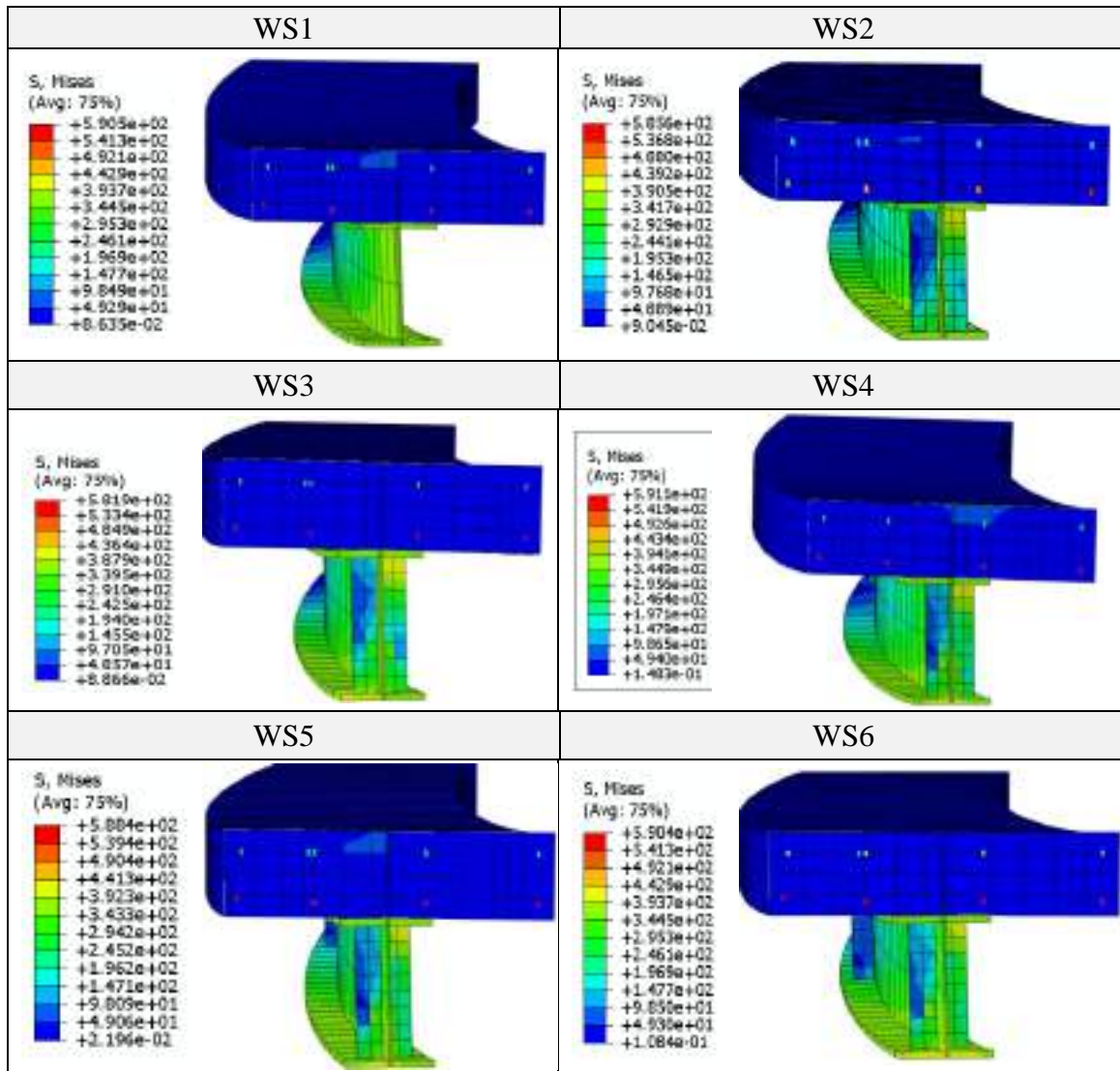
Figure (4-19): Effect of the web stiffeners on the vertical separation in the model.

The diagonal torsional cracks are effective and widen at the end supports. The compression failure in the concrete slab for the specimen WS6 is larger if compared to the other models, Fig. (4-21). The vertical separation at theses

specimens was little compared to the other specimens Fig. (4-19). The maximum load recorded for these specimens were 167.27 kN and 176.33 kN with a mid-span deflection of 163.27 mm and 137.98 mm.
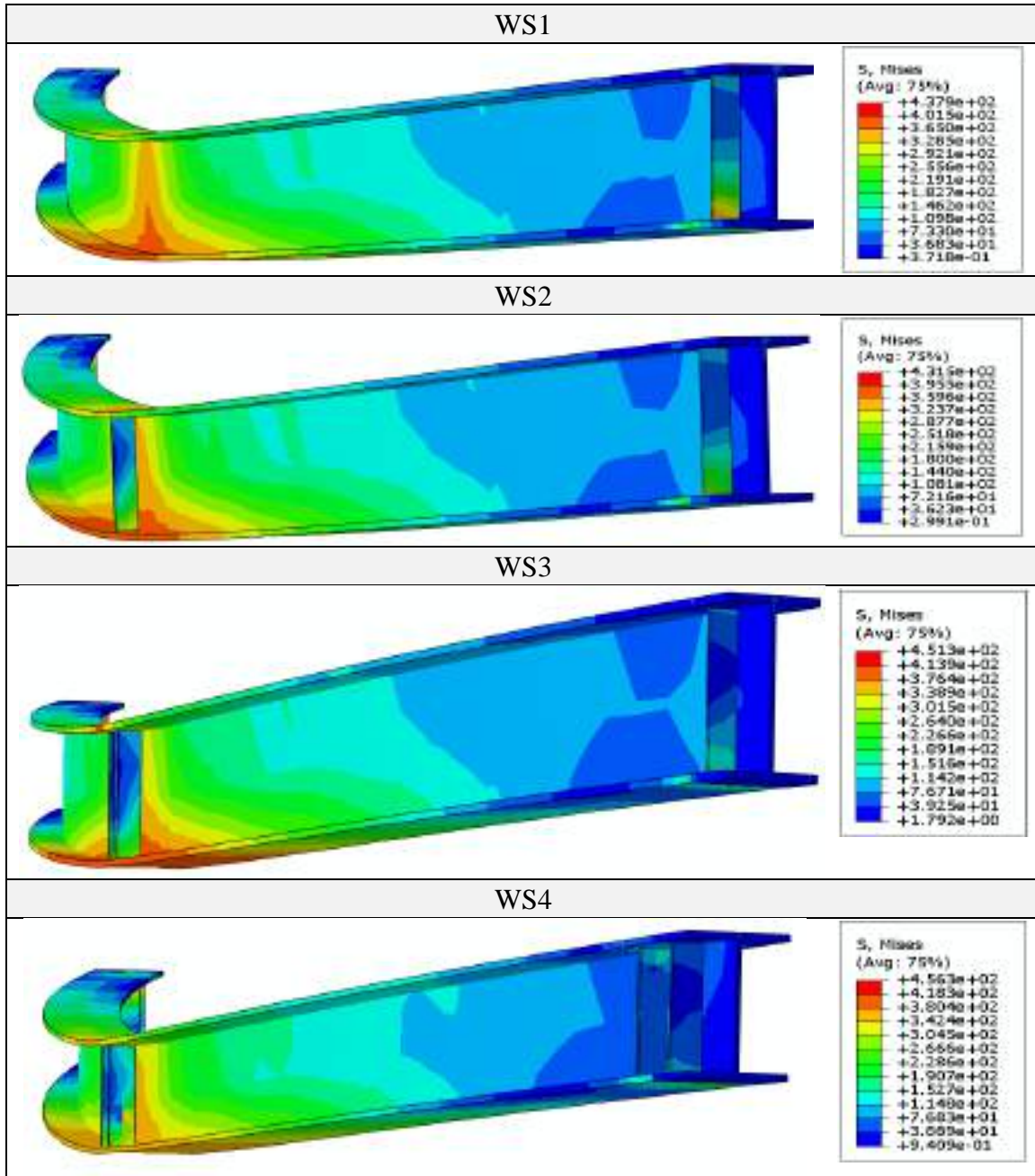
Figure (4-20): Effect of the web stiffeners on the stress distribution on the steel beam.

WS5
WS6

Figure (4-20): Continued.

Middle zone (top surface) on the concrete slab effect	
WS1	WS3
WS3	WS4
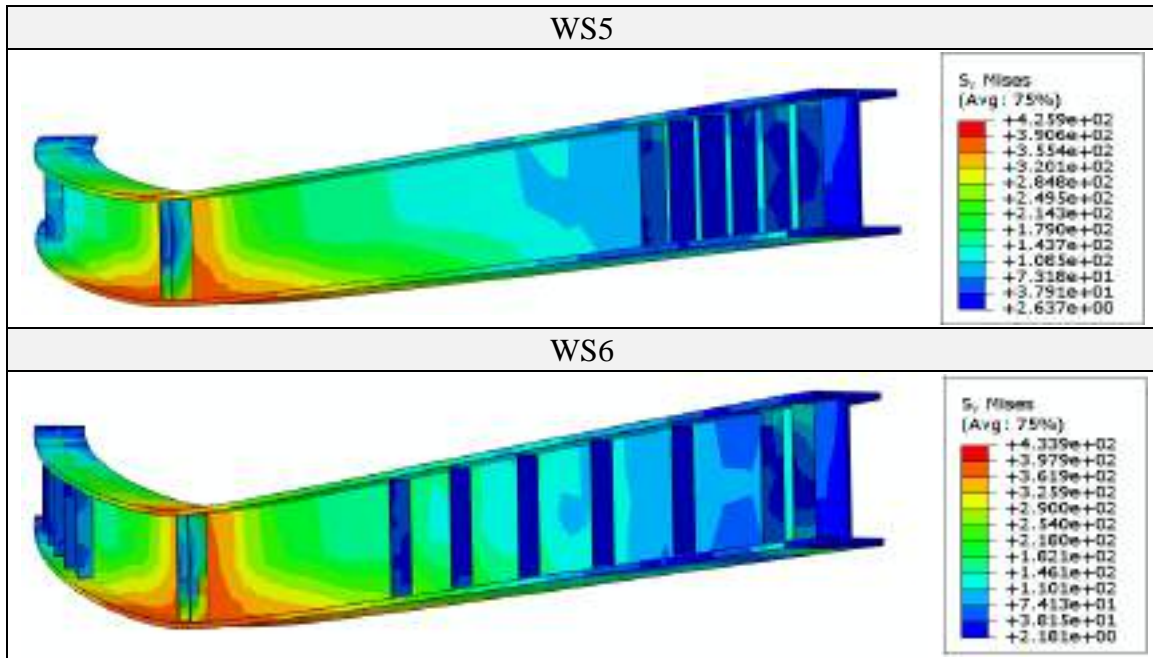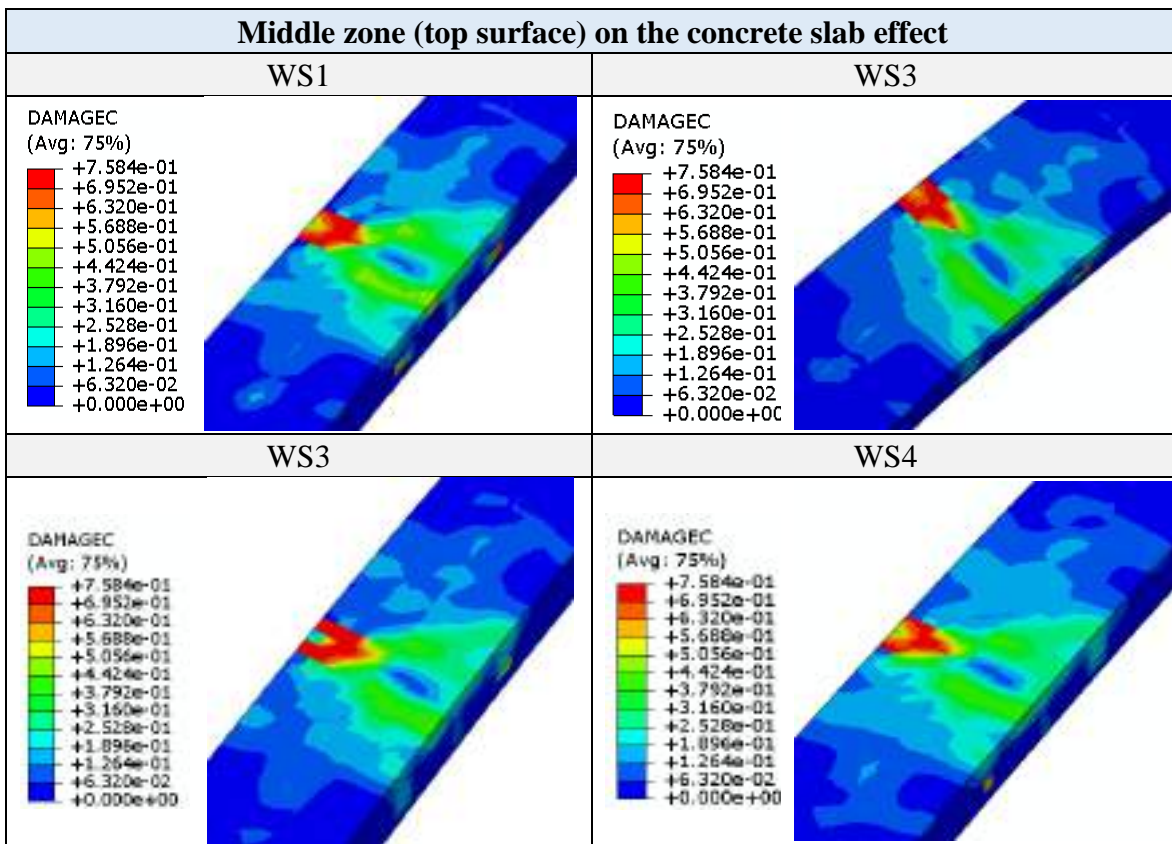
Figure (4-21): Effect of the web stiffeners on the concrete slab compression failure.

WS5	WS6
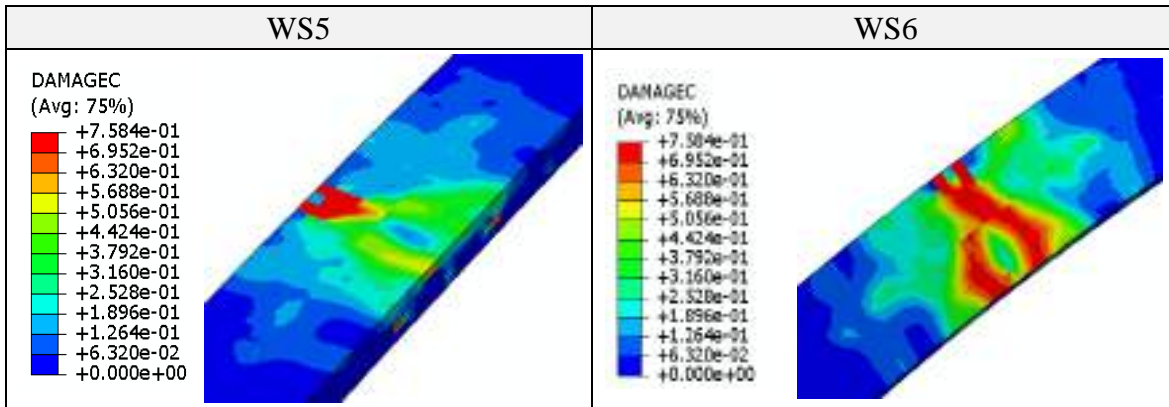
Figure (4-21): Continued.

Furthermore, Figures (4-22) and (4-23) show the comparison of the load versus the mid–span defletion and strength of the curve beams under the effect of the transverse stiffeners. Based on the outcome results, the presence of web stiffeners at different locations in the curved composite beam affected on the strength capacity of the beam. Specimens WS2 and WS3 showed a slight reduction in the beam deflection involved increasing in the beam capacity to 4.5% and 8% respectively, when compared to the WS1 model.

Meanwhile, it was shown from above that specimens with transverse stiffeners near to the support compensated for the weakness involved with enhancing the strength capacity from 22.8% to 34.43% compared to WS1. While the deflection recorded a percentage decrease from 9% to 42% compared to WS1. The observed variance in these values is due to the stiffeners' locations. Moreover, the beam began to yield at an early stage, with increases in the stiffener number, are seen in Table (4-10). Furthermore, it can be observed from the load versus vertical deflection curves in Fig. (4-22) that all the numerical curves appear to increase the ductility index of composite beams by 63% significantly with the increasing the stiffeners number as seen in Table (4-10).
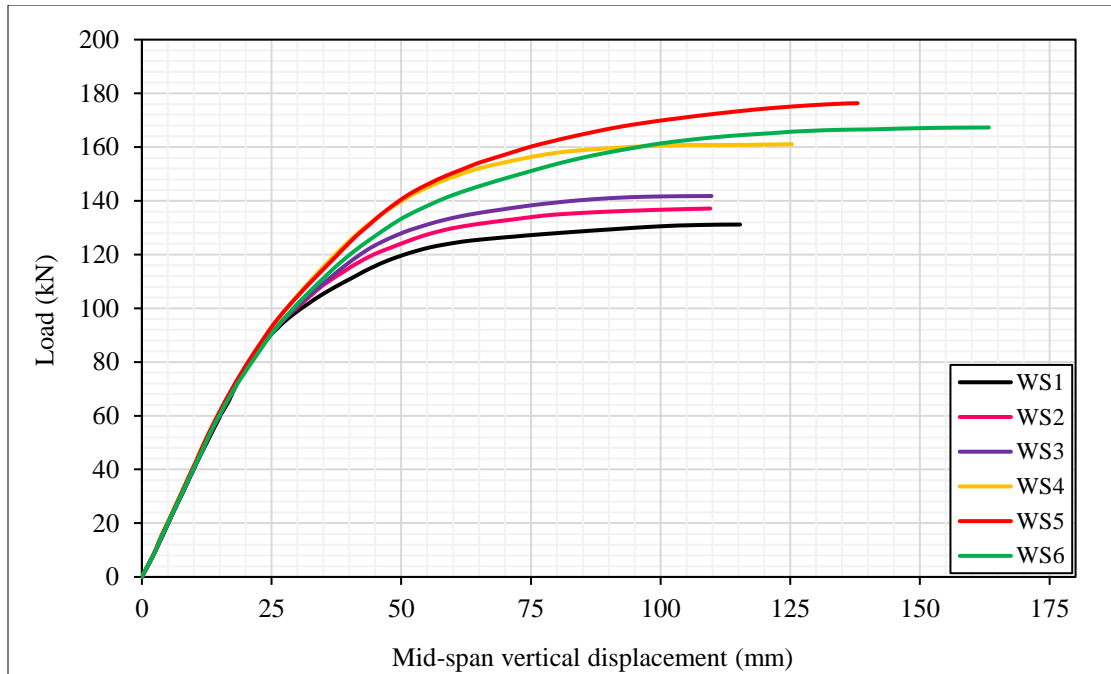
Figure (4-22): Web stiffener's effect on the load-deflection curve of the curve composite beam.
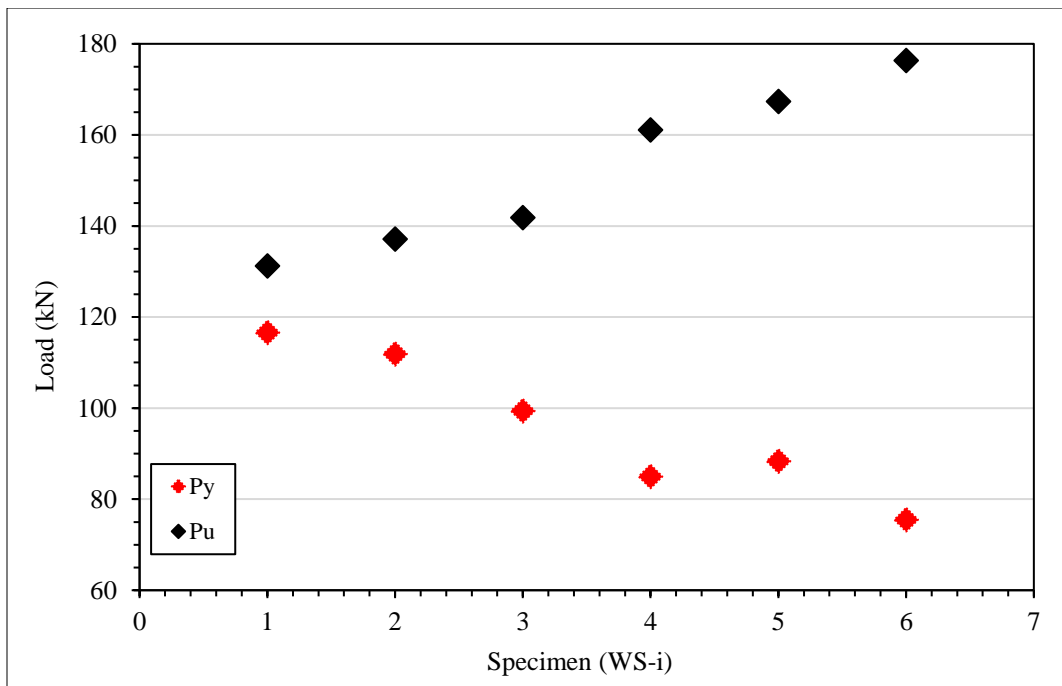
Figure (4-23): Yield and ultimate load vs specimens.

Table (4-10). Curve composite beam results under web stiffeners effect.

Specimen (WSi)	F_{yWSi} (kN)	F_{uWSi} (kN)	Δ_u (mm)	$\dfrac{F_{yWSi}}{F_{yWS1}}$	$\dfrac{F_{uWSi}}{F_{uWS1}}$	$\dfrac{\Delta_{uWSi}}{\Delta_{uWS1}}$	Ductility index (Δ_u/Δ_y)
WS1	116.60	131.17	115.32	1.00	1.00	1.00	2.5
WS2	111.28	137.12	109.57	0.95	1.05	0.95	2.9
WS3	99.38	141.79	109.80	0.85	1.08	0.95	3.8
WS4	84.97	161.08	125.32	0.73	1.23	1.09	5.6
WS5	75.43	176.33	137.98	0.65	1.34	1.20	7.3
WS6	88.31	167.30	163.27	0.76	1.28	1.42	6.8

Moreover, in which increasing the stiffeners number increase the crack progression in the slab and presented more compression and flexural cracks in the slab's center span as demonstrated in Fig. (4-20). Furthermore, the stiffeners did not affect on the interface separation between the concrete slab and the steel flange. However, transvers web stiffeners effect must be considered for the accuracy of the curve composite beam inelastic analysis. Furthermore, the strain distribution in the mid span, Fig. (4-24) show that the beams record increase in the beam strain with stiffeners number increases.
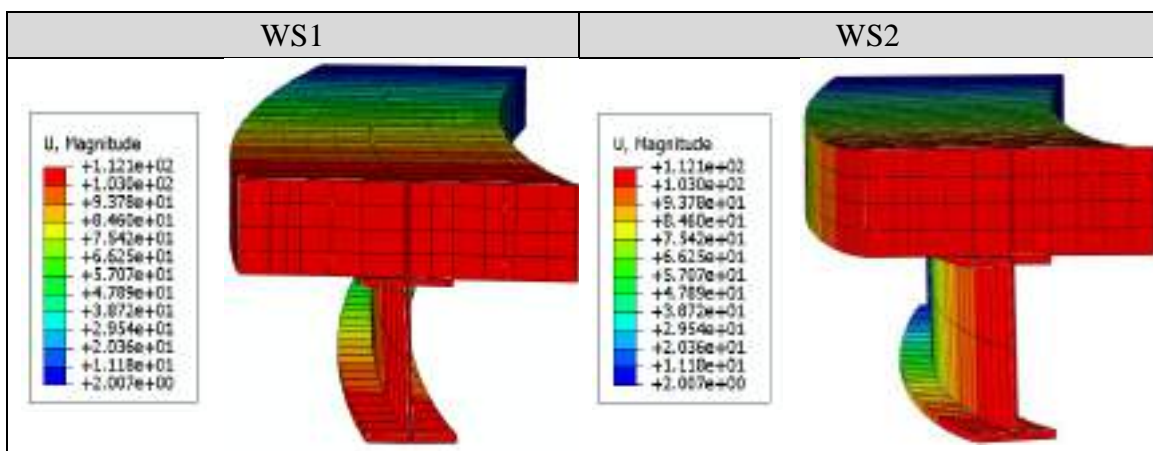
Figure (4-24): Effect of web stiffener's on strain distribution of the curve composite beam at mid-span.

WS3	WS4
WS5	WS6
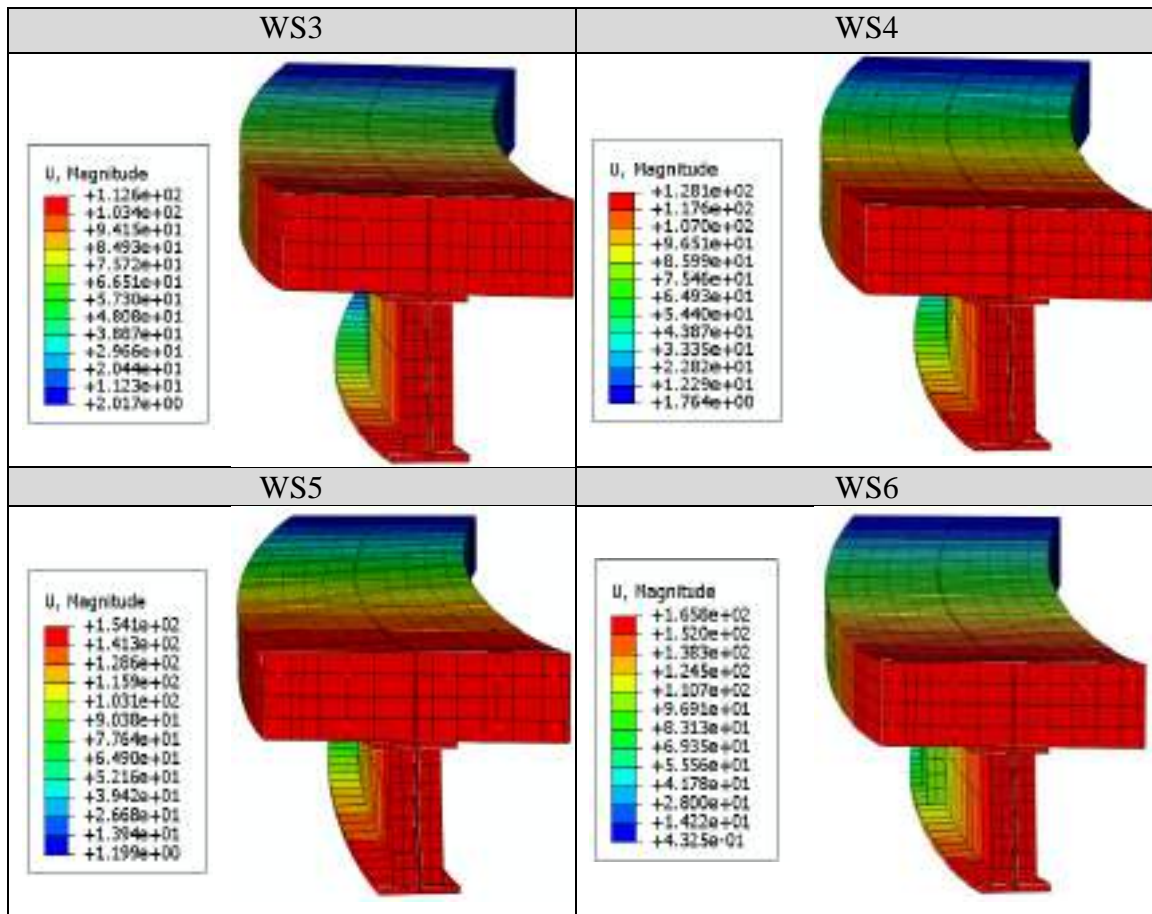
Figure (4-24): Continued.

4.6.3 The partial interaction effect

In this section, the effect of partial interaction or shear connector ratio on the composite curved beams capacity is investigated by considering different ratios of the shear connector of (0.25, 0.3, 0.4, 0.5, 0.65, 0.7, 0.8 0.9 and 1.0) on the validated model CCBP-2 by changing the connector quantity in the beam. To calculate the degree of composite action (D.C.A) Eq. (4.1) is depended:

$$D.C.A \cong \frac{Provided\ connectors}{No.of\ connectors\ for\ full\ composite\ action} * 100 \geq 25\%$$

(4.1)

Nine curved composite beams named ST8, ST10, ST12, ST16, ST20, ST22, ST24, ST26 and ST30 with a number of studs of 8, 10, 12, 16, 20, 22, 24, 26 and 30, respectively, as seen in Table (4-11). The specimens were designed by them with partial interaction. The headed studs were welded in a single row to the steel flange top surface with a diameter, length, and spacing of 19 mm, 100 mm, and 450 mm, respectively. Moreover, concrete slab compressive strength was 39.1 MPa.

Table (4-11). Curve composite beam details for partial interaction effect.

Beam type	Specimen (STi)	Partial interaction ratio (β)	Shear connection degree (%)	Shear connection number	Central angle (°)	Spacing (mm)
CCBP-2	ST30	1.00	100	30	16.85	206
	ST26	0.90	90	26	16.85	239
	ST24	0.80	80	24	16.85	260
	ST22	0.70	70	22	16.85	285
	ST20	0.65	65	20	16.85	315
	ST16	0.50	50	16	16.85	400
	ST12	0.40	40	12	16.85	545
	ST10	0.30	30	10	16.85	665
	ST8	0.25	25	8	16.85	855

Figures (4-25) and (4-26) show the load versus vertical deflection and the load versus studs number relations of composite beams. Based on the available data, a decrease in the ductility of the beam has been noticed as the partial interaction ratio increases, however this is accompanied with beam capacity increases. Furthermore, it can be observed from the load versus vertical deflection curves in Fig. (4-25) that all the numerical curves appear to decrease the ductility index of composite beams by 20% significantly with the increasing the stud ratio as seen in Table (4-12).

As can be seen in Table (4-12), the increase of ultimate load ranged between 2% to 29% for specimens compared with ST8. Also, from that Table it can be noticed that the specimen ST24, ST26 show closer enhancing in the beam capacity of ST30. Increaseing the shear connector ratio also increaseing the beam stiffeness as noticed in Fig. (4-25).
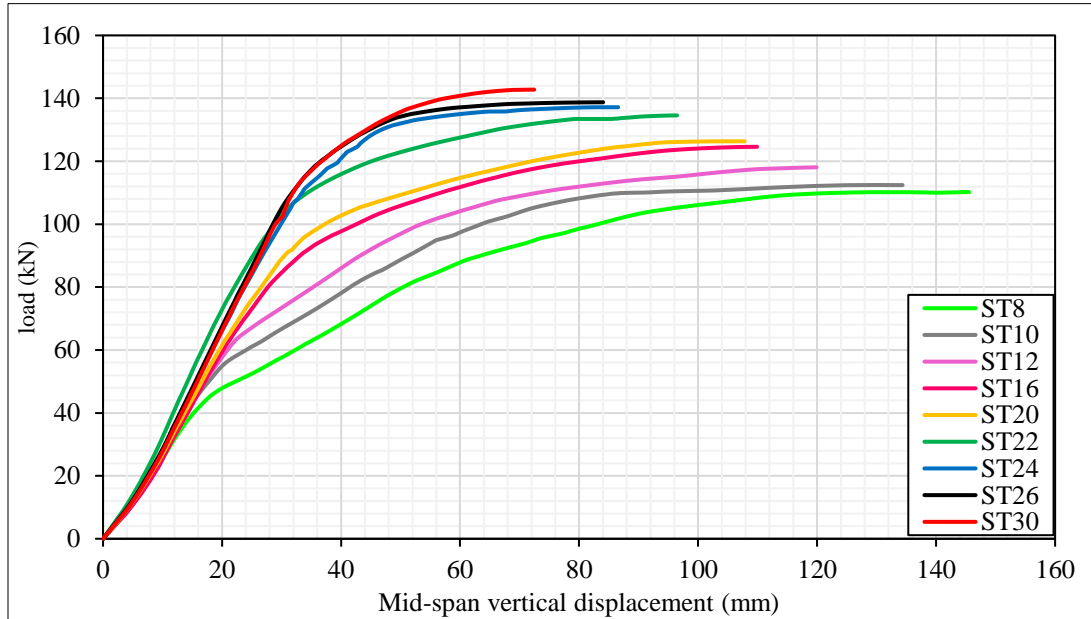
Figure (4-25): Partial interaction effect on the load-deflection curve of the curve composite beam.
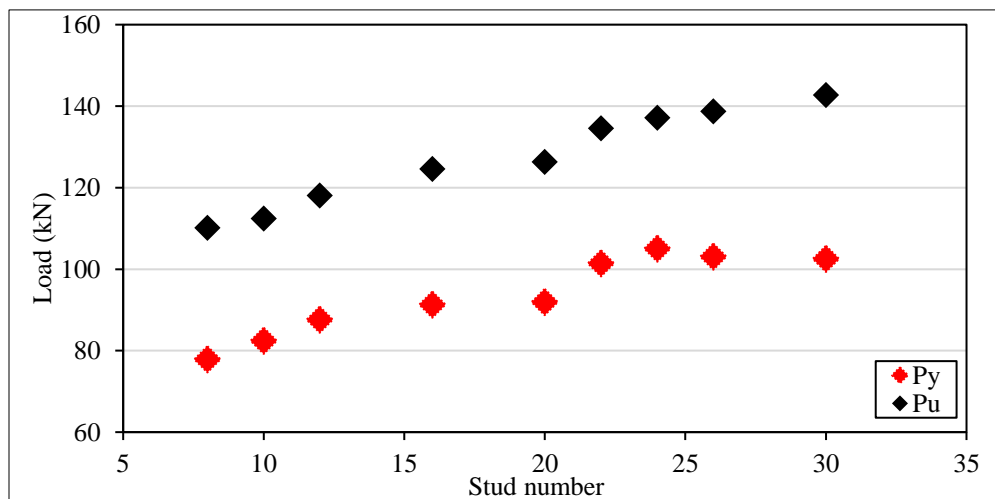
Figure (4-26): Yield and ultimate load vs stud number.

Table (4-12). Curve composite beam results under partial interaction effect.

Specimen (STi)	F_{ySTi} (kN)	F_{uSTi} (kN)	Δ_u (mm)	$\dfrac{F_{ySTi}}{F_{yST8}}$	$\dfrac{F_{uSTi}}{F_{uST8}}$	$\dfrac{\Delta_{uSTi}}{\Delta_{uST8}}$	Ductility index (Δ_u/Δ_y)
ST30	102.58	142.77	72.47	1.32	1.30	0.50	2.4
ST26	103.09	138.74	84.05	1.32	1.25	0.58	2.9
ST24	105.09	137.17	86.57	1.35	1.24	0.59	2.7
ST22	101.49	134.17	96.47	1.30	1.22	0.66	3.3
ST20	91.94	126.34	107.83	1.18	1.15	0.74	3.4
ST16	91.34	124.60	109.91	1.17	1.13	0.76	3.2
ST12	87.63	118.07	119.91	1.12	1.07	0.82	2.9
ST10	82.45	112.42	134.37	1.06	1.02	0.92	3.1
ST8	77.92	110.18	145.55	1.00	1.00	1.00	3.0

The deflection along the beam is recorded at 100 kN loading for all specimens as depicted in Fig. (4-27). Obviously, the deflection profile of specimens shows enhance in reducing the deflection of the curved composite members as the stud number increases. Specimens ST24, ST26 and ST30 show almost a very closer reduction in the deflection value by about 65% compared to ST8.
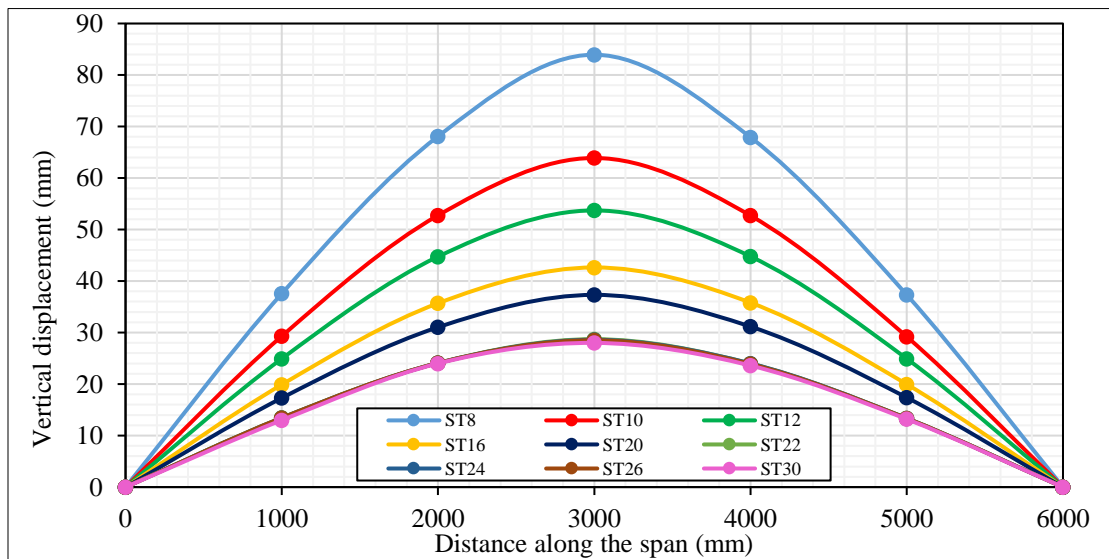
Figure (4-27): Deflection profile for the curved composite beam at 100 kN loading level.

From above it can be concluded that the observed increasing in the ultimate load can be attributed to full interaction between beam components of the beams when the stud number is increased. In which the composite member considers a beam with a full interaction when an appropriate connection maintained between the reinforced concrete slab and steel beam by an infinitely stiff and sufficient shear connector. It is found that the from Figures (4-27) and (4-28), that the interface and vertical separation decrease with increasing the partial interaction ratio. The interface separation of the specimen in which the degree of the shear connector considers with 30 shear connectors (1.00 ratio) is approximately eliminated, so it is possible to consider them as a case of the beam with full interaction comparing with the remaining beams which are of partial interaction.
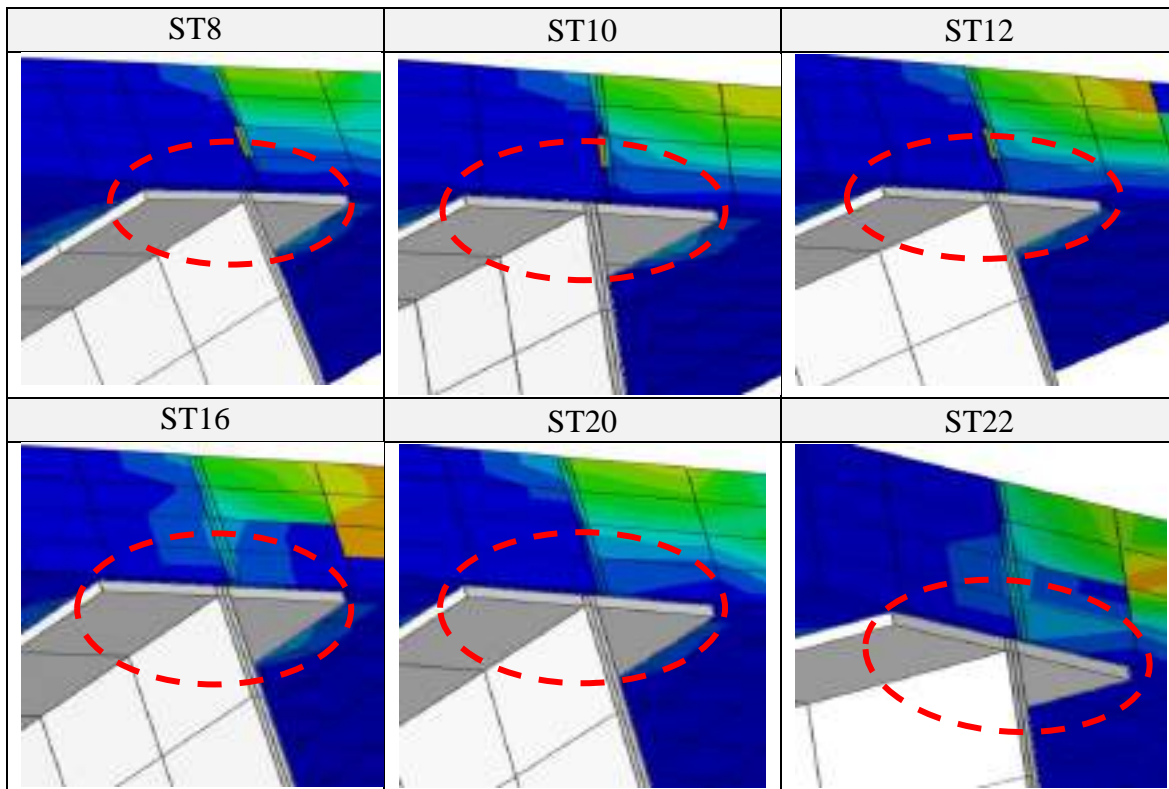
Figure (4-28): Effect of the shear connector on the interface separation between the concrete slab and the steel beam.

ST24	ST26	ST30
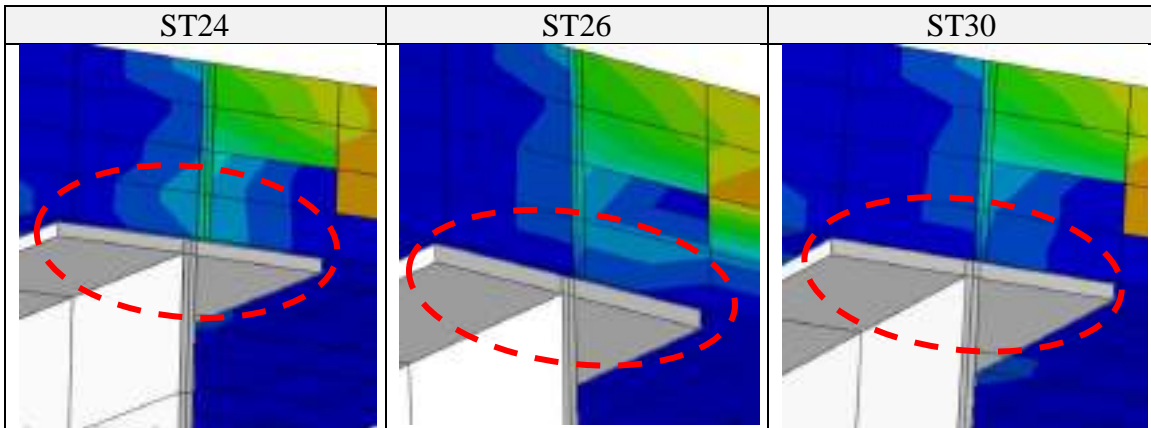
Figure (4-28): Continued.

Moreover, the distribution of flexural cracks in the tension region of concrete slab is found to be lowered as the stud number increases, where the cracks in the lower slab surface gradually decrease to include the lower middle area of a concrete slab under loading surface and the stud area as seen in Fig. (4-29). Additional cracks are observed in the slab compression face essentially in the centroid zone, in which the slab causing compresion mode failure as seen in Fig. (4-30).

ST8	ST10	ST12
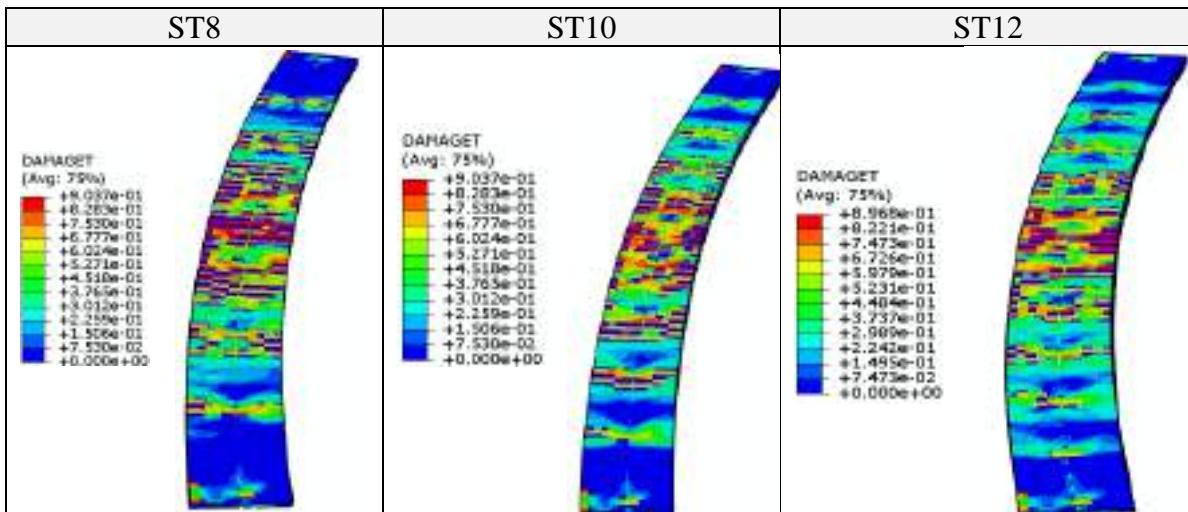
Figure (4-29): Effect of the shear connector on the tension side of the concrete slab.

ST16	ST22	ST24

ST24	ST26	ST30
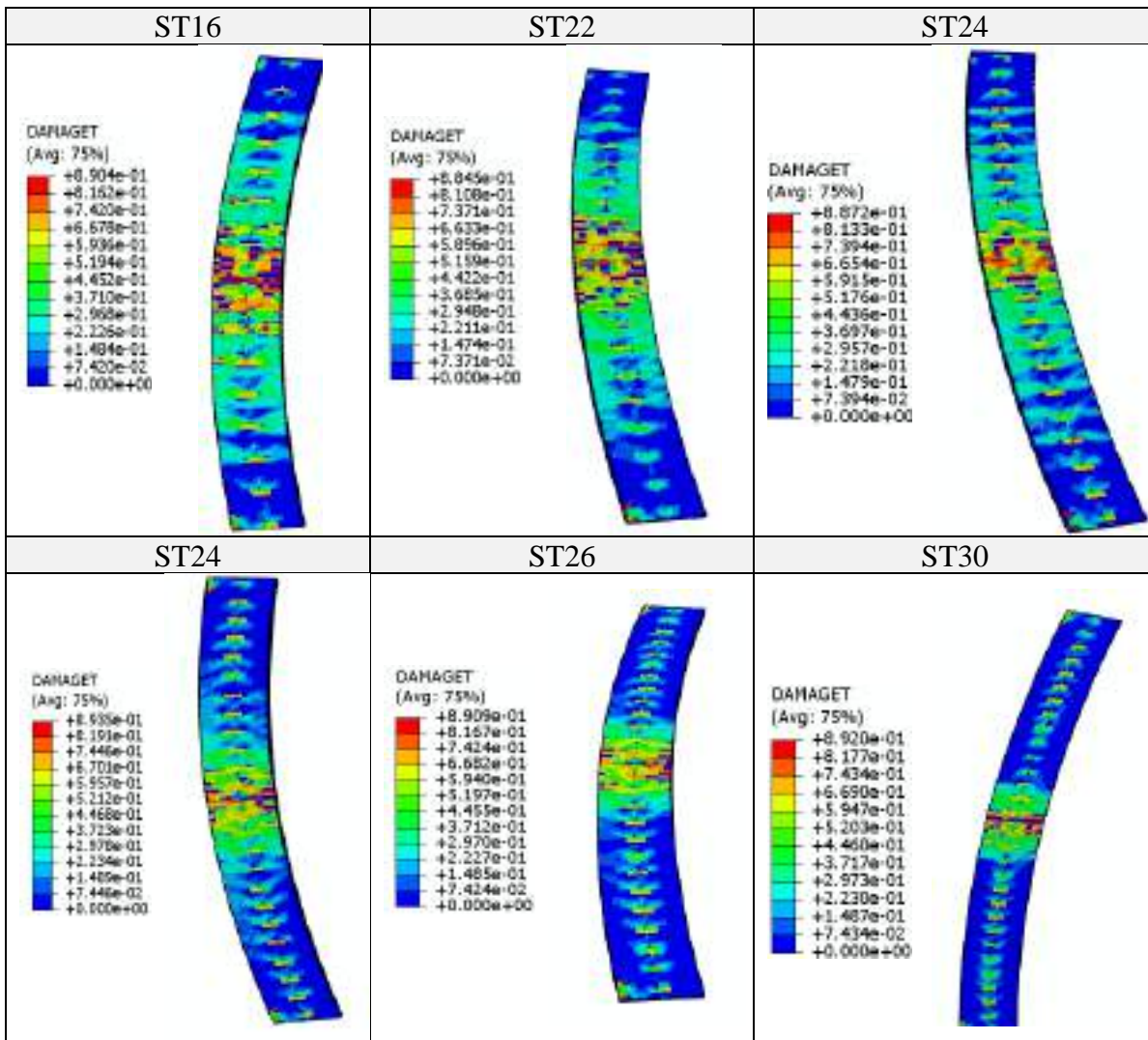
Figure (4-29): Continued.

ST8	ST10	ST12
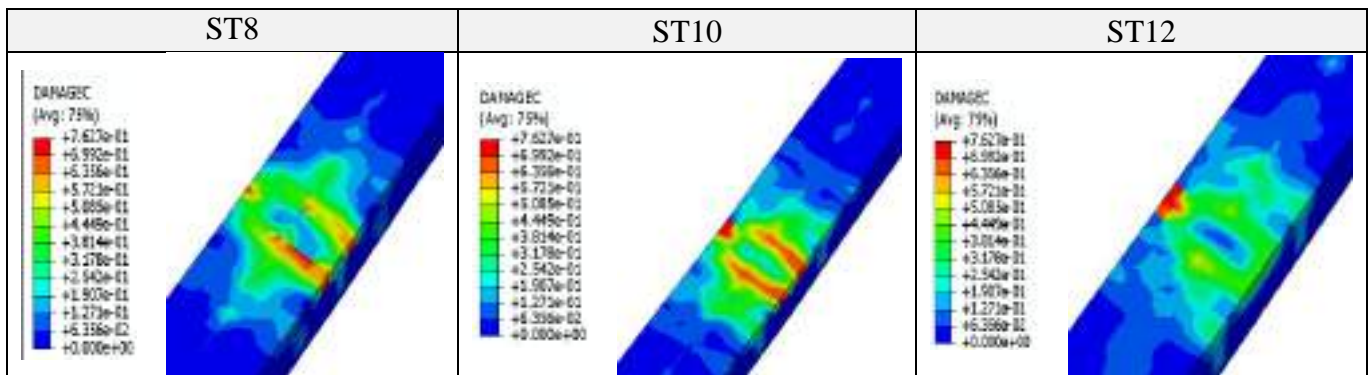
Figure (4-30): Effect of the shear connector of the concrete slab compression surface.

ST16	ST20	ST22
ST24	ST26	ST30
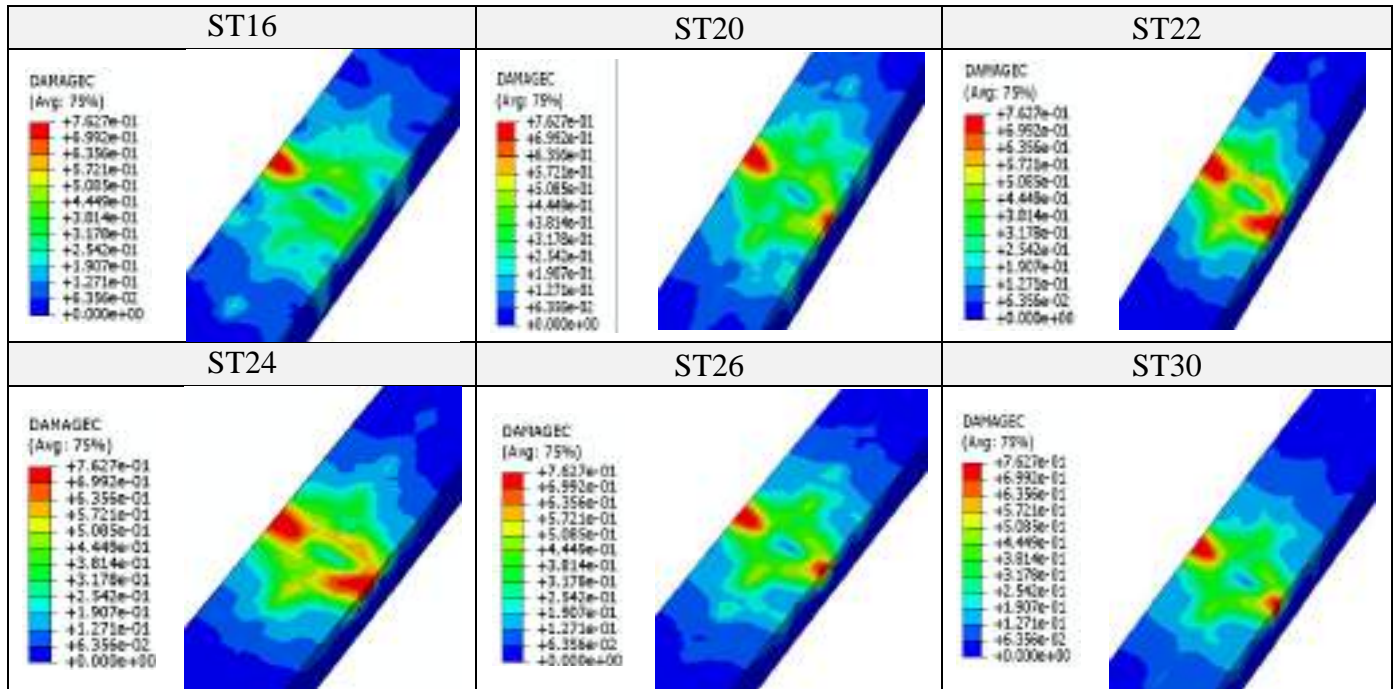
Figure (4-30): Continued.

Furthermore, the strain distribution in the mid span, Fig. (4-31) show that the beams record increase in the beam strain with partial ratio increases. Thus the partial interaction effect must be considered for the analysis accuracy. The strength and the stud shear connector stiiffness should be considered in the inelastic analysis of curved composite steel-concrete beam, whrere the full interaction assumption may overestimate the ultimate strength and underestimate the beam deflection.

ST8	ST10
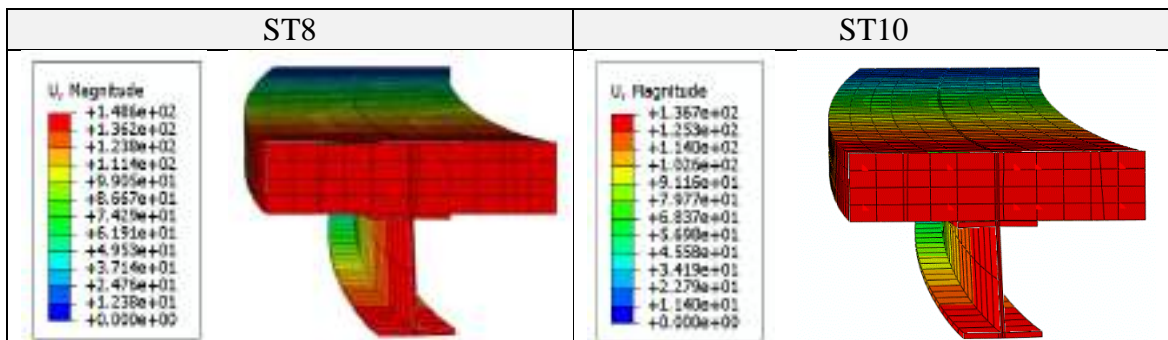
Figure (4-31): Effect of partial interaction ratio on strain distribution of the curve composite beam at mid-span.

ST12	ST16
ST20	ST22
ST24	ST26
ST30	
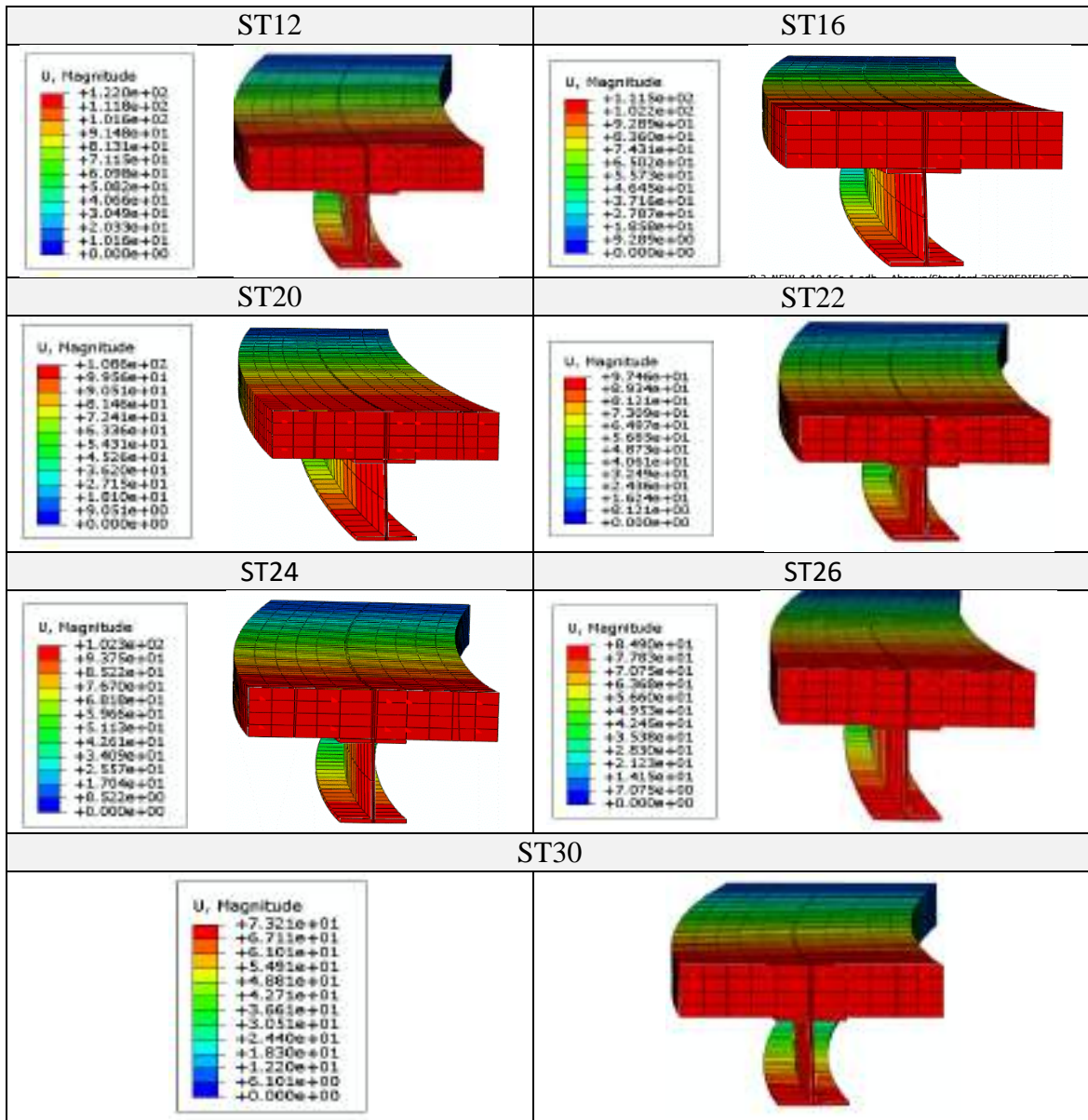
Figure (4-31): Continued.

4.6.4 The steel beam yield stress effect

The yield stress of steel beam is adapted to discuss the parameter influence on the inelastic behavior and the performance of the curved

composite beam. The model CCBP-2 was contrived to investigate the steel beam yield stress effect.

Six curved composite beams designed as simply supported, identified as S200, S250, S300, S350, S400 and S450 that represent the beams with yield stress values for the web and flanges of the steel beam are 200, 250, 300, 350, 400 and 450 MPa are seen in Table (4-13). On the steel flange top surface, the headed shear studs were welded in a single row with a diameter, length, and spacing of 19 mm, 100 mm, and 450 mm, respectively. Moreover, the concrete compressive strength is 39.1 MPa.

Table (4-13). Curved composite beam details for steel beam yield strength effect.

Beam type	Specimen (Si)	Yield strength of the steel beam f_y MPa	Central angle (°)	Degree of shear connection (%)
CCBP-2	S200	200	16.85	50
	S250	250	16.85	50
	S300	300	16.85	50
	S350	350	16.85	50
	S400	400	16.85	50
	S450	450	16.85	50

Figures (4-32) and (4-33) show different load-deflection and the load-yield stress relations of the curved composite beam. From the FE analysis, the increase of the yield stress of steel beam leads to increase both yield load and ultimate load. The ratio of increase the ultimate load of specimens (S250, S300, S350, S400 and S450) compared with that of S200 are 1.14, 1.30, 1.41, 1.47 and 1.58, respectively, as shown in Table (4-14). Also, from the same table, it can be seen that the predicted vertical deflections almost a significant increase in all specimens with a ratio ranged between (4.7-25.5) % compared

with S200. Furthermore, it can be observed from the load versus vertical deflection curves in Fig. (4-32) that all the numerical curves appear to increase in the ductility index of composite beams by 61% significantly with the increasing the steel beam yield stress as seen in Table (4-14).

Moreover, in the specimens with high yield stress, especially for S450 a number of flexural cracks can be noticed as can be illustrated in Fig. (4-34), in which the number of cracks increases as well as the stresses increase. However, the stress distribution of steel beam is found to be changed as the yield stress increases especially in specimen S450 as seen in Fig. (4-35). The vertical and interface slip effect is either negligible or ineffective as seen in Fig. (4-35). Furthermore, the strain distribution in the mid span, Fig. (4-36) show that the beams record increase in the beam strain with steel beam yield stress increases.
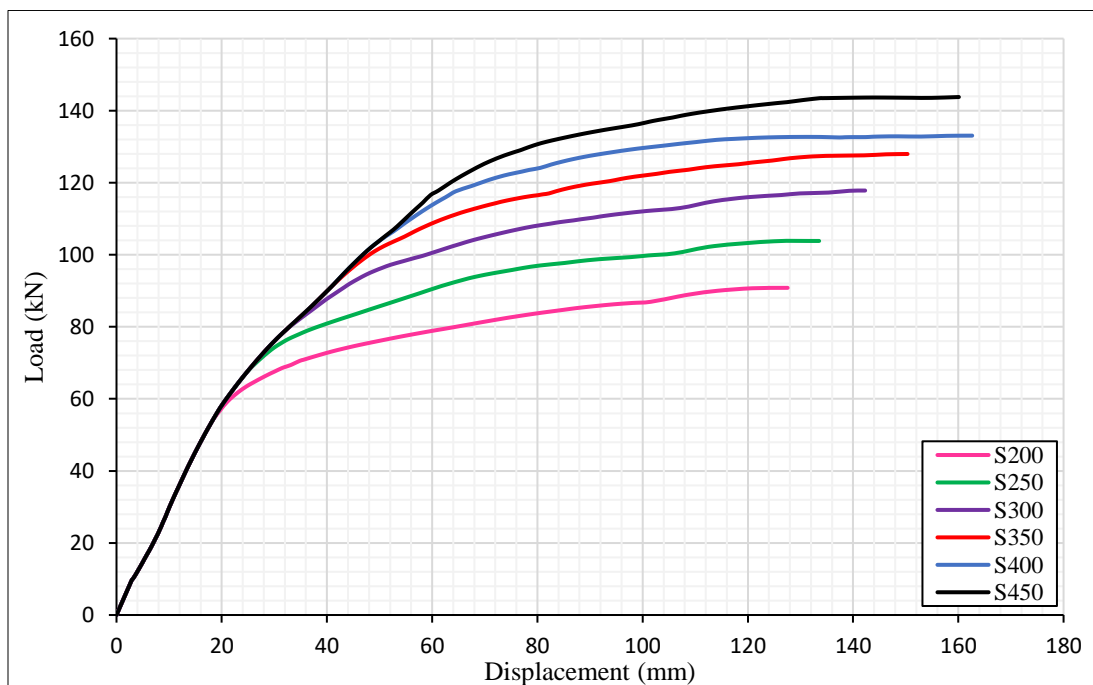
Figure(4-32): The steel beam yield stress on the load-deflection curve.
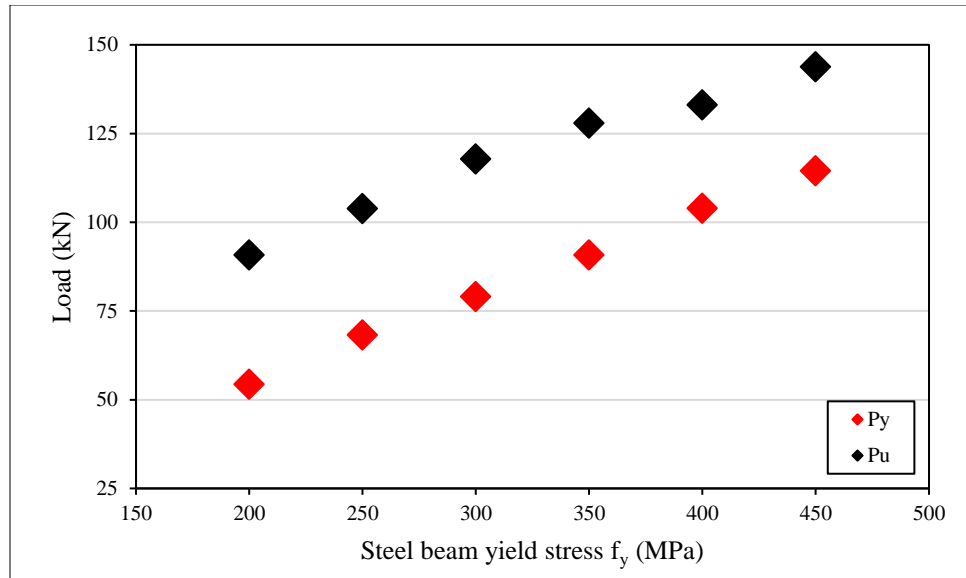
Figure (4-33): Yield and ultimate load vs yield stress.

Table (4-14): Curved composite beam results under steel beam yield stress effect.

| Specimen (Si)	F_{ySi} (kN)	F_{uSi} (kN)	Δ_u (mm)	$\dfrac{F_{ySi}}{F_{yS200}}$	$\dfrac{F_{uSi}}{F_{uS200}}$	$\dfrac{\Delta_{uSi}}{\Delta_{uS200}}$	Ductility index (Δ_u/Δ_y)
S200	54.36	90.82	127.56	1.00	1.00	1.00	2.7
S250	68.28	103.84	133.55	1.26	1.14	1.05	3.2
S300	79.06	117.83	142.83	1.45	1.30	1.12	3.7
S350	90.82	127.97	150.35	1.67	1.41	1.18	4.4
S400	105.14	133.07	162.64	1.93	1.47	1.28	5.3
S450	114.5	143.78	160.10	2.11	1.58	1.26	6.9
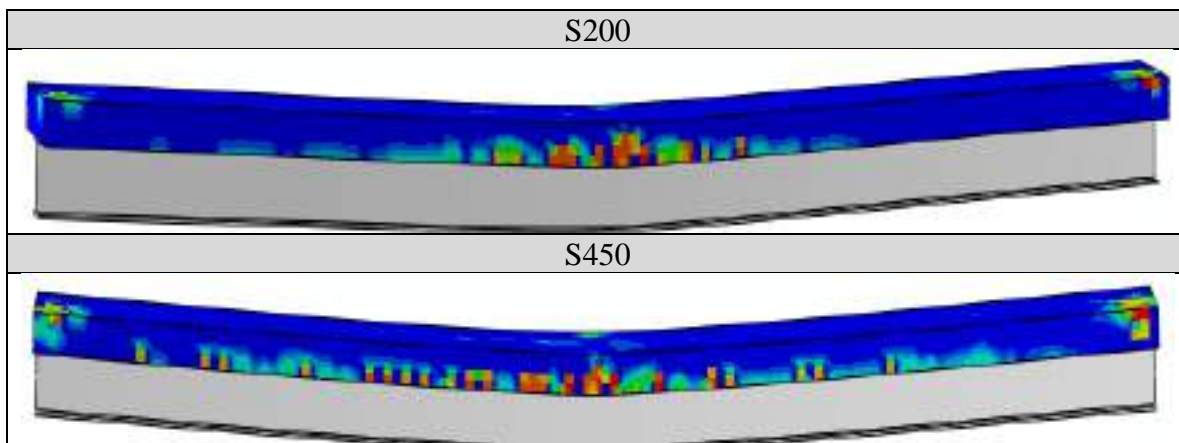
Figure (4-34): Effect of steel beam yield stress on the beam flexural cracks.

S200	S250
S300	**S350**
S400	**S450**
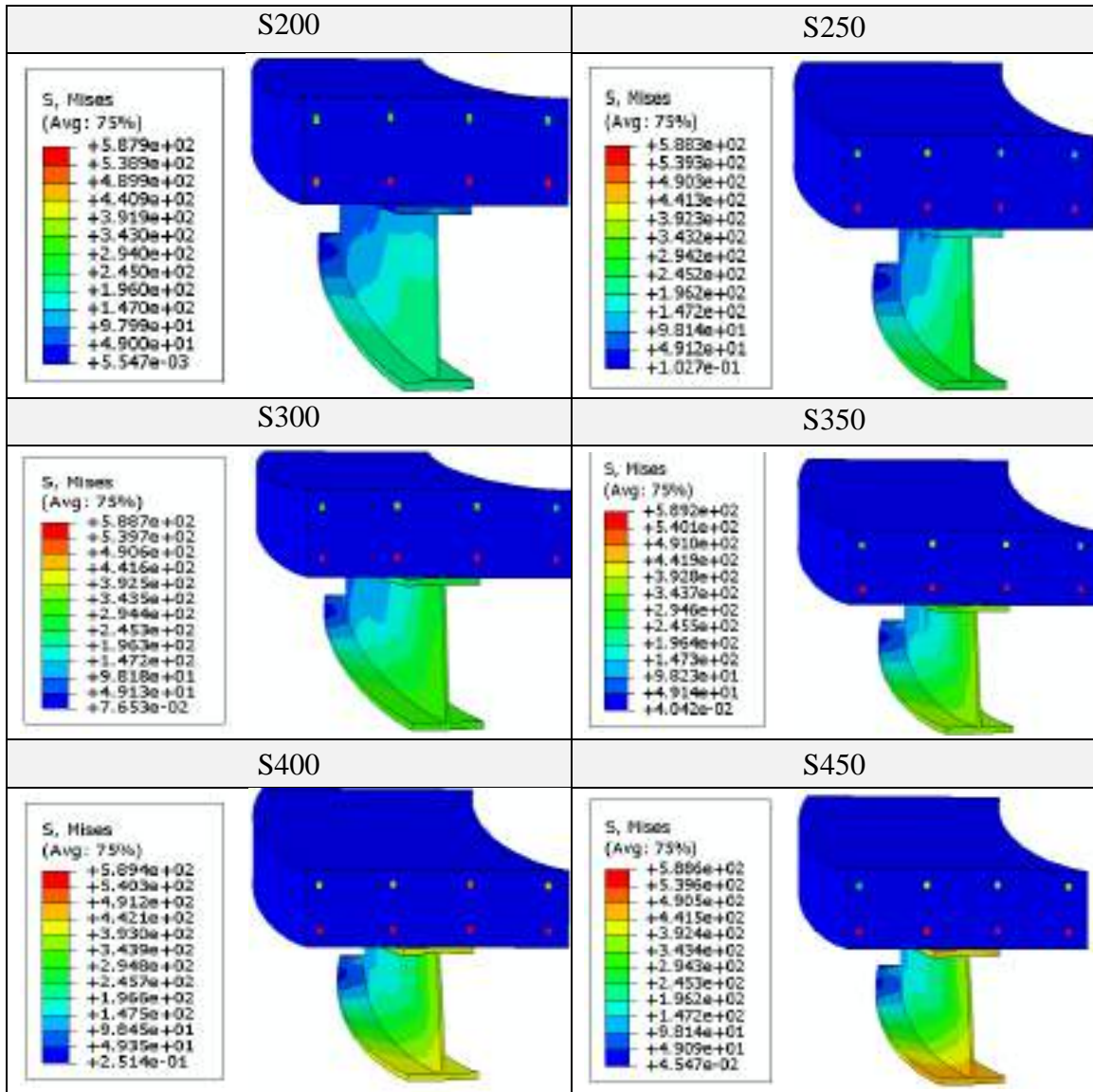
Figure (4-35): Show the stress distribution of specimen at mid-span under steel beam stress effect.

S200	S250
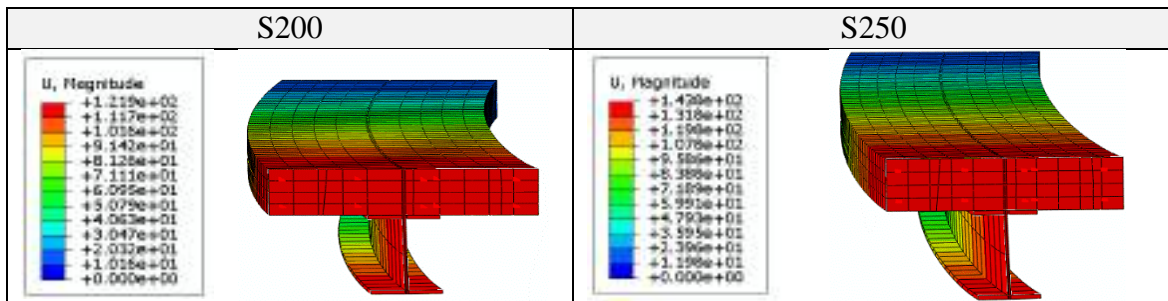
Figure (4-36): Effect of steel beam yield stress on strain distribution of the curve composite beam at mid-span.

S300	S350

S400	S450
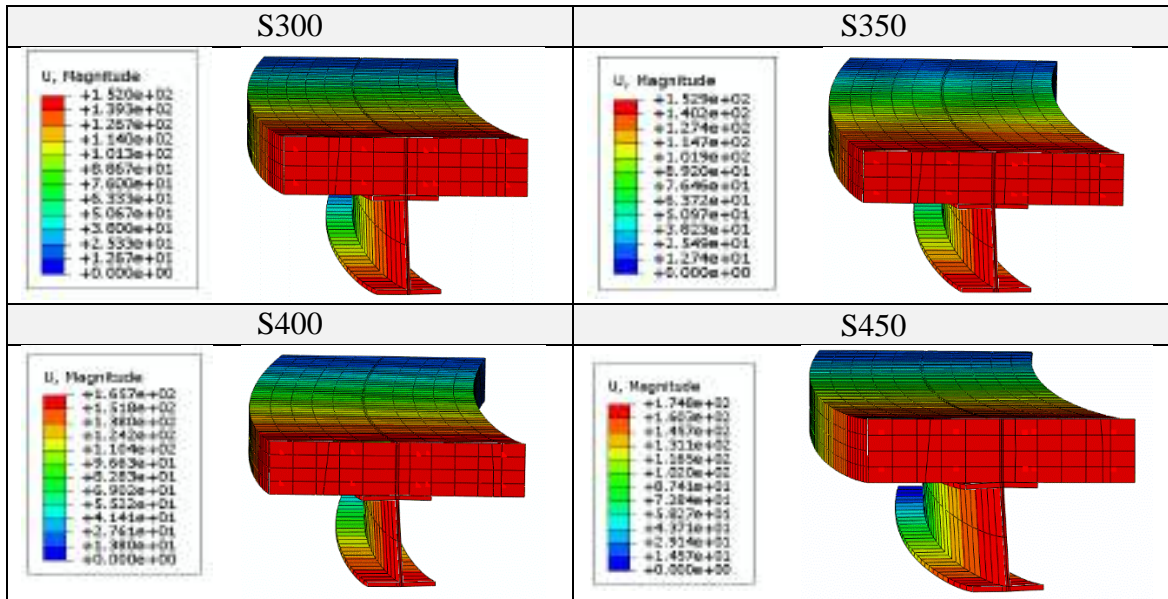
Figure (4-36): Continued.

4.6.5 The concrete slab's compressive strength effect

Concrete slab compressive strength effect is introduced by using various values for concrete grades of C30, C40, C50. These values represent the concrete compressive strength values in most design standards for normal weight concrete. The analysis is performed on the specimen A-30 (with 30° an central angle).

Table (4-15) illustrated the specimens C_{30}, C_{40} and C_{50} with concrete compressive strength 30, 40 and 50 MPa, respectively. The headed studs were welded in a single row to the steel flange top surface with a diameter, length, and spacing of 19 mm, 100 mm, and 450 mm, respectively. The properties of concrete material including the characteristic compressive strength f_{ck}, the mean value of compressive and the tensile strength f_{cm} and f_{ctm}, respectively, and the modulus of elasticity E_{cm} are in accordance to Eurocode 2 [82], Table (4-16).

Table (4-15). Detail of curved composite beam with varied compressive strength of concrete.

Beam type	Specimen (Ci)	Compressive strength (f_{cm}) MPa	Central angle (°)	Degree of shear connection (%)
A-30	C30	30	26.04	50
	C40	40	26.04	50
	C50	50	26.04	50

Table (4-16). Properties of concrete slab.

Concrete properties	Curved composite beam		
	C30	C40	C50
f_{ck} (MPa)	22	32	42
f_{cm} (MPa)	30	40	50
f_{ctm} (MPa)	2.36	3.02	3.79
E_{cm} (GPa)	30.6	33.35	35.65

Figures (4-37) and (4-38) show the load versus deflection and the load versus concrete compressive strength of the beams. It can be seen that the specimen C30 exhibits more ductility comparing with the other two beams by 29%, Table (4-17). Moreover, the load carrying capacity increases about 15.86 % and 34.4% for specimens C40 and C50 compared with C30, respectively. However, the effect of increasing compressive strength of concrete slab is slight at the yielding stage with 8.4% as maximum value. This effect becomes significant at the ultimate stage as shown in Table (4-17).

From Figures (4-37) and (4-38), it can be seen that the deflection at ultimate stage is decreased with increasing of the concrete compressive strength. The ratio of decreasing deflection is 8% and 18% for specimen C40 and C50, respectively. Concerning the flexural crack patterns, the cracks seem

to be less remarkable when compared with the above two parameters as seen in Fig (4-39). Furthermore, concrete compressive strength increases do not affect the vertical interface slip between steel flange and concrete slab as seen in Fig. (4-40). Moreover, the strain distribution in the mid span, Fig. (4-41) show that the beams record decrease in the beam strain with compressive strength increases. From results it was shown that the compressive strength was the least influential factor effect on the curve composite beam behavior.
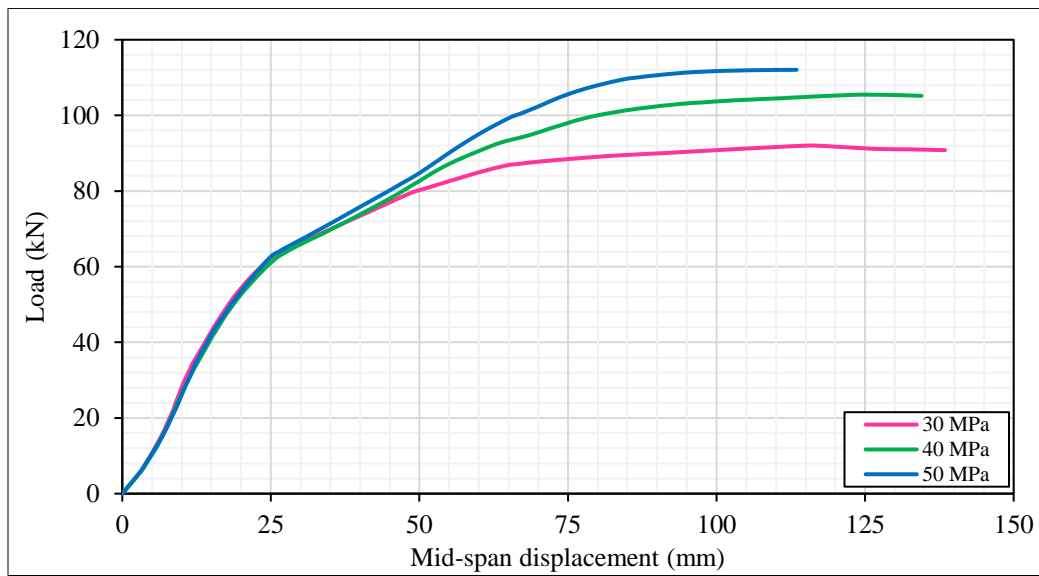
Figure (4-37): Effect of the compressive strength on the load-deflection curve.

(a) Beam strength
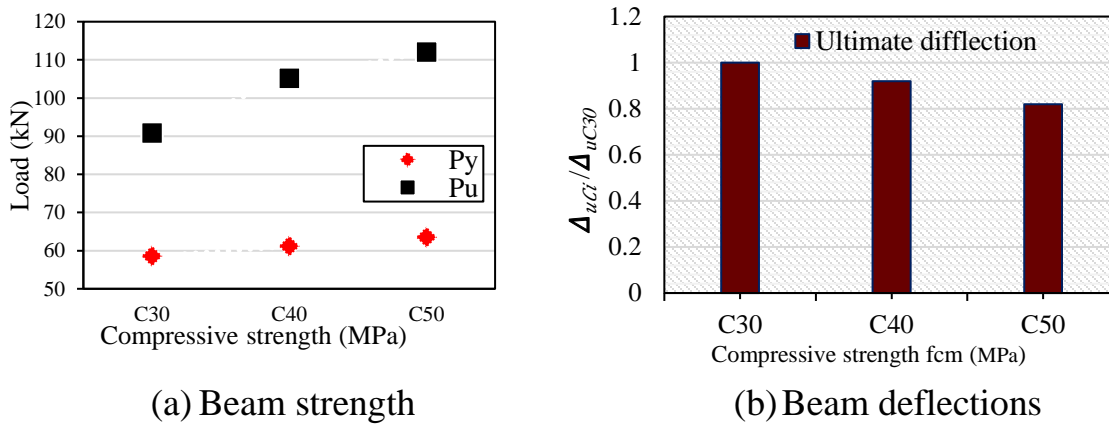
(b) Beam deflections

Figure (4-38): The concrete compressive strength effect on the ultimate strength and the ultimate deflection of the composite curved beam.

Table (4-17): Curve composite beam results under compressive strength effect.

Specimen (Ci)	F_{yCi} (kN)	F_{uCi} (kN)	Δ_u (mm)	$\dfrac{F_{yCi}}{F_{yC30}}$	$\dfrac{F_{uCi}}{F_{yC30}}$	$\dfrac{\Delta_{uCi}}{\Delta_{uC30}}$	Ductility index (Δ_u/Δ_y)
C30	58.52	90.82	138.45	1.00	1.00	1.00	6.2
C40	60.17	105.2	127.37	1.03	1.16	0.92	5.2
C50	63.45	112.04	113.48	1.08	1.23	0.82	4.4
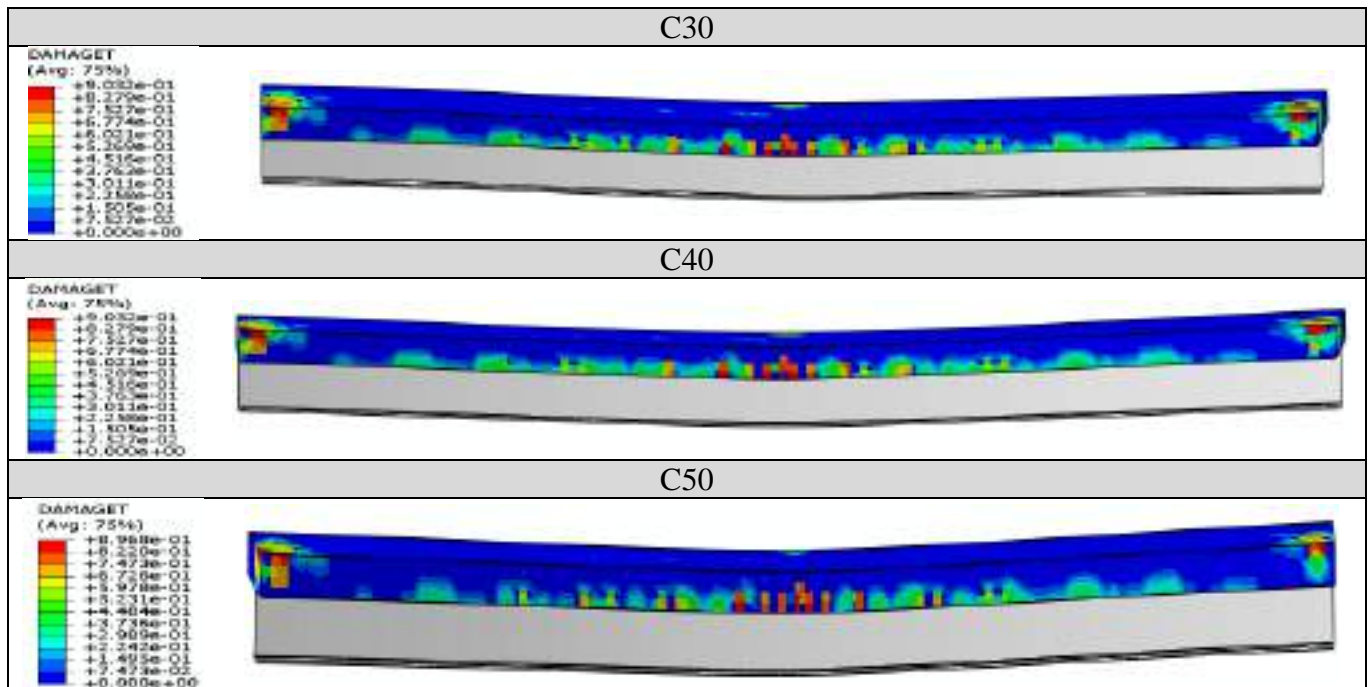
Figure (4-39): Effect of concrete slab compressive strength on the beam flexural cracks.
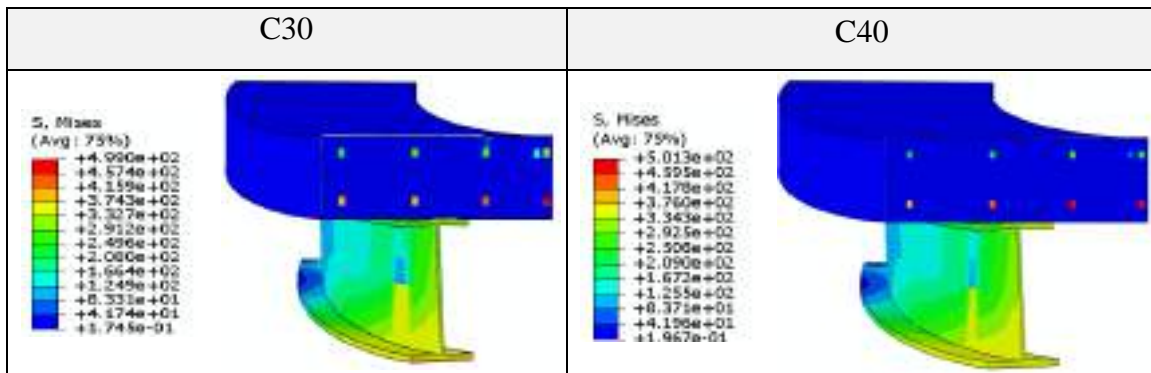
Figure (4-40): Effect of the compressive strength on the vertcial separation between the concrete slab and the steel beam.

C50
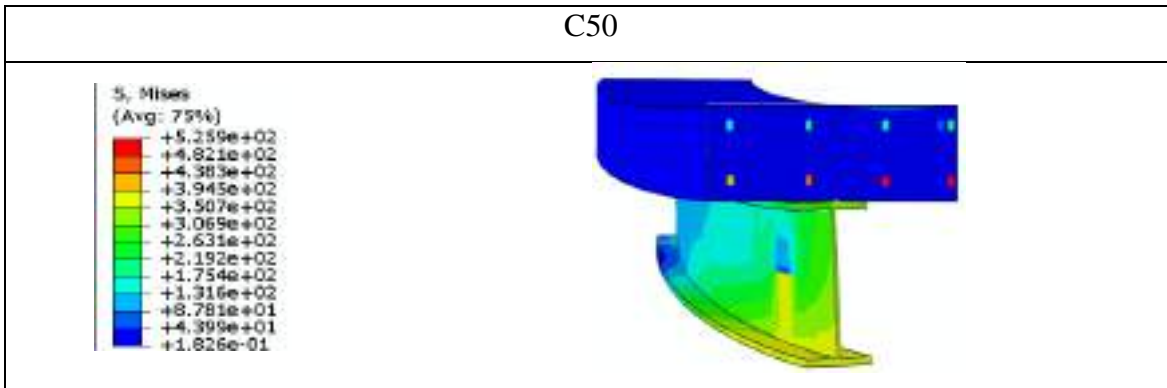
Figure (4-40): Continued.

C30	C40
C50	
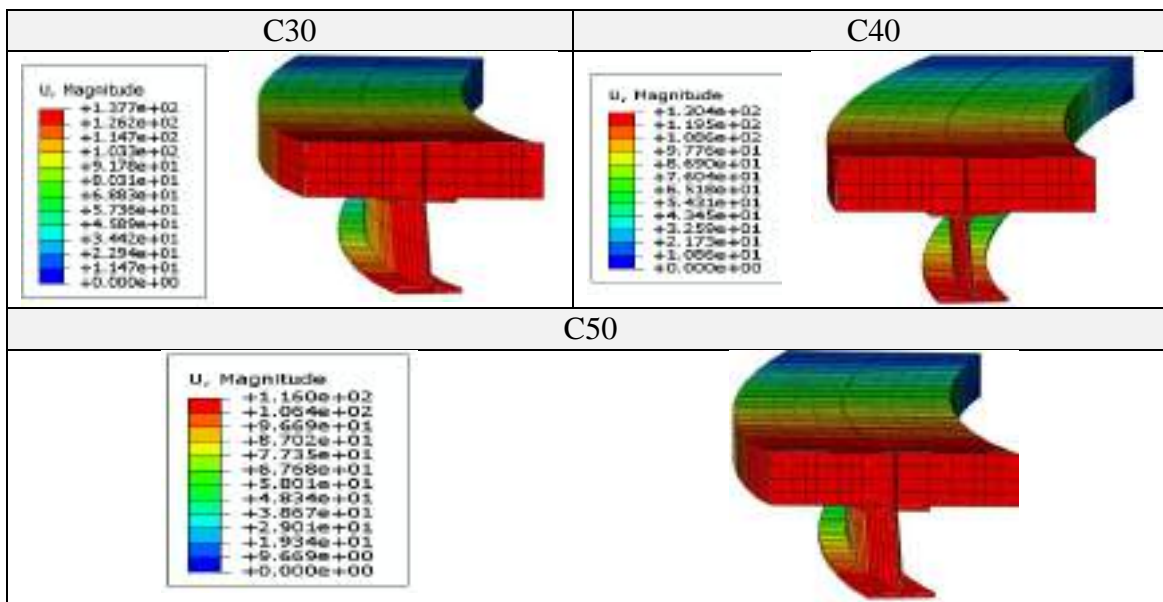
Figure (4-41): Effect of compressive strength on strain distribution of the curve compoeite beam at mid-span.

4.6.6 Effect of steel beam opening

The use of composite beam with opening is a practical solution when it is required to pass service ducts through the structural zone of the beams. A common method of incorporating services within the floor–ceiling zone of buildings using in the construction is to create large openings in the webs of the I-sections. In recent years, some of the curved steel members that used in

modern building systems are designed with opening to reduce the wight of the member. The openings may be rectangular or circular, and may be in the form of discrete openings, or a series of openings, along the beam [92].

In this thesis the influence of the opening was investigated with various situations to demonstrate the curve composite beam behavior; opening depth, shape and strengthening effect by web stiffeners. The model CCBF-2 with central angle 17.4° was contrived to investigate the opening influence on the curve composite beam inelastic behavior.

Ten models were designed as simply supported as seen in Fig. (4-42) and Table (4-18), and were designed by them with full shear connection by two rows with a diameter, length, and spacing of 19 mm, 100 mm, and 450 mm, respectively. Moreover, concrete slab nominal compressive strength was 41.5 MPa.
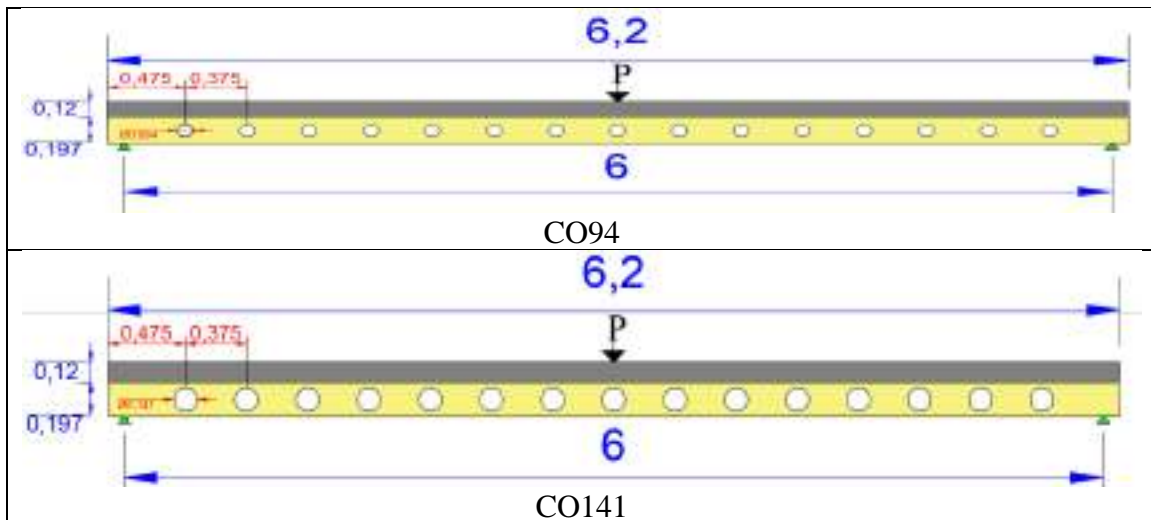
Figure (4-42): Geometry and dimensions of the curved composite steel–concrete beam with opening (unit: m).
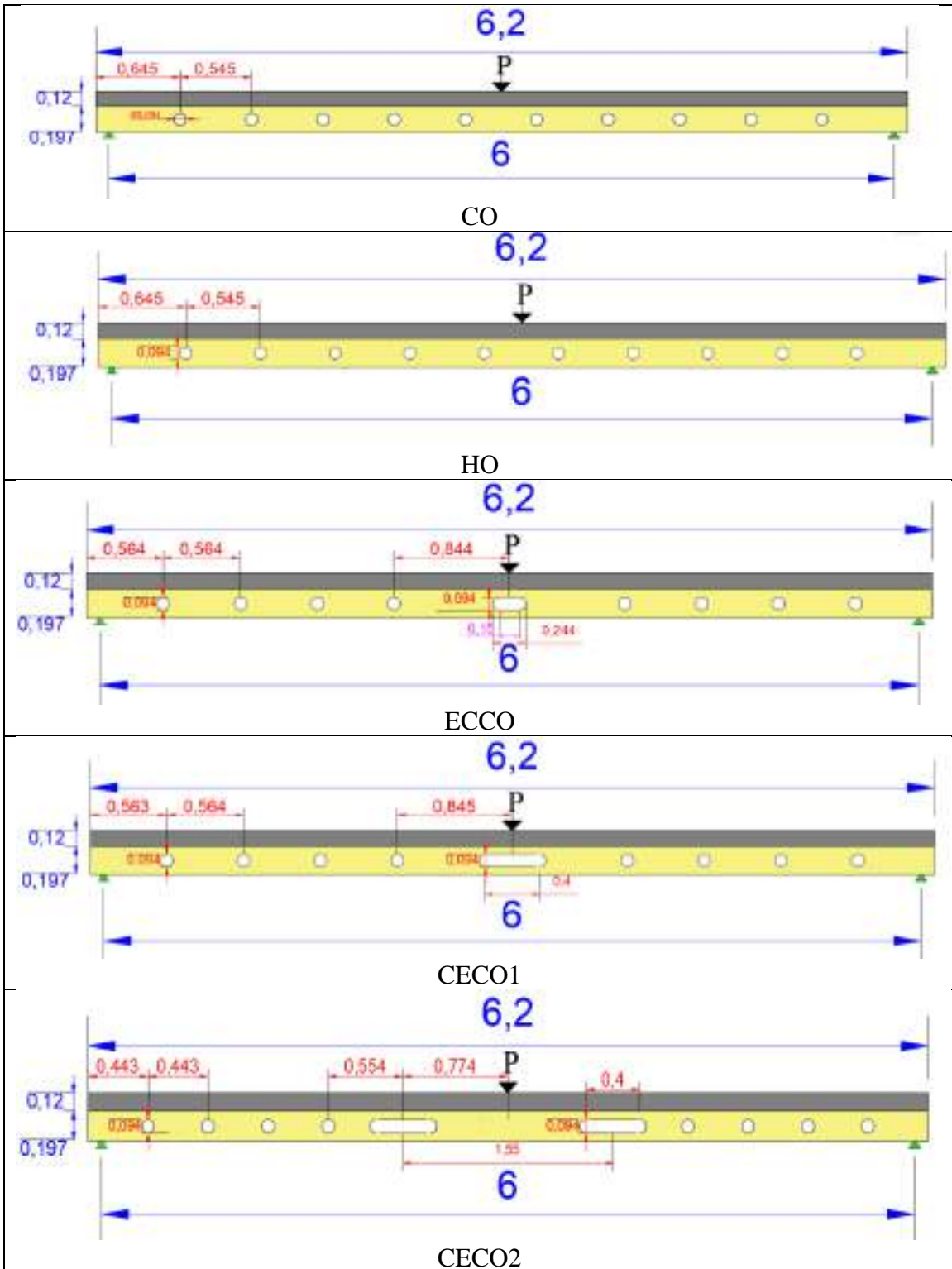
Figure (4-42): Continued.
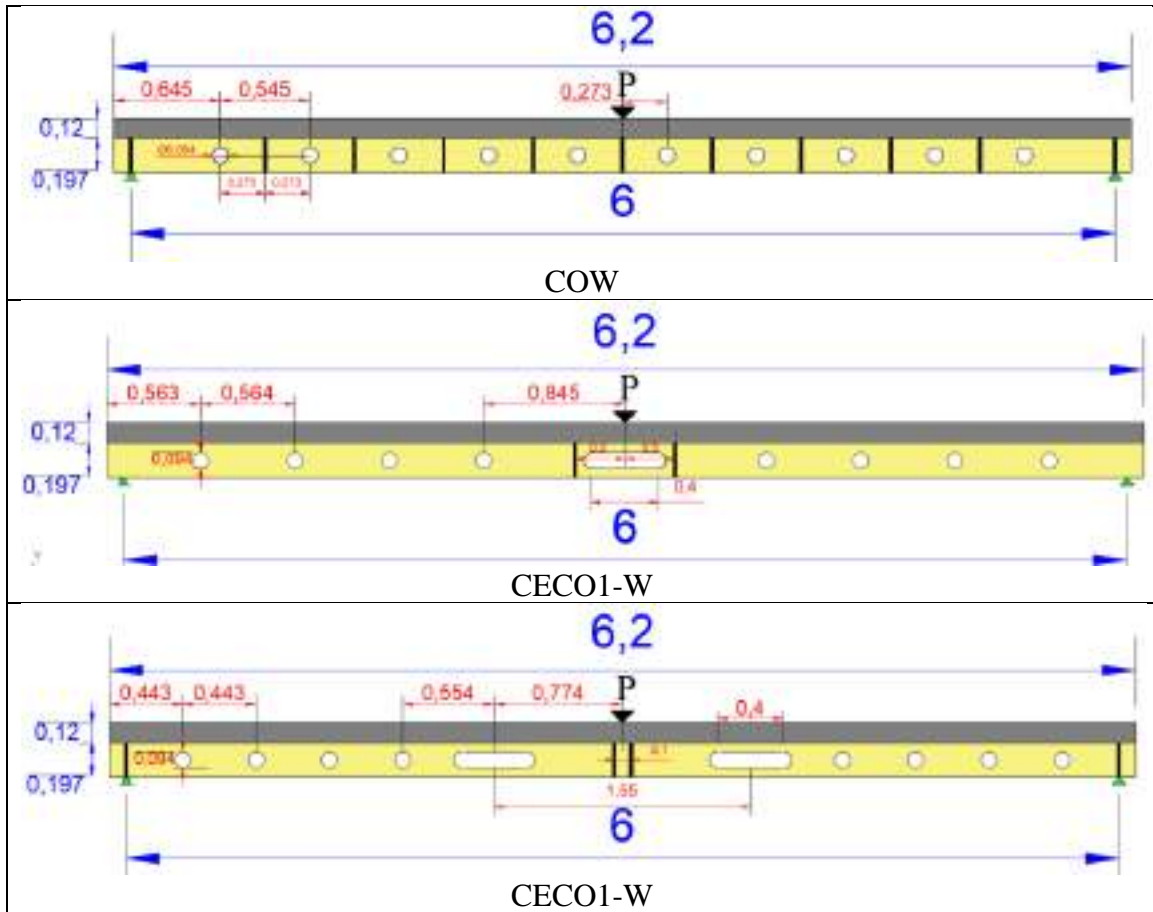
Figure (4-42): Continued.

Table (4-18). Curve composite beam details for opening effect.

Beam type	Specimen	Opening shape	Opening size (mm)	Opening number	Opening depth from web (ih)	Stiffeners number
CCBF-2	CO94	Circle	94	15	0.5h	-
	CO141	Circle	141	15	0.75h	-
	CO	Circle	94	10	0.5h	-
	HO	Hexagonal	94	10	0.5h	-
	ECCO	Elongated circle-circle	244×94	1-8	0.5h	-
	CECO1	Circle-elongated circle	494×94-94	8-1	0.5h	-

Table (4-18). Continued, Curve composite beam details for opening effect.

Beam type	Specimen	Opening shape	Opening size (mm)	Opening number	Opening depth from web (ih)	Stiffeners number
CCBF-2	CECO2	Circle-elongated circle	494×94-94	8-2	0.5h	-
	COW	Circle	94	10	0.5h	11
	CECO1-W	Circle-elongated circle	494×94-94	8-1	0.5h	4
	CECO2-W	Circle-elongated circle	494×94-94	8-2	0.5h	4

A. Opening size

Two beams are considered to study the opening size effect (CO94 and CO141) with circular opening 0.5h and 0.75h; respectively, in which h is the steel beam height, placed from web vertex at distance 47 and 23.5 mm, respectively.

Form the model's analysis, for CO94 and CO141, the flexural cracks developed when increasing the applied load slightly to 55.54 kN and 46.51 kN for CO94 and CO141; respectively, while the diagonal torsional cracks of concrete are observed at beam. The maximum recorded load is 95.66 kN and 88.40 kN with vertical deflection of 66.09 mm 63.10 mm. Furthermore, it was noticed that the beam suffers from excessive twisting at mid-span as well as the opening depth increase as shown in Fig. (4-43).

Furthermore, from Fig. (4-44) of the load versus vertical deflection at mid span, it can be noted that increasing the opening depth show reduction in

the stiffness and beam capacity while the ductility index shows an approximate behavior to the beam without opening. The model begins yield to develop at an early stage compared to the specimen without opening (CCBF-2) as seen in Table (4-19). Table (4-19) shows a comparison between CCBF-2 (model without opening) with the models CO94 and CO141 (with 0.5h and 0.75h opening depth), in which the records of yield load, ultimate load and vertical deflection decrease by (26% and 48), (11% and 18%) and (4% and 8%); respectively.

CO94	CO141
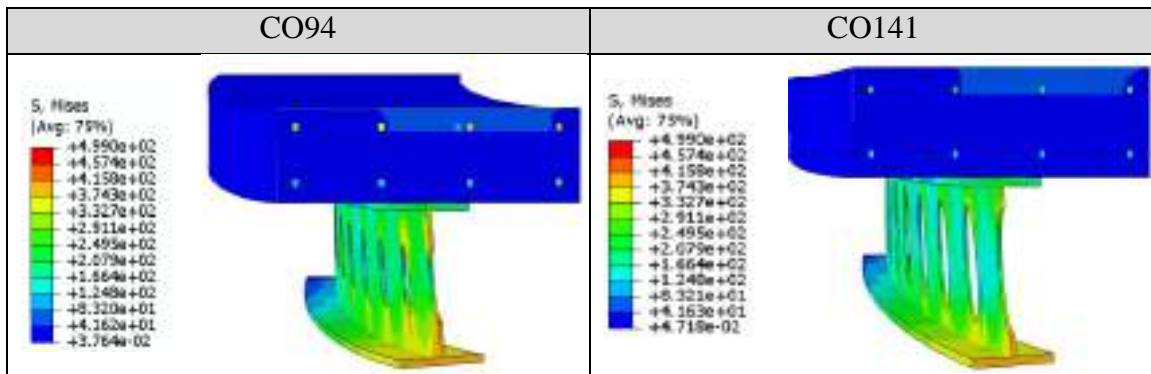
Figure (4-43): Efect of the opening depth on the composite beam twisting at mid-span.

Furthermore, it can be noted that increasing the opening depth causing the reduction in the stiffness of the curved composite beams. The steel beam twisting is significantly be evident as the opening depth increase which is attribute to the effect of torsion. This leads to conclude that the yielding of the beams becomes earlier with increasing the opening size. Moreover, the crack patterns of the curved beams show that the diagonal torsional cracks developed earlier and tension crack was found to concentrate in the centroid zone then widened and propagated toward the whole slab when the depth of the opening increased. The stress distribution for the specimens is show in

Fig. (4-45). Fig. (4-46) show the strain distribution under opening depth effect.
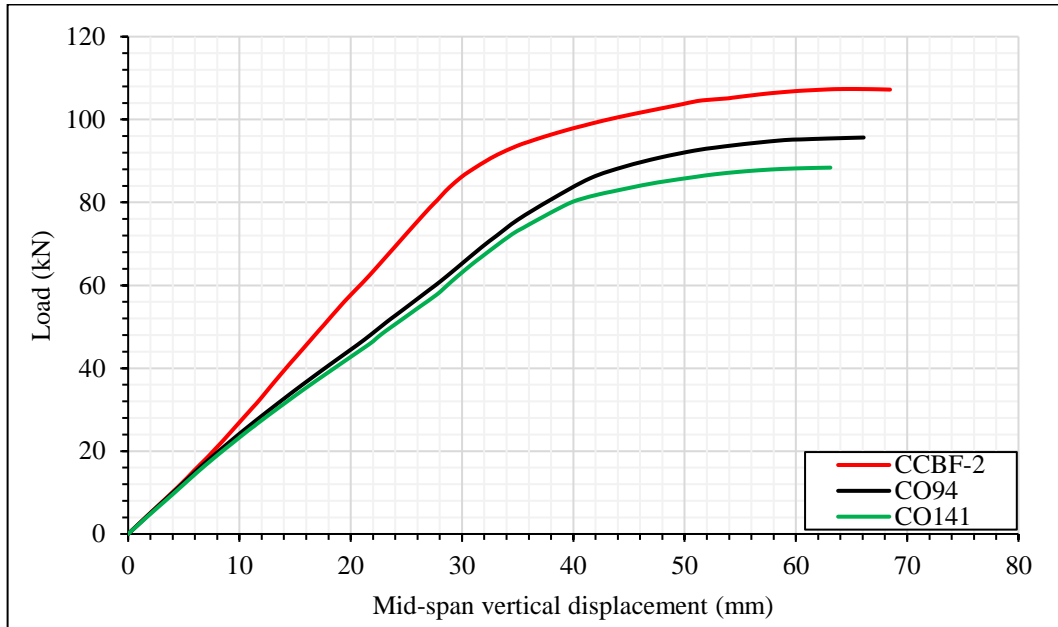
Figure (4-44): Opening depth effect on the load-deflection curve of the curve composite beam.

Table (4-19). Curve composite beam results under opening size effect.

Specimen	F_y (kN)	F_u (kN)	Δ_u (mm)	$\dfrac{F_{yCOi}}{F_{yCCBF-2}}$	$\dfrac{F_{uCOi}}{F_{uCCBF-2}}$	$\dfrac{\Delta_{uCOi}}{\Delta_{uCCBF-2}}$	Ductility index (Δ_u/Δ_y)
CCBF-2	86.12	107.37	68.46	1.00	1.00	1.00	2.3
CO94	64.17	95.66	66.09	0.75	0.89	0.97	2.2
CO141	44.81	88.40	63.10	0.52	0.82	0.92	2.2
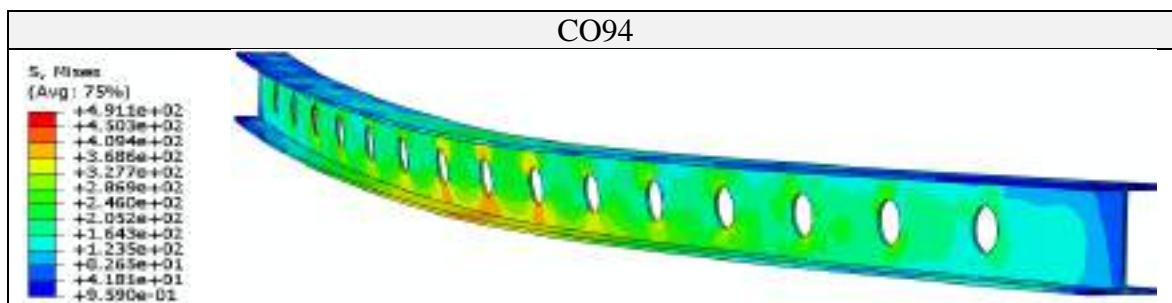
Figure (4-45): Effect of the opening depth on the steel beam stress distribution.

CO141
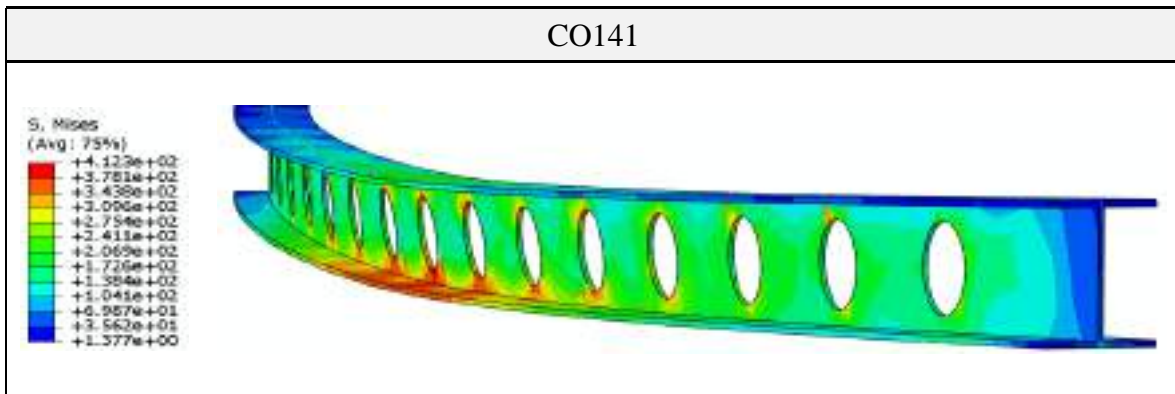
Figure (4-45): Continued.

CO94	CO141
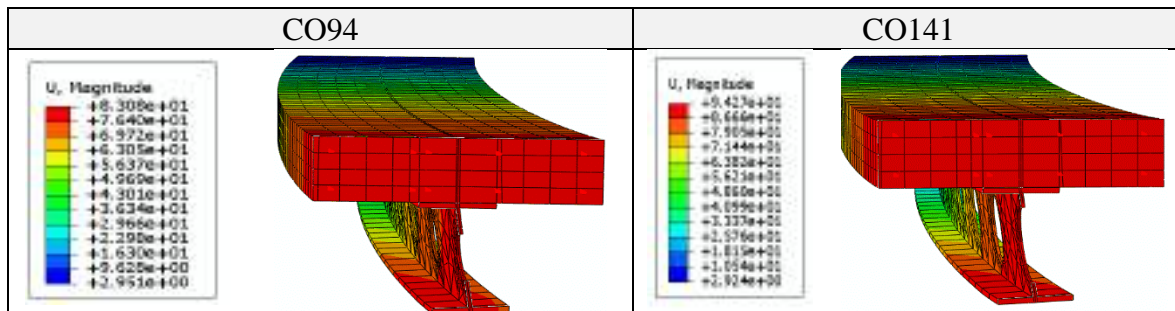
Figure (4-46): Effect of opening depth on strain distribution of the curve composite beam at mid-span.

B. <u>Opening shape</u>

Three beams are considered for opening shape effect, which are CO, HO and ECCO with circular, hexagonal and combined elongated circular and circular opening with 0.5h depth, in which h is the steel beam height, placed from web vertex at distance 47 mm.

In specimens CO and HO the ultimate capacity reduction was by approximatly 10% compared to the CCBF-2 (which was designed without opening). In these specimens stiffeness are decrease with opening providence, while the deflection are enhanced with a slight value. The diagonal torsional

cracks in the beam HO developed earlier compared to the beam without opening (CCBF-2). Furthermore, the flexural concrete cracks had been observed immediately as the load is applied incorporating with diagonal torsional cracks. The twisting at mid-span found to be increase Fig. (4-47).

Moreover, model ECCO began to yield at an early stage by 23% comparing with CO. Moreover, presence of elongated circular opening at the beam mid-span reduce the ductilty index by 14% and loading capacity of the specimen by about 24% as can be seen in Fig. (4-48) and Table (4-19) for ECCO compared to CCBF-2 (beam without opening). Moreover, the Von Misses stress distribution shows high stress concentration intensity in the beam mid-span for specimen ECCO as shown in Figures (4-47) and (4-49). Fig. (4-50) show the strain distribution under opening depth effect.
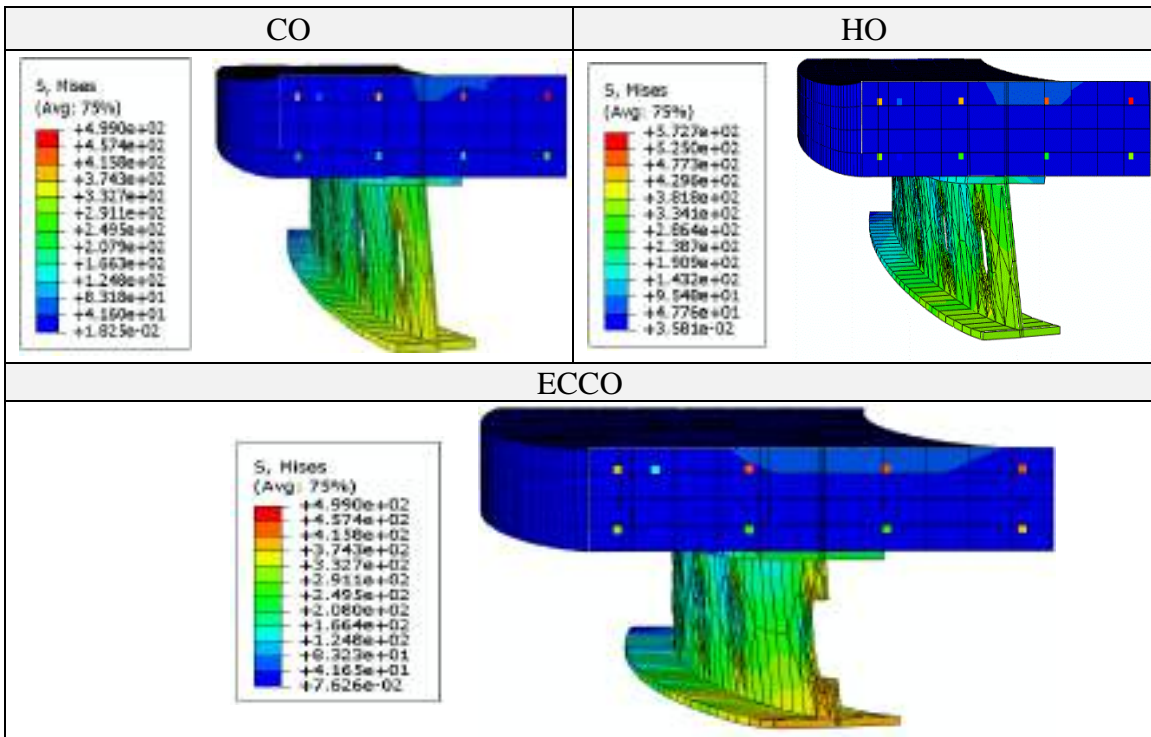
Figure (4-47): Effect of the opening shape on the steel beam twisting and stress distribution at mid-span.
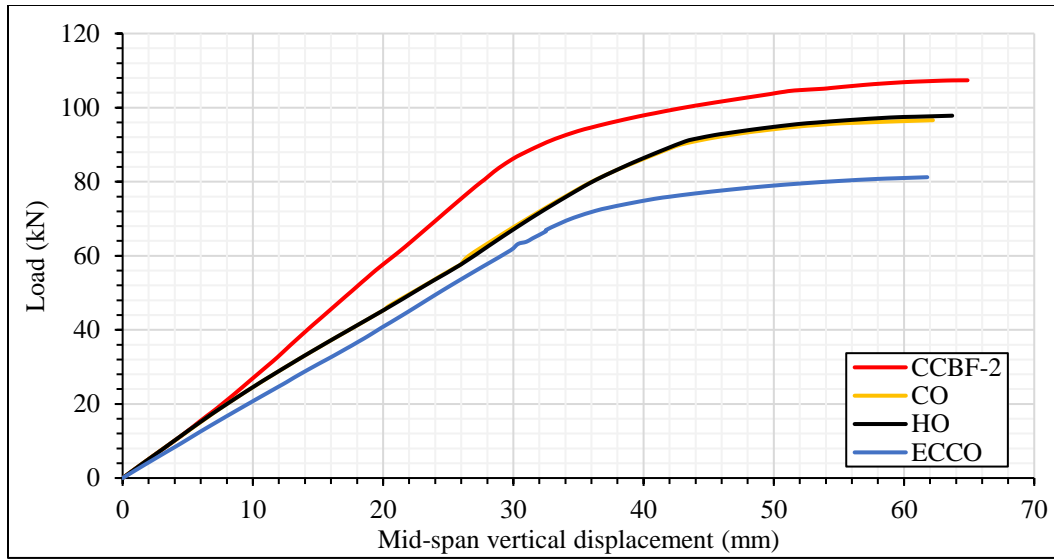
Figure (4-48): Effect of the opening shape on the load-deflection curve.

Table (4-20). Curved composite beam results under opening shape effect.

Specimen (i)	F_y (kN)	F_u (kN)	Δ_u (mm)	$\dfrac{F_{yi}}{F_{yCCBF-2}}$	$\dfrac{F_{ui}}{F_{uCCBF-2}}$	$\dfrac{\Delta_{ui}}{\Delta_{uCCBF-2}}$	Ductility index (Δ_u/Δ_y)
CCBF-2	86.12	107.37	66.09	1.00	1.00	1.00	2.2
CO	77.54	96.93	62.22	0.90	0.90	0.94	2.1
HO	76.94	98.05	63.70	0.89	0.91	0.96	1.8
ECCO	66.96	81.21	61.78	0.77	0.76	0.93	1.9

From above it can be concluded that the strength capacity reduced by about 24 % for beam designed with elongated circular opening at mid-span, the response of the specimens is softening and it yields in early stage. From Fig (4-48), it is evident that the elongated circular opening was the most effective shape on the beam strength, ductility and stiffness. Moreover, the torsion is found to be dominate and influential on the failure mechanism and inelastic behavior of the beam, especially in specimens with elongated circular opening (ECCO).
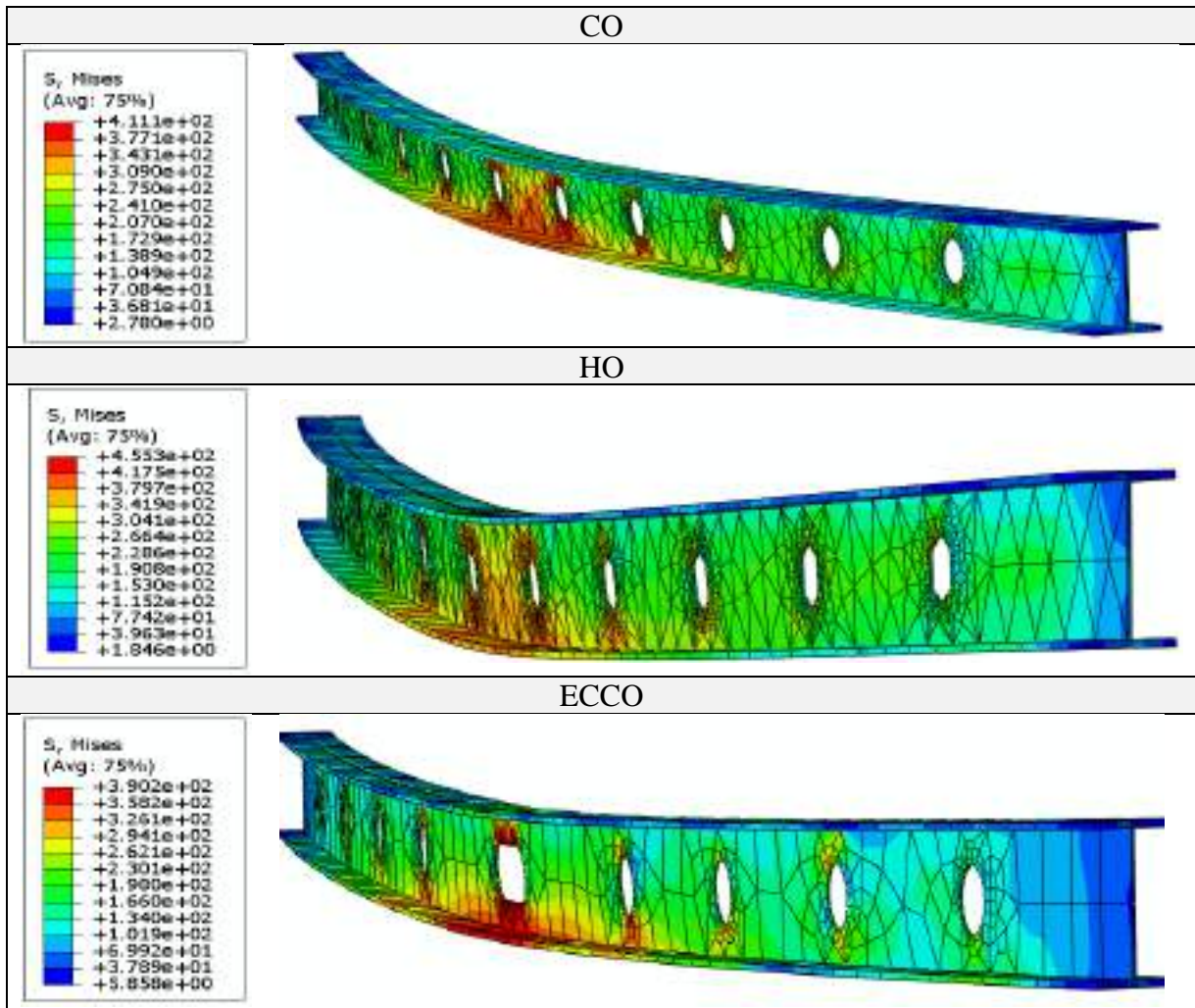
Figure (4-49): Efect of the opening shape on the steel beam stress distribution.
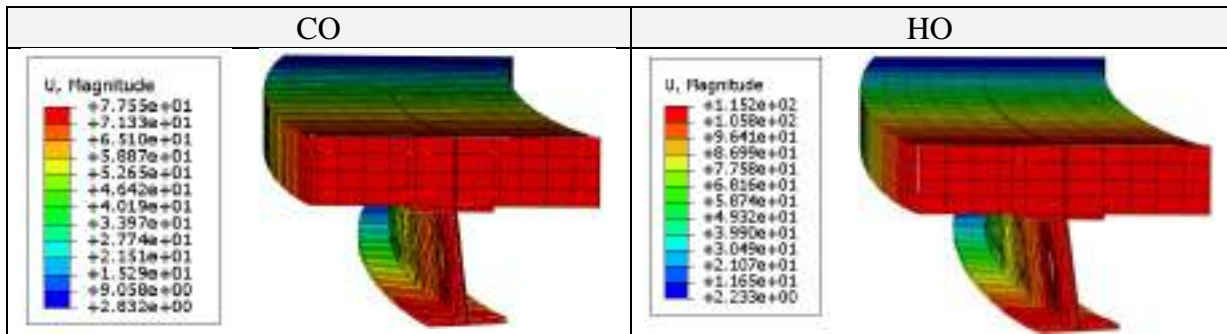
Figure (4-50): Effect of opening shape on strain distribution of the curve composite beam at mid-span.
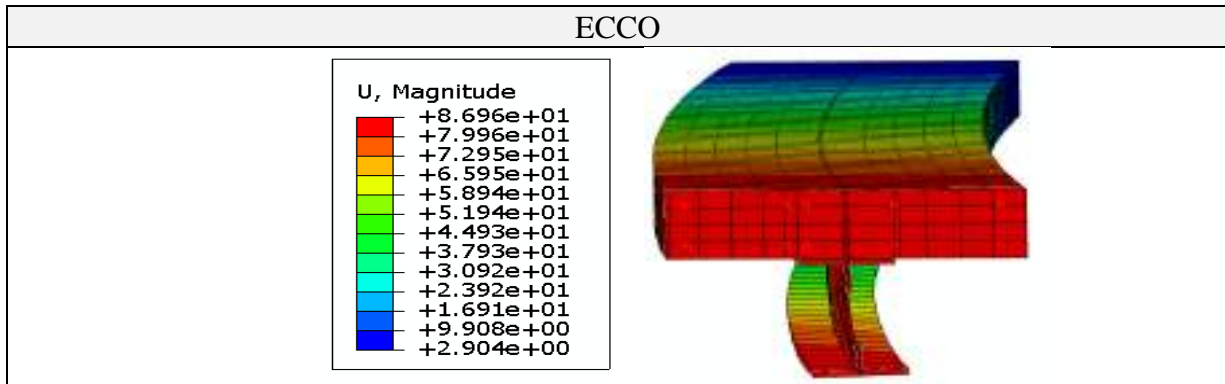
Figure (4-50): Continued.

Thus the effect of the opening shape should be taken into account for the analysis accuracy. Furthermore, however it is not possible to define an optimum shape because it depends on the opening location along the beam length.

C. Opening with stiffeners

Five beams are considered for web stiffeners study, to investigate their effect on the performance of composite curved beams with opening. For this purpose, specimen's COW, CECO1-W and CECO2-W with circular, combined opening of elongated circular and circular opening of 94 mm opening depth (0.5h) in which h is the steel beam height, placed from web vertex at distance 47 mm are prepared.

From analysis result for COW, it is shown that srengthening the composite besm by web stiffeners along the span length enhance the beam strength with 11% with slight decreasing the deflection beam as shown in Table (4-21), incorporating with increasing the diagonal torsional cracks, due to high stiffeners providence by the web stiffeners. Furthermore, presence of web stiffeners enhance the beam stiffeness as exhibited in Figures (4-51) to

(4-53). Furthermore, it can be observed from the load versus vertical deflection curves and Table (4-20) that the ductility index of composite beams decreases by 23% and 41% for CECO1 and CECO2; respectively, while the COW (strengthening by web stiffeners along the span) have approximate ratio to the beam without opening.

Moreover, in specimens CECO1 and CECO2 where designed with opening the recorded ultimate capacity reduction were by 26% and 15% compared to the CCBF-2 (which was designed without opening), this can be restored by using steel stiffeners by 10%. In these specimens stiffeness are increased with stiffeners providence, while the deflection are enhanced with a slight value. Furthermore, the flexural concrete cracks had been observed immediately as the load is applied incorporating with diagonal torsional cracks. The twisting at mid-span found to be decrease slightly. The stress and strain distribution for the specimens is show in Figures (4-54) and (4-55).
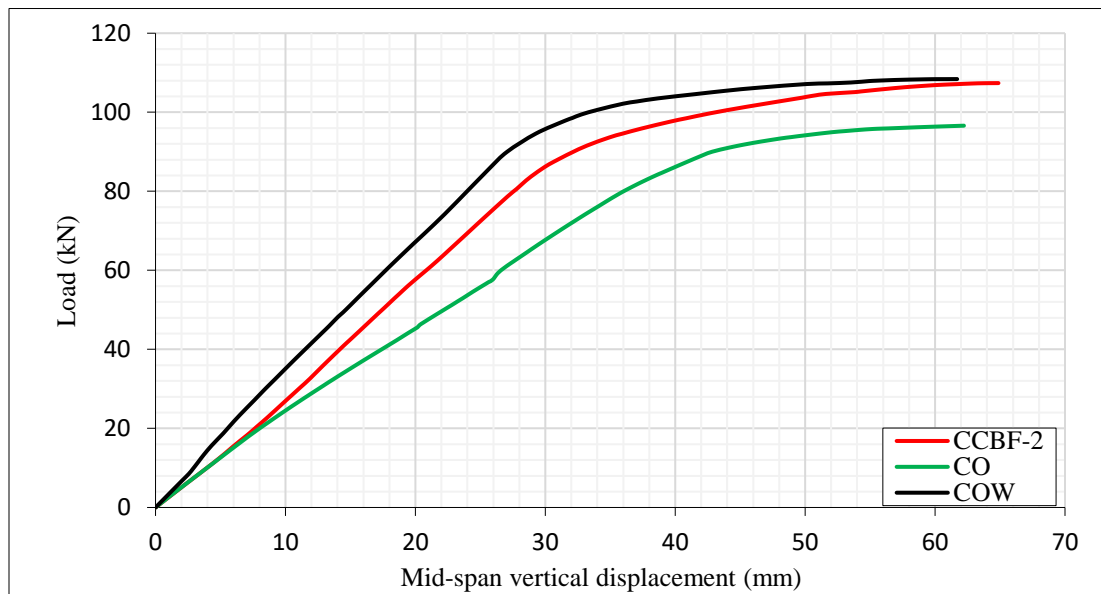
Figure (4-51): Load-vertical deflection curve for curve composite beam strengthening by web stiffeners along the span.
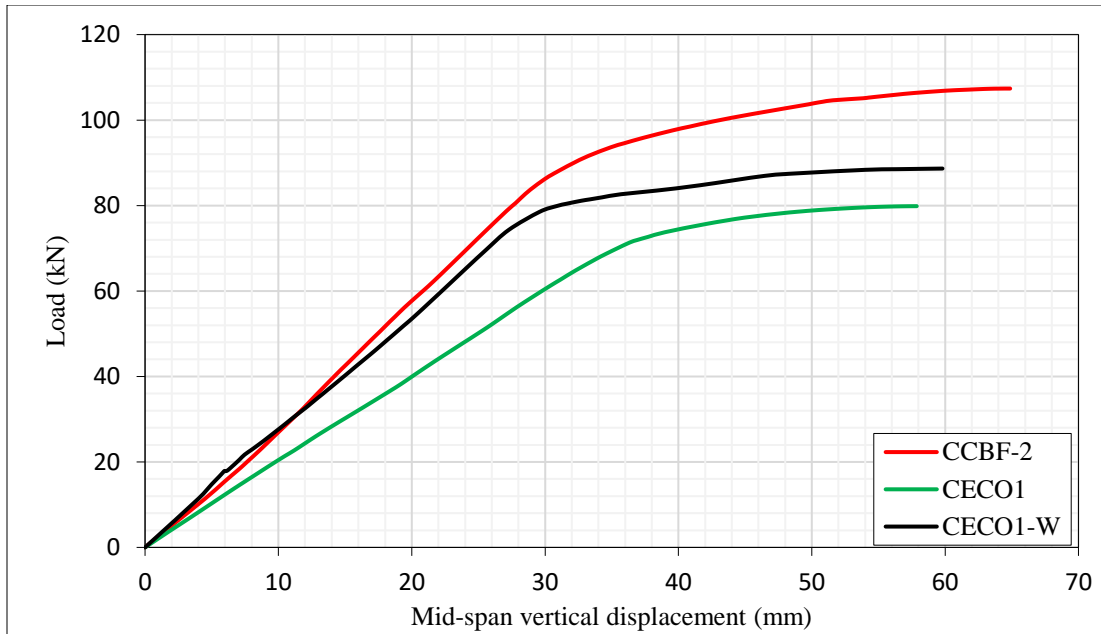
Figure (4-52): Load-vertical deflection curve for curve composite beam strengthening by web stiffeners beside the opening.
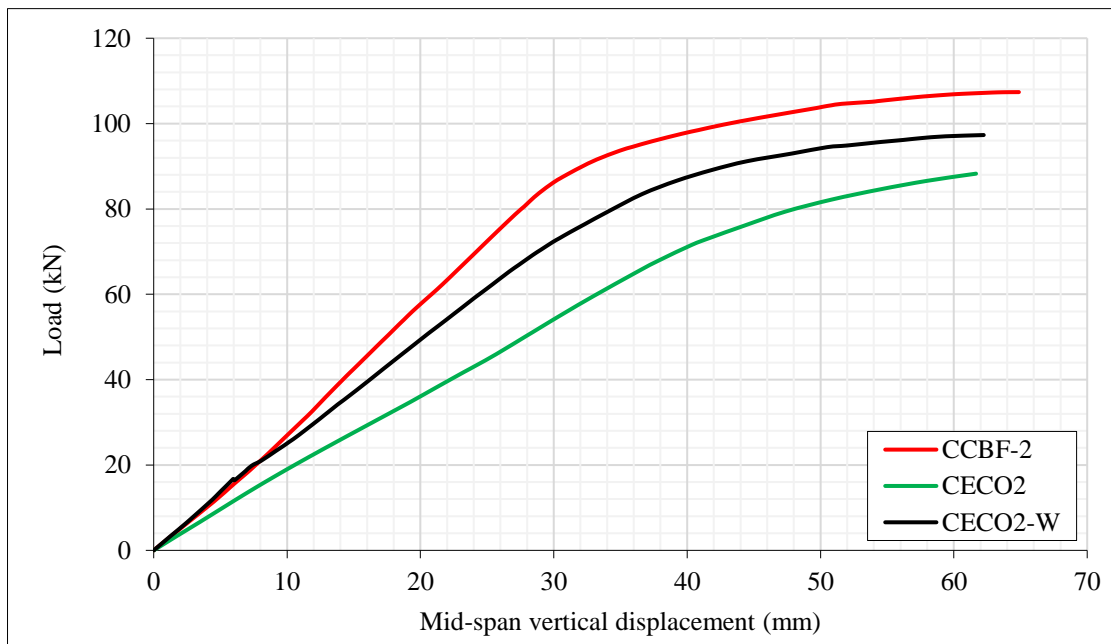
Figure (4-53): Load-vertical deflection curve for curve composite beam strengthening by web stiffeners at the mid-span.

Table (4-21). Curve composite beam results under web stiffeners effect on beam with opening.

Specimen (i)	F_y (kN)	F_u (kN)	Δ_u (mm)	$\dfrac{F_{yi}}{F_{yCCBF-2}}$	$\dfrac{F_{ui}}{F_{uCCBF-2}}$	$\dfrac{\Delta_{ui}}{\Delta_{uCCBF-2}}$	Ductility index (Δ_u/Δ_y)
CCBF-2	86.12	107.37	66.09	1.00	1.00	1.00	2.2
CO	77.54	96.93	62.22	0.90	0.90	0.94	2.1
COW	94.59	108.39	61.70	1.10	1.01	0.93	2.1
CECO1	69.02	79.85	57.88	0.80	0.74	0.88	1.7
CECO1-W	78.52	88.65	59.80	0.91	0.83	0.91	2.0
CECO2	79.37	91.55	61.66	0.92	0.85	0.93	1.3
CECO2-W	70.42	97.32	62.24	0.82	0.91	0.94	2.1
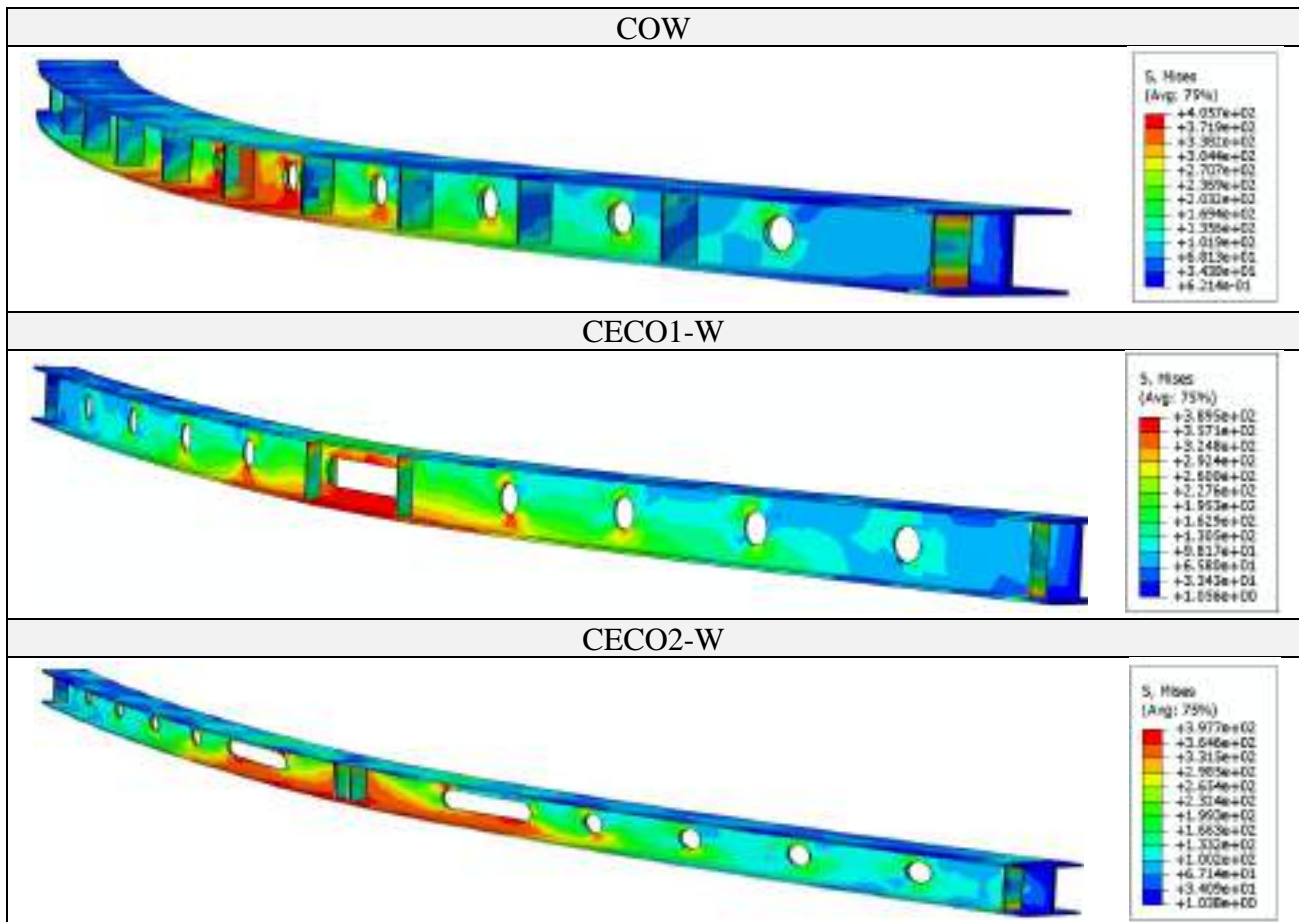
Figure (4-54): Efect of exsiting the web stiffenerss on the steel beam stress distribution.

COW	CECO1-W

CECO2-W
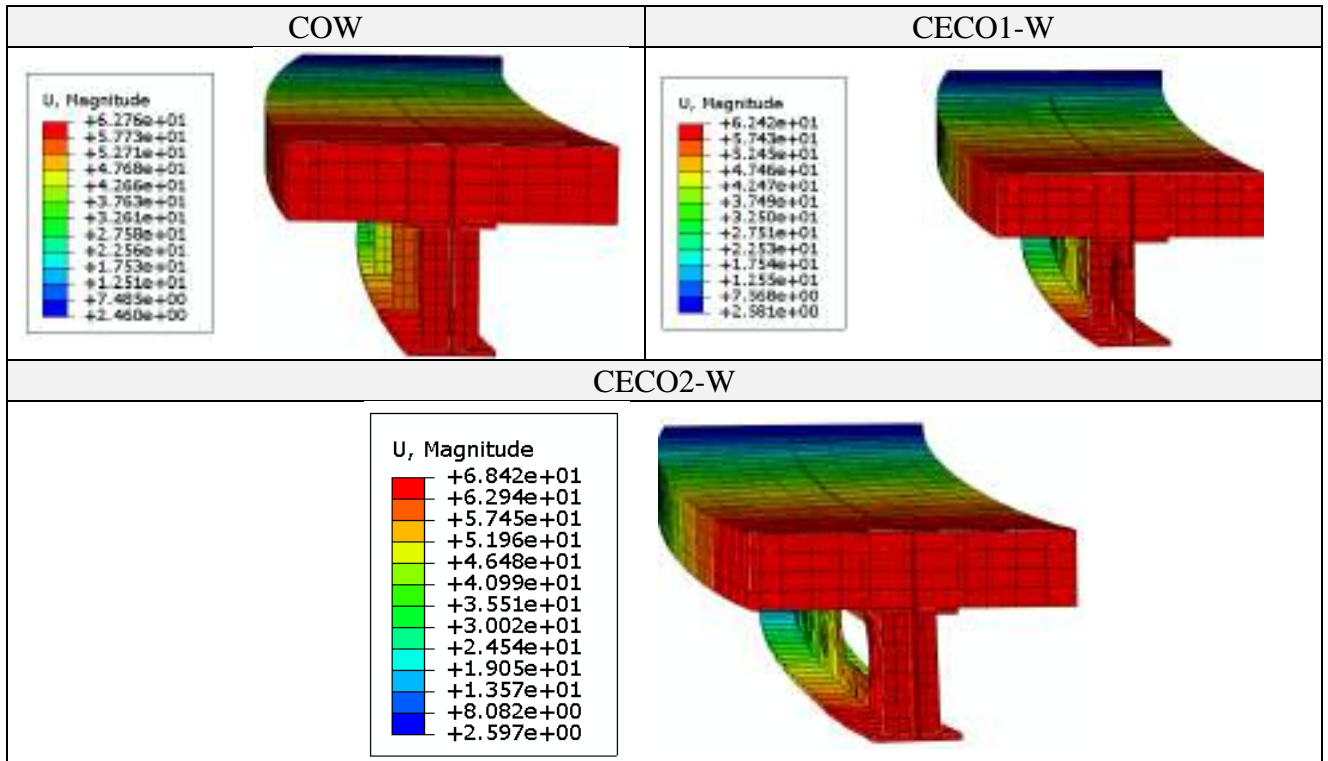
Figure (4-55): Effect of stiffeners on strain distribution of the curve composite beam with opening at mid-span.

CHAPTER FIVE

CHAPTER 5

Conclusions and Future Research

5.1 Conclusions

Three dimensions nonlinear finite element analysis are employed to simulate the composite steel-concrete curved in plane beam until failure using a powerful ABAQUS/Standards package, to investigate the inelastic beams behavior under static loading including various parameters. According to the results obtained numerical analysis, following points were deduced:

1) Increasing the beam central angle to 40° decrease the ultimate capacity and the beam deflection by 50% and 52%; respectively, incorporating with increasing the diagonal and flexural concrete crack.

2) The beam suffers from excessive twisting, vertical and interface separation at the beam mid-span against increases the curvature ratio to 0.698. Moreover, the beams exhibited less ductility by 41% and the

specimens softening and yielding at an early stage incorporating with changing the failure of the beam from flexural to a combined effect of flexure and torsion.

3) Existing of transverse stiffeners near to the support shows compensation all the weakness in the beam separation and twisting, incorporating with enhancing the strength capacity by 57% to the beam without transverse stiffeners. But with stiffeners number increases, the beam record early yielding by 24% and enhance in the ductility index by 63% incorporating with reducing web twisting and vertical separation at the beam mid-span transferring the failure to the concrete slab. Moreover, increase of the stiffener's numbers presented more flexural cracks in the concrete slab mid-span.

4) Increasing the stud numbers show a significant reduction in the vertical and interface separation between the steel beam flange and concrete slab and the ductility index by 20%. The capacity of the specimens observed to increase with stud number increases. The specimen designed with 30 stud shear connectors (full shear connector) recorded 30% higher resistance and decreasing the deflection by 50% compared to the designed model with 8 studs (partial shear connector), due to relative increase in the stiffness of the beams. Also, some cracks were observed in the concrete slab tension surface, as these cracks receded to include the loading area and the area under the stud's surfaces.

5) The yield and ultimate capacity of the curved composite beam increased as the yield stress of the steel beam increased. A 58.31% of

loading capacity was improved using 450 MPa yield stress compared to the 250 MPa steel beam yield stress. The effect of yielding stress of steel beam on the flexural cracks appears to be small and negligible on both bottom and top faces of the reinforced concrete slab, while the ductility index shows an enhancement by 61%.

6) The study shows that increasing the concrete slab compressive strength f_{cm} reduce the ductility by 41% of the curve composite beam and increase the composite beam capacity by 20%, while the cracks pattern in the flexural zone doesn't affect by changing the f_{cm}.

7) Increasing the opening web depth in steel section leads to reduce the strength capacity and stiffness of the beam. Maximum reduction in yield load, ultimate load and vertical deflection were recorded for 75%h opening depth by approximately 48%, 18% and 8% for curve composite beam compared to the beam without opening. An increasing in the flexural and diagonal torsional cracks has been observed when the opening depth increases.

8) Presence of elongated circular opening in the curved composite beams reduce the beams capacity by 24%. The beams exhibit less ductility by 14% and the response of the specimens softening and the beams yield in an early stage. Moreover, the torsion is found to be dominate and influential on the inelastic behavior and failure mechanism of the beam, especially in specimens with elongated circular opening.

9) Using web stiffeners is considered a good way to enhance the beam capacity. Web stiffeners provided a semi complete restoring to the

strength loss due to the presence of opening in steel beam with improvement in the beam performance by 11%.

5.2 Future Research Recommendation

For the structural behavior study purpose of the curve composite steel-concrete, the following future recommendations may be taken into consideration:

- Curved composite steel-concrete beams behavior investigation when strengthened with CFRP bar and GFRP sheet can be adapted.

- Three-dimensional modeling must be extended to model the continuous curved composite girder behavior under the various parameters with box-girder or twin or multi I-girder in various profile cross section.

- Different parameters can be investigated using the FE model; Profile steel sheeting, various types of shear connector and the reinforcement bars.

- The response of the curve composite steel-concrete beams with open webs should be investigated under the effect of the impact, cyclic and dynamic loading.

- Studying the strengthening of longitudinal stiffeners of torsional-flexural capacity.

- Studying the strengthening of transverse stiffeners from on side of the curvature.

- Studying the effect of lateral bracing type of maintaining the strength of curved beams.

REFRENCES

[1] Johnson, R.P., Composite structure of steel and concrete: beams, slabs, columns and frames for building, Crosby Lockwood Staples, London. Vol.1, pp.210, 1975.

[2] https://www.alamy.com/stock-photo, "Mission Arched Shaped Concrete Towers of the Curved Coronado Bridge 35180162.html", 2010.

[3] https://www.dreamstime.com, "Nathan Phillips square of New City hall in Toronto", 2018.

[4] Lin, W., Yoda, T., "Numerical study on horizontally curved steel-concrete composite beams subjected to hogging moment", International Journal of Steel Structures. Vol.14, pp.557-569, 2014.

[5] Hall, D.H., Grubb, M.A., and Yoo, C.H., "Improved design specifications for horizontally curved steel girder highway bridges", No. 424, NCHRP Project 12-38 Final Report,1999.

[6] AISC., "A. 360-specification for structural steel buildings", American Institute of Steel Construction. 2005.

[7] Eurocode 2. "Design of concrete structures. part 1.1: general rules and rules for buildings", British Standards Institution: London, 2004.

[8] Federal Highway Administration; Department of Transportation, "steel bridge design handbook; design example: three-span continuous curved i-girder beam bridge". U.S., FHWA. 2015.

[9] Bouazaouia L., Jurkiewiezb B., Delmasa Y., and Lia A., "Static behavior of a full-scale steel-concrete beam with epoxy-bonding connection", Engineering Structures. Vol. 30, pp. 1981-1990, 2008.

[10] Oehlers, D.J. and Bradford, M.A., "Elementary behaviour of composite steel and concrete structural members", Butterworth Heinemann, London, pp. 259, 1999.

[11] Johnson, R.P. and May, I.M.," Partial interaction design of composite beams", Institution of Structural Engineer. Vol.8, pp. 305-311, 1975.

[12] Kumar, M., " Numerical modelling of partial interaction in steel concrete composite beams", Master Thesis, Indian institute of technology Roorkee, Uttarakhand, India, 2016.

[13] Raguvaran, B. and Baskar, R., "Study on behaviour of angle shear connector in steel-concrete composite structures", International Journal of Steel Structures. Vol.16, pp. 807-811, 2016.

[14] Wang. H.Y., Yue, J., Liu, J. and Chen, F.Y., "Experimental and numerical analysis of steel-block shear connectors in assembled monolithic steel–concrete composite beams", Journal of Bridge Engineering. Vol.24, pp. 1-12, 2019.

[15] Sudharsan, S. and Vinoth K.N., "Experimental investigation of cold-formed steel composite beams with shear connectors", International Advanced Research Journal in Science, Engineering and Technology. Vol.5, pp. 28-38, 2018.

[16] Lam, D. and El-Lobody, E., "Behavior of headed stud shear connectors in composite beam", Journal of Structural Engineering. Vol.131, pp. 96-107, 2005.

[17] Sharitati, M., Sulong, H.R., Arabnejad, M. and Mohoution, M., "Shear resistance of channel shear connectors in plain, reinforced and lightweight concrete", Scientific Research and Essays. Vol.6, pp. 977-983, 2011.

[18] Design of compsoite highway bridges curved in plan. British, 2014.

[19] Liew, J.Y.R., Thevendran, V., Shanmugam, N.E. and Tan, L.O. "Behaviour and design of horizontally curved steel beams", Journal of Constructional Steel Research. Vol.32, pp.37-67, 1995.

[20] AASHTO "AASHTO LRFD Bridge Design Specifications", Washington, DC. American Concrete Institute (1971)". Building code requirement for reinforced concrete, (ACI 318-71), Detroit, pp. 78, 2007.

[21] Tan, E.L. and Uy, B., "Experimental study on curved composite beams subjected to combined flexure and torsion", Journal of Constructional Steel Research. Vol.65, pp. 1855-1863, 2009.

[22] Nagoya Expressway Corporation. "Design specification of steel structures". Nagoya, Japan. 1984.

[23] Umanskii, A. A., Spatial structures. Moscow, Russian, 1948.

[24] Structural Stability Research Council-Task Group 14, "Horizontally curved girders-A look to the future", Annual Report, SSRC Workshop, 14-15, Chicago, Illinois, 1991.

[25] Konishi, I. and Komatsu, S, "Three-dimensional analysis of curved girder with thin-walled cross-section". ABSE, Zurich, Switzerland. Vol.25, pp.143-203, 1965.

[26] United States Steel, "Highway structural design handbook". Vol.1, ADUSS, pp.88-2222, 1965.

[27] Watanabe, N., "Theory and calculation of curved girder". Gihodo, Tokyo, Japanese, 1967.

[28] Conrad, P. and Heins, Jr, "Curved girder bridge analysis", Computers and Structures. Vol. 2, pp.785-797, 1972.

[29] Yoo, C.H., Evick, D.R., and Heins, C.P., "Non-prismatic curved girder analysis", Computers and Structures. Vol.4, pp. 675-698, 1974.

[30] Heins, C.P. and Oleinik, J.C., "Curved box beam bridge analysis", Computers and Structures. Vol.6, pp. 65-73, 1976.

[31] Heins, C.P. and Sheu, F.H., "Design/analysis of curved box girder bridges", Computers and Structures. Vol.15, pp. 241-258, 1982.

[32] Fukumoto, Y. and Nishida, S., "Ultimate load behaviour of curved I-beams", Journal of Engineering and Mechanics Division. Vol.107, pp.367-385, 1981.

[33] Rosen A. and Abromovich H., "Galerkin method as a tool to investigate the planar and non-planar behavior of curved beams", Computers and Structures. Vol.18, pp.165-174, 1984.

[34] Yang, Y.B. and Kuo, S.R., "Effect of curvature on stability of curved beam", Journal of Structural Engineering, ASCE. Vol.113, pp.1185-1202, 1987.

[35] Liew, J.Y.R., Thevendran, V., Shanmugam, N.E., and Tan, L.O., "Behavior and design of horizontally curved steel beams", Journal of Conational Steel Research. Vol.32, pp.37–67, 1995.

[36] Yoo, C.H., Kang, Y.J., and Davidson. J.S., "Buckling analysis of curved beams by finite-element discretization", Journal of Engineering Mechanics, ASCE. Vol.122, pp. 762-770, 1996.

[37] Davidson, J. S. and Yoo, C. H., "Cross-frame spacing and parametric effects in horizontally curved I-girder bridges", Journal of Structural Engineering, ASCE, Vol.122, pp. 1089-1096, 1997.

[38] Pi, Y.L., Bradford, M.A., and Trahair, N.S. "Inelastic analysis and behavior of steel I-beams curved in plan", Journal of Structural Engineering, ASCE. Vol.126, 772–779, 2000.

[39] Pi, Y.L., and Bradford, M.A. "Strength design of steel i-section beams curved in plan", Journal of Structural Engineering, ASCE, Vol.127, 639-646, 2001.

[40] Jung, S.K., and White, D.W., "Shear strength of horizontally curved steel I-girders-finite element analysis studies", Journal of Conational Steel Research, Vol.62, 329-342, 2006.

[41] AASHTO. 3rd ed. 2005, "AASHTO LRFD bridge design specifications, Interim Provisions", Washington (DC), 2004.

[42] Kim, W.S., Laman, J.A., and Linzell, D.G., "Live load radial moment distribution for horizontally curved bridges", Journal of Bridge Engineering, ASCE. Vol.12, pp.727-736, 2007.

[43] Madhavan, M. and Davidson, J.S., "Theoretical evaluation of flange local buckling for horizontally curved I-girders", Journal of Bridge Engineering, ASCE. Vol.14, pp. 424-435, 2009.

[44] Hayder, M. and Kadhim, A., "The analytical study of strengthening the bottom flange of steel I-section simply supported horizontally curved beams", Journal of University of Babylon/Engineering Sciences, Vol.21, pp.1520-1530, 2013.

[45] El-Khoury, G.I., Linzell, D.G. and Geschwindner, L.F., "Computational studies of horizontally curved longitudinally stiffened plate girder webs in flexure", Journal of Constructional Steel Research. Vol.93, pp.97–106, 2014.

[46] Visuvasam, J., Kumar P.S., Susan, B. "Study of bending behavior of horizontally curved steel beams using ANSYS", Journal of Chemical and Pharmaceutical Sciences. Vol.10, pp.275-279, 2017.

[47] Colville, J., "Tests of curved steel-concrete beams", Journal of the Structural Division, ASCE. Vol.99, pp.1555-1570, 1973.

[48] Heins, C.P., "Box girder bridge design state-of-the-art", AISC Engineering Journal. Vol.15(4), pp. 126-142, 1978.

[49] Arizumi, Y., Oshiro, T., and Hamada, S, "Finite strip analysis of curved composite girders with incomplete interaction", Computers and Structures. Vol.15, pp.603-612, 1982.

[50] Maeda, Y., et al. "Static test of two-span continuous curved composite girders", Determent of Civil Engineering, Osaka University, 1973.

[51] Yoda, T. and Hirashima M., "Finite displacement theory of curved and twisted thin-walled members", Journal of Theoretical and Applied Mechanics. Vol.28, pp.105-117, 1980.

[52] Yoda, T., Hirashima, M., and Kojima, M., "Nonlinear analysis of one-dimensional curved and twisted members", Journal of Theoretical and Applied Mechanics. Vol.30, pp.115-120, 1981.

[53] Nakai, H. and Murayama, Y., "Distortional stress analysis and design aid for horizontally curved box girder bridges with diaphragms", Proceedings of JSCE, No.309, pp.25-39, 1981.

[54] Arizumi, Y., Oshiro, T., and Hamada, S., "Finite strip analysis of curved composite girders with incomplete interaction", Computers and Structures. Vol.15, pp. 603-612, 1982.

[55] Arizumi, Y., Hamada, S., and Oshiro, T., "Experimental and analytical studies on behavior of curved composite box girders", Bulletin of the Faculty of Engineering, University of the Ryukyus. No.34, pp.175-195, 1987.

[56] Arizumi, Y., Hamada, S., and Oshiro, T., "Behavior study of curved composite box girders", Journal of Structural Engineering, ASCE. Vol.114, pp.2555-2573, 1988.

[57] Ng, S.F, Cheung, M.S. and Hachem H.M., "Study of a curved continuous composite box girder bridge", Canadian Journal of Civil Engineering. Vol.20, pp.107–119, 1993.

[58] Thevendran, V., Chen, S., Shanmugam, N.E. and Liew, J.Y.R, "Nonlinear analysis of steel-concrete composite beams curved in plan", Finite Elements in Analysis and Design, Vol.32, pp.125-139, 1999.

[59] Thevendran, V., Chen, S., Shanmugam, N.E. and Liew, J.Y.R, "Experimental study on steel-concrete composite beams curved in plan" Engineering Structures. Vol.22, pp.877-889, 2000.

[60] Sennah, K., Kennedy, J.B., and Nour, S., "Design for shear in curved composite multiple steel box girder bridges", Journal of Bridge Engineering. Vol.8, pp.144-152, 2003.

[61] Al hashimy, A., "Load distribution factors for curved concrete slab-on-steel I-girder bridge" M.Sc. Thesis, College of Engineering, Ryerson Unversity, Canda, 2005.

[62] Samaan, M., Kennedy, J.B. and Sennah, K., "Impact factor for curved continuous composite multiple-box girder bridges", Journal of Bridge Engineering. Vol.12, pp.80-88, 2007.

[63] Erkmen, R.E. and Bradford, M.A., "Nonlinear elastic analysis of composite beams curved in-plan", Engineering Structures, Vol.31, pp.1613-1624, 2009.

[64] Erkmen, R.E. and Bradford Mark, A., "Nonlinear quasi-viscoelastic behavior of composite beams curved in-plan", Journal of Engineering Mechanics. Vol.137, 238-247, 2011a.

[65] Erkmen, R.E. and Bradford, M.A., "Time-dependent creep and shrinkage analysis of composite beams curved in-plan", Computers and structures. Vol.89, pp.67-77, 2011b.

[66] Liu, X., Bradford Mark, A. and Erkmen, R.E., "Time-dependent response of spatially curved steel-concrete composite members. ii: curved-beam experimental modeling", Journal of Structural Engineering. Vol.139, 2013.

[67] Liu, X., Bradford, M.A. and Erkmen, R.E., "Non-linear inelastic analysis of steel-concrete composite beams curved in-plan", Engineering Structure. Vol.57, pp.484-492, 2009.

[68] Tan, E.L. and Uy, B. "Nonlinear analysis of composite beams subjected to combined flexure and torsion", Journal of Constructional Steel Research. Vol.67, pp.790-799, 2011.

[69] Lin, W. and Yoda, T. "Numerical study on horizontally curved steel-concrete composite beams subjected to hogging moment", International Journal of Steel Structures. Vol.14, pp.557-569, 2014.

[70] Zhang, Y., Hou, Z., Li, Y. and Wang, Y., "Torsional behavior of curved composite beams in construction stage and diaphragm effects", Journal of Construction Steel Research. Vol.108, pp.1-10, 2015.

[71] Xi, Q.X., Han, L.B, Chan, W.L and Zheng, G.W., "A Trigonometric analytical solution of simply supported horizontally curved composite i-beam considering tangential slips", Mathematical Problems in Engineering. Vol.1, pp.1-12, 2016.

[72] Qin, X., Wu, C., Liu, H., Xiang, C., "Lateral distribution calculation of multi-I beam composite curved bridge with slip effect", VIBROEngineering International LTD Journal. Vol.11, pp.1-6, 2017.

[73] Androus, A., Afefy, H.M. and Sennah, K., "Investigation of free vibration and ultimate behavior of composite twin-box girder bridges", Journal of Construction Steel Research. Vol.130, pp.177-192, 2017.

[74] Izzet A.F, Mohammed, A.R., "Experimental study on curved composite i-girder bridge subjected to iraqi live loading for road bridges", Journal of Engineering Science and Technology, Vol.13, pp.226-241, 2018.

[75] Abdullah, S.S., "Behavior of composite concrete - steel castellated beams under combined flexure and torsion". PhD. Thesis, University of Baghdad, 2017.

[76] Reddy, J.N., "An Introduction to Nonlinear Finite Element Analysis", Texas, Oxford University Press, 2004.

[77] Abaqus, F. E. A. "ABAQUS analysis user's manual". Dassault Systemes, Vélizy-Villacoublay, France. 2009.

[78] Karlsson, B.I. and Sorensen, E.P. ABAQUS, "Analysis User's Guide Volume III: Materials", Pawtucket, Rhode Island, Hibbitt Publication. 2006c.

[79] Ellobody, E., "Finite element analysis and design of steel -concrete composite bridges", Archives of Civil and Mechanical Engineering. Vol.11, pp.623-636, 2014.

[80] P. Kmiecik and M. Kami_Ski., "Modelling of reinforced concrete structures and composite structures with concrete strength degradation taken into consideration", Archives of Civil and Mechanical Engineering. Vol.11, pp.623-636, 2011.

[81] Amar, K., "Introduction to finite element analysis using MATLAB and ABAQUS 1st Edition", 2013.

[82] Eurocode 2, "Design of concrete structures. part 1.1: general rules and rules for buildings", British Standards Institution, London, 2004.

[83] Nguyen, H.T., Kim, S.E. "Finite element modeling of push-out tests for large stud shear connectors", Journal of Constructional Steel Research. Vol.65, pp.1909-1920, 2009.

[84] Byfield, M.P., Kemp, A.R. and Nethercot, D.A., "Effect of strain hardening on flexural properties of steel beams", The Institution of Structural Engineering. Vol.80, pp.29-34, 2009.

[85] Liang, Q.Q. and Uy, B., "Theoretical study on the post-local buckling of steel plates in concrete-filled box column", Journal of Computers and structures. Vol.75, pp.479-490, 2000.

[86] Liang, Q.Q., Uy, B., Wright, H.D. and Bradford, M.A., "Local buckling of steel plates in double skin composite panels un-der biaxial compression and shear", Journal of Structural Engineering. Vol.130, pp.443-451, 2004.

[87] Karlsson, B.I. and Sorensen, E.P. ABAQUS, "Analysis user's guide volume II: Analysis", Pawtucket, Rhode Island, Hibbitt Publication, 2006c.

[88] Karlsson, B.I. and Sorensen, E.P. ABAQUS, "Analysis user's guide volume IV: Elements", Pawtucket, Rhode Island, Hibbitt Publication, 2006c.

[89] Karlsson, B.I. and Sorensen, E.P. ABAQUS, "Analysis user's manual volume V: Prescribed conditions", constraints and interactions, Pawtucket, Rhode Island, Hibbitt Publication, 2006c.

[90] Rakhshanimehr, M., Esfahani, M.R., Kianoush, M.R., Mohammadzadeh, B.A. and Mousavi, S.R., "Flexural ductility of reinforced concrete beams with lap-spliced bars", Canadian Journal of Civil Engineering. Vol.41, pp.594-604, 2014.

[91] Abdulraheem, M.S., Kadhum, M.M., M.R., "Experimental investigation of fire effects on ductility and stiffness of reinforced reactive powder concrete columns under axial compression", Canadian Journal of Civil Engineering. Vol.20, pp.750-761, 2018.

[92] Chung, K.F., Lawson, R.M., "Simplified design of composite beams with large web openings to Eurocode 4", Journal of Constructional Steel Research. Vol.57, pp.135-163, 2001.

[93] P.H. Mans, "Full scale testing of composite plate girder constructed using 70-ksi high performance steel". MSc Thesis, University of Nebraska-Lincoln, USA, 2001.

APPENDIX-A

APPENDIX

A

Material Properties Modeling

A.I Introduction

ABAQUS is a powerful finite element package vastly used in civil engineering practice. Particularly used for modeling the reinforced concrete structure. Concrete damaged plasticity is one of the most appropriate models that deals with concrete behavior considering possible failure modes; the tensile cracking and compressive crashing. A program input of concrete and steel reinforcement modelling for specimen A-30 with 37.7 MPa compressive strength is given as an example for material modeling and all special definitions about the property of elements are described below.

A.2 Material Properties Modeling

A.2.1 Material properties

All parameters for the material models were illustrated in Tables. (A-3) to A-7). ABAQUS element needs some properties for proper entities which are elastic and plastic properties. The stress-strain curve of the concrete that

obtained from the equations (3.3), (3.5) and (3.9) is used in the modeling of the nonlinear behavior.

Table (A-1): Elastic properties of concrete.

Type	Youngs Modulus (MPa)	Poisson's Ratio
Isotropic	32758.58	0.2

Table (A-2): Plastic properties of concrete.

Dilation Angle (ψ)	Eccentricity (ϵ)	Strength ratio $(\frac{\sigma_{b0}}{\sigma_{c0}})$	K_c	Viscosity parameter (η)
34	0.1	1.16	0.667	0.0001

Table (A-3): Concrete compressive behavior.

Yield stress (MPa)	Inelastic strain	d_c
7.25827	0	0
13.72208	2.63918E-05	0.000889
19.39883	7.57399E-05	0.018503
24.2958	0.000148892	0.04593
28.42021	0.000245627	0.079551
31.77918	0.000365728	0.117284
34.37974	0.000508981	0.15785
36.22883	0.000675173	0.20042
37.33333	0.000864096	0.244432
37.7	0.001075541	0.289494
37.56379	0.001215725	0.335322

Table (A-3): Cont. concrete compressive behavior.

Yield stress (MPa)	Inelastic strain	d_c
37.15618	0.001364194	0.363607
36.47867	0.001520902	0.392062
35.53273	0.001685803	0.420654
34.31987	0.001858854	0.449357
32.84154	0.002040008	0.478147
31.09919	0.002229221	0.507005
29.09429	0.002426449	0.535913
26.82826	0.002631649	0.564856
24.30253	0.002844776	0.593821
21.51852	0.003065788	0.622796
18.47763	0.003294641	0.651772
15.18125	0.003531293	0.651772
11.63078	0.003775702	0.70969
7.82758	0.004027826	0.738618
3.773025	0.004287623	0.767515

Table (A-4): Concrete tensile behavior.

Yield stress (MPa)	Cracking strain	d_t
2.877126	0	0
2.122795	0.000123027	0.262182
1.789613	0.000233198	0.377986
1.588388	0.00033934	0.447925
1.449124	0.000443592	0.496329
1.344969	0.000546771	0.53253
1.140462	0.000853014	0.603611

Table (A-4): Cont. concrete tensile behavior.

Yield stress (MPa)	Cracking strain	d_t
1.015105	0.001156841	0.647181
0.927665	0.00145951	0.677572
0.86195	0.001761516	0.700413
0.810092	0.002063099	0.718437
0.767735	0.002364392	0.733159
0.711515	0.002866108	0.7527
0.667489	0.003367452	0.768002
0.631727	0.003868544	0.780431
0.601884	0.004369455	0.790804
0.576456	0.004870231	0.799642
0.542543	0.005671266	0.811429
0.514722	0.006472116	0.821099
0.49133	0.00727283	0.829229
0.471281	0.008073442	0.836197
0.449809	0.009074097	0.84366
0.431413	0.010074659	0.850054
0.415407	0.011075147	0.855617
0.357943	0.016076901	0.87559
0.321218	0.021078023	0.888355
0.29501	0.026078823	0.897464
0.275028	0.031079433	0.904409

Table (A-5): Material properties for Ø12 rebar (longitudinal reinforcement for top and bottom).

Elastic properties		
Type	**Youngs Modulus (MPa)**	**Poisson's Ratio**
Isotropic	200000	0.3
Plastic properties		
Hardening	**Yield stress (MPa)**	**Plastic strain**
Isotropic	586	0
	683	0.0485

Table (A-6): Material properties for Ø10 rebar (stirrups steel).

Elastic properties		
Type	**Youngs Modulus (MPa)**	**Poisson's Ratio**
Isotropic	200000	0.3
Plastic properties		
Hardening	**Yield stress (MPa)**	**Plastic strain**
Isotropic	399	0
	498	0.0495

Table (A-7): Material properties for steel beam type 200UB29.8.

Elastic properties		
Type	**Youngs Modulus (MPa)**	**Poisson's Ratio**
Isotropic	200000	0.3
Plastic properties		
Hardening	**Yield stress (MPa)**	**Plastic strain**
Isotropic	360.5	0
	503.5	0.0715

Table (A-8): Material properties for stud shear connector.

Elastic properties		
Type	**Youngs Modulus (MPa)**	**Poisson's Ratio**
Isotropic	200000	0.3
Plastic properties		
Hardening	**Yield stress (MPa)**	**Plastic strain**
Isotropic	395	0
	499	0.052

# APPENDIX-B

Modeling Example

B.I Introduction

In this section, modeling is performed on simply supported straight composite steel-concrete beam as an example for performing the modeling procedure as described below.

B.2 Finite Element Modeling

B.2.1 Modeling of the specimen

Three dimensions finite element models using ABAQUS software are developed to model the straight composite steel-concrete beam tested by Mans [93]. The structural steel used in the test was a high-strength steel HPS70W having a nominal yield stress of 482 MPa. The general layout and dimensions of composite plate girder are shown in Fig. (B-1) the composite plate girder had an overall length of 12,801 mm and a length between supports equal to 12,192 mm. The steel plate girder had a web of 760.4 x 8.9 mm and upper and lower flanges of 182.6 x 19.6 mm. The measured flange and web portions of the steel plate girder had yield and ultimate tensile stresses of 556, 700 MPa and 583, 656 MPa, respectively. The web of the steel plate girders was strengthened by stiffeners as shown in Fig. (B-1) to prevent shear failure.

a) Elevation (unit: m)

b) Cross section (unit: mm)
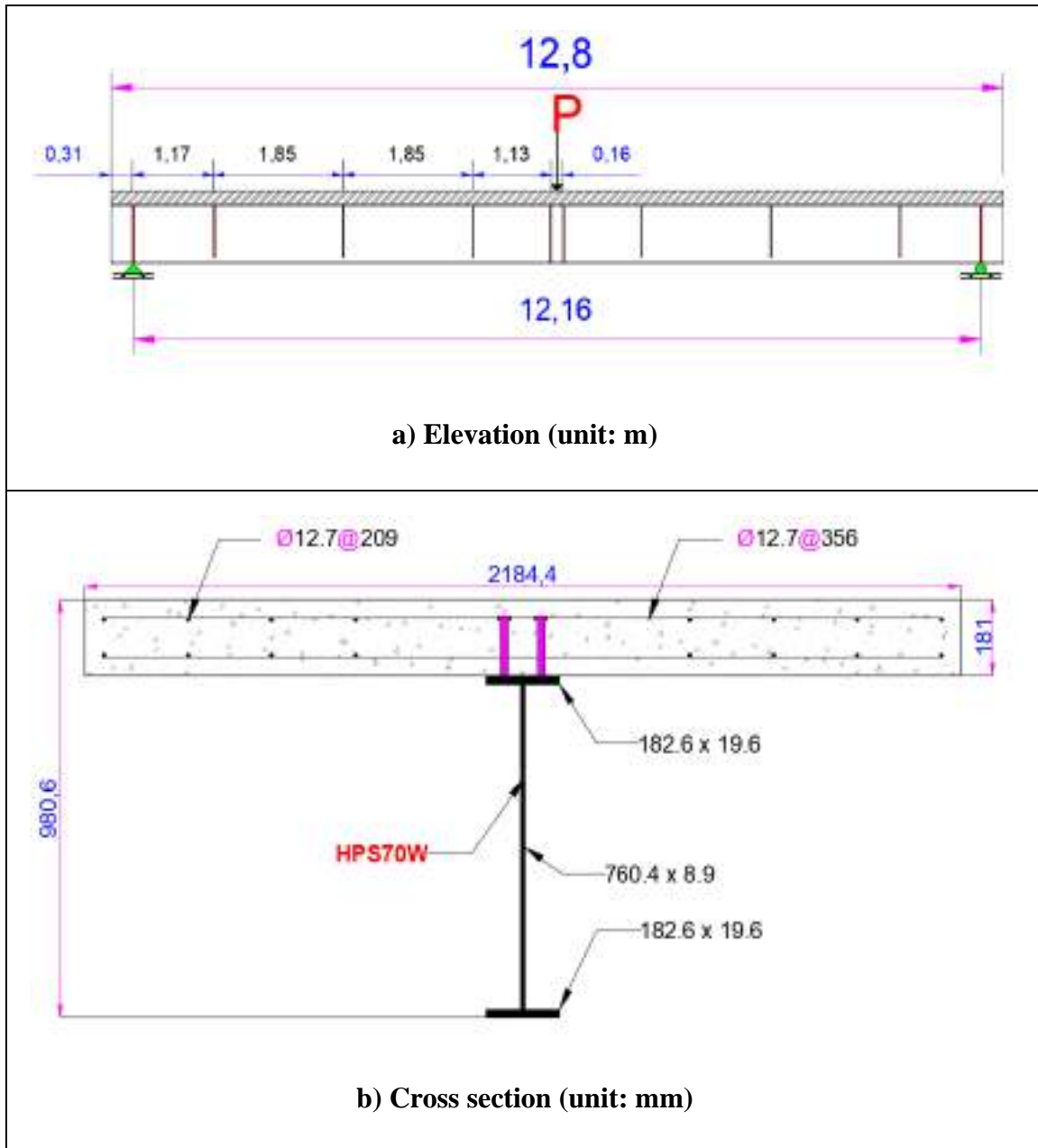
(B-1): Show elevation and cross section of composite beam.

The concrete slab had a width of 2184 mm and a depth of 181 mm. The composite plate girder had an overall height of 980 mm. The measured concrete cylinder strength was 52.5 MPa. The concrete slab had reinforcement steel bars of Grade 60 having a yield stress of 413 MPa. The reinforcement bars were spaced at 209 mm longitudinally and 356 mm transversely. The top

and bottom reinforcement bars had a cover of 44 mm. The shear connectors were headed studs having a diameter of 19 mm and a height of 114 mm. Sixty pairs of headed studs were used in the composite plate girder. The composite plate girders were subjected to a single concentrated load applied at midspan via a spreader beam.

For the modeling process achieved in this example, five parts are simulated including: concrete slab, shear connectors, reinforcement bars, steel beam, and steel stiffeners. The reinforced concrete slab, shear connectors, web stiffeners and steel beam are simulated as a solid element. While the steel rebars as a truss element. All parameters for the material models are illustrated in Table (B-1). The stress-strain curve of the concrete that obtained from the equations (3.3), (3.5) and (3.9) are used in the modeling of the nonlinear behavior.

Table (B-1): Material properties of the composite beam.

Material	Material property	Value (MPa)
Concrete	Compressive strength f_{cm}	52.5
Steel web	Yield strength f_y	583
	Ultimate strength f_u	656
Steel flange	Yield strength f_y	556
	Ultimate strength f_u	700
Steel reinforcement	Yield strength f_y	415
	Ultimate strength f_u	550
Stud shear connector	Yield strength f_y	680
	Ultimate strength f_u	900

Once all parts were assembled at an appropriate location, a proper constraint was used to describe the interaction between components. Three types of interaction are presented in this example as seen in Table (B-2).

Table (B-2): Interaction type of the composite beam.

Interaction Type	Components according to the type of interaction
Surface to surface	Between the steel beam and the concrete slab
Tie	Welding simulating of shear connector to the steel beam.
	Welding simulating of transverse stiffeners to the steel beam.
Embedment	Reinforcement to concrete slab
	Stud shear connector to the concrete slab

In order to simulate the test specimen, one end of the bottom steel flange of the FE model was prevented from translation in x, y and z directions while the other end restrained in x and y directions. The load was applied in increments as concentrated static loads at midspan, which is identical to the experimental investigation. Prescribed boundary conditions are summarized in Fig. (B-2).
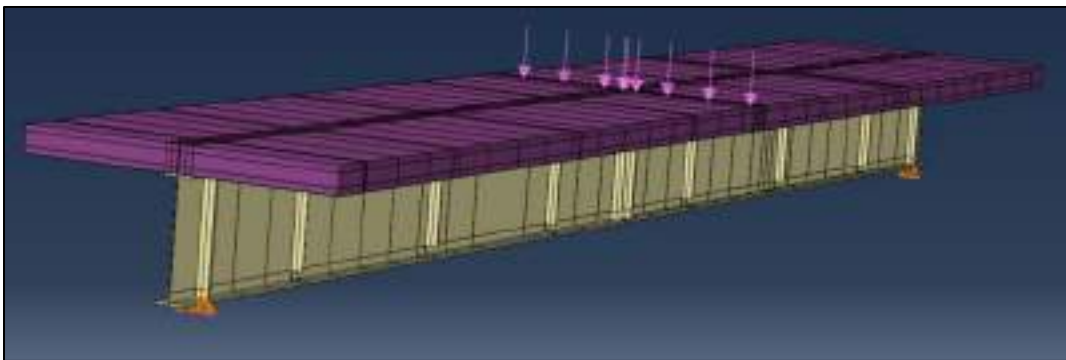

Figure (B-2): Boundary and applied loading conditions for the model.

B.2.3 Comparison with experimental results

The load-deflection relationship for the numerical and the experimental test results is demonstrated in Fig. (B-3). The finite element results showed good agreement with the experimental results. The ultimate loads and displacement are 1481 kN, 177.57 mm, 1432 kN and 177.8 mm for the model

and the tested beam, respectively as shown in Table (B-3). The stiffness, strength and ductility are good for both experiment and FE during each loading stage.
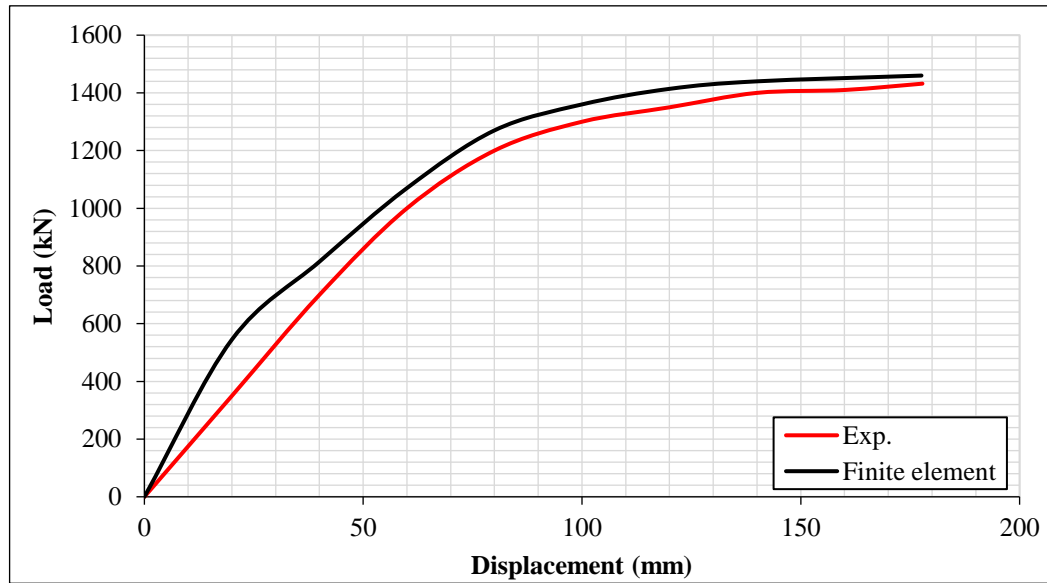

Figure (B-3): Comparison of the numerical and experimental load-displacement curve.

Table (B-3): Comparison between the numerical and experimental results.

Specimen	$P_u(kN)$		$\dfrac{P_{EXP}}{P_{FEA}}$	$\Delta_u(mm)$		$\dfrac{\Delta_{Exp}}{\Delta_{FEA}}$
	P_{EXP}	P_{FEA}		Δ_{EXP}	Δ_{FEA}	
Model	1432	1481	0.97	177.8	177.57	1.00

الخلاصة

تناولت هذه الدراسة التحريات النظرية حول سلوك العتبات الخرسانية-الفولاذية المركبة المنحنية في المخطط, للتحقق من تأثير معاملات مختلفة لسلوك هذه العتبة. اذ تم استخدام العتبة الخرسانية-الفولاذية المركبة ذات المقاومة العادية مع أو بدون فتحات للعتبة الفولاذية مصممة باسناد بسيط. علاوة على ذلك ، تم إجراء تقنية تقوية عن طريق إضافة شرائح فولاذية داخلية.

تم العمل على خمسة وأربعين نموذج مصمم ببساطة بطول ٦ أمتار. تم إنشاء العينات من بلاطة خرسانية بعرض ٥٠٠ مم وعمق ١٢٠ مم متصلة بشعاع فولاذي ملفوف من النوع UB29.8٢٠٠ باستخدام ست معاملات مختلفة. اذ تم استخدام تحليل العناصر المحددة ثلاثية الأبعاد باستخدام البرنامج التجاري (ABAQUS) للتأكد من دقة وصحة الخطوات المستخدمة في الحل. أثبتت فعالية تحليل العناصر المحددة من خلال مقارنة النتائج العددية مع الاختبارات التجريبية التي تم الحصول عليها من الدراسات السابقة من خلال منحني القوة- الازاحة، الحمل النهائي ، الانحراف النهائي ، ونمط التشقق. تم أُستخدم النماذج التي تم التحقق من صحتها لتقييم بعض المعاملات الرئيسية مثل مدى نسبة الانحناء ، والتقوية المستعرضة ، والارتباط الجزئي ، وقوة الانضغاط الخرسانية ، والإجهاد الناتج عن الحزمة الفولاذية ، وعمق وشكل الفتحة ، واستخدام شرائح فولاذية داخلية لاستعادة النقص الحاصل نتيجة وجود الفتحة. اظهرت النتائج التي تم الحصول عليها، أن مدى نسبة الانحناء يؤثر على قدرة التحميل، الخضوع، الازاحة والمطيلية بنسبة ٥٠٪, ٥٣٪, ٥٢٪ و ٤١٪ مع انحناء الحزمة الفولاذية بسبب تأثير عزم الالتواء. ان أثر وجود التقوية باستخدام الشرائح الفولاذية في مواقع مختلفة في العتبة الفولاذية المركبة له تاثير على قوة القص وعلى تعزيز مقاومة المقطع والمطيلية بنسبة ٥٧٪ و ٦٣٪. بالإضافة إلى ذلك ، تساهم زيادة الشرائح الفولاذية في تقليل الفصل الرأسي والتواء الحزمة الفولاذية عند منتصف العتبة بسبب انخفاض عزم الالتواء، ونقل الفشل إلى الحزمة الخرسانية. علاوة على ذلك، تظهر زيادة نسبة الارتباط الجزئي انخفاضًا كبيرًا في الفصل الرأسي والواجهة بين البلاطة الخرسانية وحافة العارضة الفولاذية, مع زيادة قدرة العتبات المركبة بنحو ٣٠٪. مع انخفاض في الازاحة والمطيلية بنسبة ٥٠٪ و ٦١٪ بزيادة قابلية التحمل للحزمة الفولاذية ، في حين يبدو أن الشقوق المرنة صغيرة ولا يكاد يذكر في الوجوه السفلية والعلوية للبلاطة الخرسانية المسلحة ، مقارنة بالمعايير الأخرى.

تؤدي زيادة عمق الفتح إلى تقليل قدرة قوة العتبة المركبة ويصبح خضوع العتبة في وقت أبكر اذ سجلت نسبة انخفاض بالخضوع وقابلية التحمل والازاحة العمودية بنسبة ٤٨٪, ١٨٪, ٨٪ تقريبًا عندما يكون عمق الفتحة بنسبة ٧٥٪ من ارتفاع العتبة الفولاذية. وقد لوحظت زيادة في الشقوق الالتوائية عند زيادة عمق الفتح. علاوة على ذلك ، فإن وجود فتحة دائرية ممدودة في العتبات المنحنية المركبة تقلل من قدرة العتبة بنسبة ٢٤٪ تقريبً اما المطيلية فكانت بنسبة ١٤٪، حيث أظهرت العتبة ليونة أقل وخضوع في مرحلة مبكرة. اذ وجد أن الالتواء هو المسيطر على السلوك غير المرن وآلية فشل الحزمة، خاصة في العتبات ذات الفتحة الدائرية الممتدة. تعتبر مقويات العتبة الفولاذية طريقة جيدة لتعزيز قدرة العتبة المركبة. اذ انها توفر استعادة شبه كاملة للقوة المفقودة بنسبة ١١٪ بسبب وجود الفتحات مع تعزيز في أداء العتبة.

جمهورية العراق
وزارة التعليم العالي والبحث العلمي
جامعة ميسان
كلية الهندسة
قسم الهندسة المدنية

التحليل العددي للعتبة الخرسانية ــ الفولاذية المركبة المنحنية في المخطط

رسالة
مقدمة الى كلية الهندسة في جامعة ميسان
كجزء من متطلبات نيل درجة الماجستير في علوم الهندسة المدنية/ انشاءات

من قبل
صبا ليث كريم
(بكالوريوس هندسة مدنية ٢٠١٦)

بأشراف
الاستاذ الدكتور: عبد الخالق عبد اليمة جعفر

ربيع الاول ١٤٤٢   تشرين الاول ٢٠٢٠